RADC-TDR-64-461
FINAL REPORT

1 November 1964

PROJECT WIDE BAND FINAL REPORT

Dr. Walter A. Flood

Cornell Aeronautical Laboratory, Inc.
Buffalo, New York 14221
CAL Report No. UB-1363-P-6

DDC

JAN 1965

DDC-IRA B

Rome Air Development Center
Research and Technology Division
Air Force Systems Command
Griffiss Air Force Base, New York

Qualified requesters may obtain copies from ASTIA. Orders will be expedited if placed through the librarian or other person designated to request documents from ASTIA.

If this copy is not needed, return to RADC, (EMASA/V. Coyne).

Qualified requesters may obtain copies from DDC.

DDC release to OTS is authorized.

RADC-TDR-64-461
FINAL REPORT

1 November 1964

PROJECT WIDE BAND FINAL REPORT

Dr. Walter A. Flood

Cornell Aeronautical Laboratory, Inc.
Buffalo, New York 14221
CAL Report No. UB-1363-P-6

Contract No. AF 30(602)-0277
Project 5579
Task 557902

Rome Air Development Center

Research and Technology Division

Air Force Systems Command

Griffiss Air Force Base, New York

FOREWORD

Evaluation of Contract AF 30(602)-2077

The objective of the effort was to experimentally determine the influence of the atmosphere on radar resolution in range, angle and velocity. The approach was to utilize satellite borne transmitters and ground based receivers designed such that measurements could be made of (1) the spectrum of phase fluctuations, (2) the angular spectrum, and (3) dispersion.

Technical and financial problems negated the possibility of conducting the satellite experiment. Radio astronomy experiments were performed however to deduce the phase fluctuations contributed by the ionosphere and aircraft borne sources were utilized to deduce the phase fluctuations induced by the troposphere. The tropospheric measurement of phase fluctuations was limited by the inability to accurately determine aircraft position; therefore the resultant spectrum of phase fluctuations was contaminated by aircraft induced phase variations. It is still useful within limits however.

Estimates of achievable resolution were made based on data collected by the contractor and the National Bureau of Standards. The following conclusions were reached:

(1) Angular resolution of 0.1 milliradian can be achieved at frequencies greater than 100 mcs for targets of equal cross section. At X-band the cross section may vary as much as 13 db and still be resolved.

(2) Velocity resolution of 0.1 ft per second can be attained for targets of equal cross section. At X-band, this degree of resolution can be achieved on targets whose cross section differs by 13 db.

(3) Range resolution of 1.0 foot can be achieved at frequencies greater than 4,000 mcs for targets of equal cross section. Although difficult to evaluate it is expected that a difference of target cross section of 30 db will still permit resolution to 1.0 foot.

The above estimates are considered to represent worst case conditions; therefore system designers can utilize these values with confidence. It is evident from this effort that worst case estimates of the atmospheric influence on radar resolution can be provided utilizing indirect measurement techniques but that the validity of these estimates become highly questionable when it is necessary to establish limits. It is conceivable that, as radar resolution requirements become more stringent, processing techniques will be required which will utilize statistical descriptions of a signal in time and space to negate the degrading influence of the medium. It has been realized from this effort that costly, sophisticated approaches are necessary to obtain the required statistical representation.
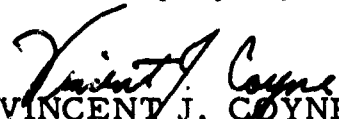
VINCENT J. COYNE
Project Engineer

i
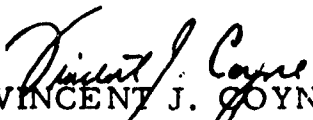
ABSTRACT

The results of a theoretical and experimental program to determine the influence of the atmosphere on radar resolution are presented. The limits imposed by the atmosphere on resolution in range, angle and velocity are treated theoretically and estimated values are presented based on current experimental data. General expressions are derived which permit assessment of the atmospheric influence on resolution as a function of frequency. Consideration is given to multipath dispersion, phase fluctuations and unequal target cross sections.

A description of a radio astronomy experiment which was performed to deduce the phase fluctuations incurred by a wave traversing the ionosphere is presented with the results obtained. Similarly an experiment performed to determine the tropospheric contribution to phase path fluctuations is presented along with a discussion of the validity of the data as limited by the measurement technique employed. An application of the data is included which provides an assessment of the influence of phase fluctuations on the performance of a focussed, multiple antenna, communications system.

PUBLICATION REVIEW

This report has been reviewed and is approved. For further technical information on this project, contact Vincent J. Coyne, EMASA, X-3107.

Approved:

VINCENT J. COYNE
Project Engineer

Approved:

THOMA. B. BOND, JR.
Colonel, USAF
Ch, Surveillance and
Control Division

FOR THE COMMANDER:

IRVING J. GABELMAN
Chief, Advanced Studies Group

TABLE OF CONTENTS

up

INTRODUCTION

The Wide Band Program was instituted to determine the limitations imposed upon radar resolution in angle, range and velocity as a consequence of propagation through the atmosphere of the earth. Insofar as the effects of a nuclear detonation upon radar resolution are represented by naturally occurring auroral phenomena, the Wide Band program would also determine the effects of a high altitude nuclear detonation upon radar resolution.

The Wide Band program embraces both theoretical and experimental investigations. The experimental investigations were to include but not necessarily be limited to the following techniques:

1) A passive satellite experiment utilizing ground-based transmitters and receivers;

2) An active satellite experiment with ground based receivers and satellite-borne transmitters;

3) An aircraft experiment using airborne transmitters and ground-based receivers;

4) A radio astronomy experiment using an extra-terrestrial radio source.

This is the summary report for the Wide Band Program. We shall briefly review the theoretical aspects of resolution, indicate those experimental techniques that were deemed desirable and feasible and discuss the reasons for rejecting certain of the experiments. The above discussions will be somewhat brief since many of these topics have been treated in some detail in referenced Wide Band reports. The report will conclude with a summary of our best estimates of the atmospheric limitations to radar resolution.

1. RADAR RESOLUTION

Although the general concepts of radar resolution are readily
comprehended, a discussion of the resolution of specific radar systems
is not at all straightforward. The general concepts of resolution,
derived from the classical optical "Rayleigh" resolution, criterion
(Jenkins and White, 1950) define resolution as the ability to distinguish
between two radar targets (of equal cross section) which differ in only
one coordinate angle (azimuth or elevation), range or velocity. In
the cases of interest however, the two targets may have far different
radar cross sections and the radar echoes from each target may be
time varying because of target motion or atmospheric effects. The
time varying nature of the signal complicates the problem of system
evaluation.

Before discussing the detailed relationship among resolution,
radar system parameters and atmospheric effects, it might be useful
to reiterate the well known definition of radar cross section:

$$\sigma = P_r \times \frac{16\pi^2 R^4}{P_T G_T A} = \overline{|E_s|^2} \times \frac{16\pi^2 R^4}{P_T G_T A}$$

$$\sigma = \overline{|E_s(t)|^2} \times \frac{16\pi^2 R^4}{P_T G_T A}$$

3

where σ = radar cross section

P_r = received power

R = range to target

P_T = transmitted power   .

G_T = antenna gain

A = effective aperture of the antenna

$E_s(t)$ = temporal variation of the received signal voltage

It is important to note that since the cross section is defined
in terms of the received power (and the system parameters) there is
an integration time required to ascertain the received power. Whenever
there is relative motion between the target and the radar system (due
to either translation or rotation or both) the received signal voltage
will vary for all targets except a single point target. When one takes
signal-to-noise ratios or propagation fluctuations into account, the
received signal voltage for even a single point target will also vary
with time. With no a priori knowledge of the characteristics of the
target, we are required to average the received signal to determine
the cross section.

The preceding remarks have been included to indicate that when
discussing resolution in terms of relative target "cross section" and
real radar systems, a certain amount of time averaging will be required
for each and every system. If the averaging time required to account

for the relative motions of the targets and the actual signal-to-noise ratio is very short compared to the time necessary for the atmospheric effects to change noticeably, then the effects of the atmosphere upon radar resolution, may be negligible.

It would seem however, that the integration time of most systems is such that one should consider the effects of the atmosphere upon radar system resolution limitations.

2. ANGULAR RESOLUTION

Angular resolution is usually defined as the ability of a system to resolve two targets, of equal cross section at the same range, differing only in their angular coordinates. Note that this definition says nothing about the accuracy of location of a single target. The angular resolution of a monostatic radar system is approximately equal to the antenna beamwidth.

The antenna beamwidth and its sidelobe levels are defined in terms of the output power of the antenna for different orientations of the antenna in the presence of a simple plane wave. In a real atmosphere, due to ever-present -albiet normally weak forward scattering by inhomogeneities of refractive index,multipath propagation can exist and the incoming signals cannot be completely represented by a single plane wave but rather must be represented by a summation of plane waves in angle space. Due to the random nature of the forward scattering process giving rise to the multipath propagation, the phase relationship between the plane wave components in the voltage angular spectrum is random and it is usual to speak of the time averaged angular power spectrum of plane waves which describes the power associated with each component of the angular spectrum. Under these circumstances the antenna is said to act as a space filter described by the antenna power pattern and the average power output is the integral,over all angle space, of the product of the antenna power pattern and the angular power spectrum.

6

The angular power spectrum describes on the <u>average</u>, the
distribution of power in the received signal as a function of the angle
of arrival. The emphasis given to the term on the average is warranted.
The angular power spectrum does not describe the time history of
the angle of arrival of radio waves. When assessing the effects of
diffractive scattering upon resolution, it is important to consider
the statistics of the incoming signal on the same time basis as the
time required to move the antenna through an angular distance equal
to at least two resolution elements. If one could move the antenna through
this angular distance in a time very short compared to the time constant
of the atmospheric processes (say for example 10 milliseconds), one
might observe the energy coming from a direction slightly different
from the line of sight path between the observer and the target, but
the beam pattern of the antenna would be preserved. Two targets
separated by more than the angular beamwidth of the antenna might be
resolved on the basis of this short sample if the target field strengths
were well above noise. Some time later, the apparent angles of arrival
of the two targets might be different from before but again the beam
pattern of the antenna might be preserved. Under these circumstances
the effect of multipath propagation would cause the instantnaeous signal
to "glint" over a range of directions centered on the line of sight path.

m.

So far we have described the principles which might be used to determine the effects of multipath or forward scatter upon angular resolution. We must now qualitatively assess these effects upon radar resolution.

2.1 Angular Spectrum and Angular Resolution

Bramley (1951) has derived the angular spectrum of plane waves produced by a phase changing screen in which the spatial autocorrelation function of the fluctuations of phase was of the form

$$\rho_\phi(x) = exp - \left(\frac{x}{x_0}\right)^2 \tag{1}$$

and found that the angular power spectrum is given by (equation 36 of Bramley)

$$\overline{|F(s)|^2} = exp - \sigma^2 \left[\delta(s) + \frac{\pi^{1/2}}{2} x_0 \sum_1^\infty \sigma^{2n} \frac{exp - \frac{\pi^2 s^2 x_0^2}{n}}{n! \sqrt{n}} \right] \tag{2}$$

where   is the mean squared phase fluctuation

is the "correlation distance" of the phase fluctuations measured in wavelengths

is the sine of the angle of arrival measured from the vertical

is a delta function

8

The delta function in equation (2) represents the zero order undeviated plane wave - that wave which would propagate in the absence of the phase fluctuations. As the mean square phase fluctuations increase, power is abstracted from the zero order undeviated wave and is fed into the continuous spectrum of plane waves represented by the second term of equation (2). One would expect, then, that as the mean squared refractive index fluctuations increase the power in the delta function in the spectrum will decrease to a value such that it is indistinguishable from the continuous spectrum and the incoming spectrum is then spread over a range of angles. In Appendix A we show that when σ is of the order of 1.5 radians the power associated with the delta function is 1/10 of the power associated with the continuous spectrum and the angular spectrum has a half-width, $\Delta\theta$ given by

$$\Delta\theta = 1.5 \times .46 \frac{\lambda}{x_0} = .69 \, x_0$$

and that therefore the minimum angular resolution which can be expected is $2\Delta\theta$

$$2\Delta\theta \approx \frac{\lambda}{x_0}$$

2.2 Resolution Limitations Imposed By The Auroral Ionosphere

An experiment to determine the ionospheric limitations to angular resolution was conducted under the Wide Band Program. This experiment utilized emissions from the radio source in Cassiopeia A and observed

9

the phase fluctuations introduced by the auroral ionosphere on frequencies
of 52 and 147 Mcs simultaneously on baselines of 300, 600, and 900 feet
East-West and 1000 and 200 feet North-South. A complete description
of the experimental technique and the detailed results can be found in
the Cornell Aeronautical Laboratory Report No. UB-1363-P-4, January
1962. A supplementary report, covering an additional six months of
work is appended to this report as Appendix B. To sum up the results
of the experimental investigations of the ionosphere, it appears that
a radio wave, traversing the entire ionosphere will suffer phase
fluctuations whose mean square value σ^2 is given by $\sigma^2 \approx \lambda^2$
square radians and d_s , the correlation distance of the phase fluctuations
is of the order of 200-300 meters.

For frequencies well in excess of 300 Mcs ($\lambda = 1$ meter) the
mean squared phase fluctuations in the ionosphere will be much less than one
square radian and the angular spectrum of the wave as received at
the ground will consist of a well-defined angle of arrival with some weak
continuous scatter. For such frequencies, the radar system angular
resolution will be limited only by tne physical size of the aperture.
"Resolution" in the preceding sentence is used in the context of
distinguishing two targets of equal or nearly equal cross section.

10

For frequencies less than 300 Mcs ($\lambda \gtrsim 1$ meter) ionospheric phase fluctuations will set a limit to the maximum obtainable resolution. In Radio Astronomy Report No. UB-1363-P-4 we developed the formula (derived a little more elegantly in Appendix A) $2 \Delta\theta = \lambda^2/d$ where d is the correlation distance, approximately, 200-300 meters. Table I lists our estimates of the limitations to angular resolution imposed at VHF-UHF frequencies by the auroral ionosphere.

Table I

Limitations to Angular Resolution Imposed by Auroral Ionosphere

Frequency in Mcs	50	100	200	300
Minimum Angular Separation in Radians	.12	.03	.0075	.003

2.3 Limitations of Angular Resolution Imposed by the Troposphere

At the time of the initiation of the Wide Band program, there was a definite paucity of available data on the magnitude of tropospheric path fluctuations. In the first Wide Band report, extensive use was made of the path length fluctuation data obtained by the National Bureau of Standards from a 10 mile path in Colorado. Since that time NBS has collected additional Colorado data and extensive Hawaiian data. Figure 1 is a composite of the NBS data reported by Thompson, Janes and Kirkpatrick (1960). The data presented are median spectral data and the variance of the
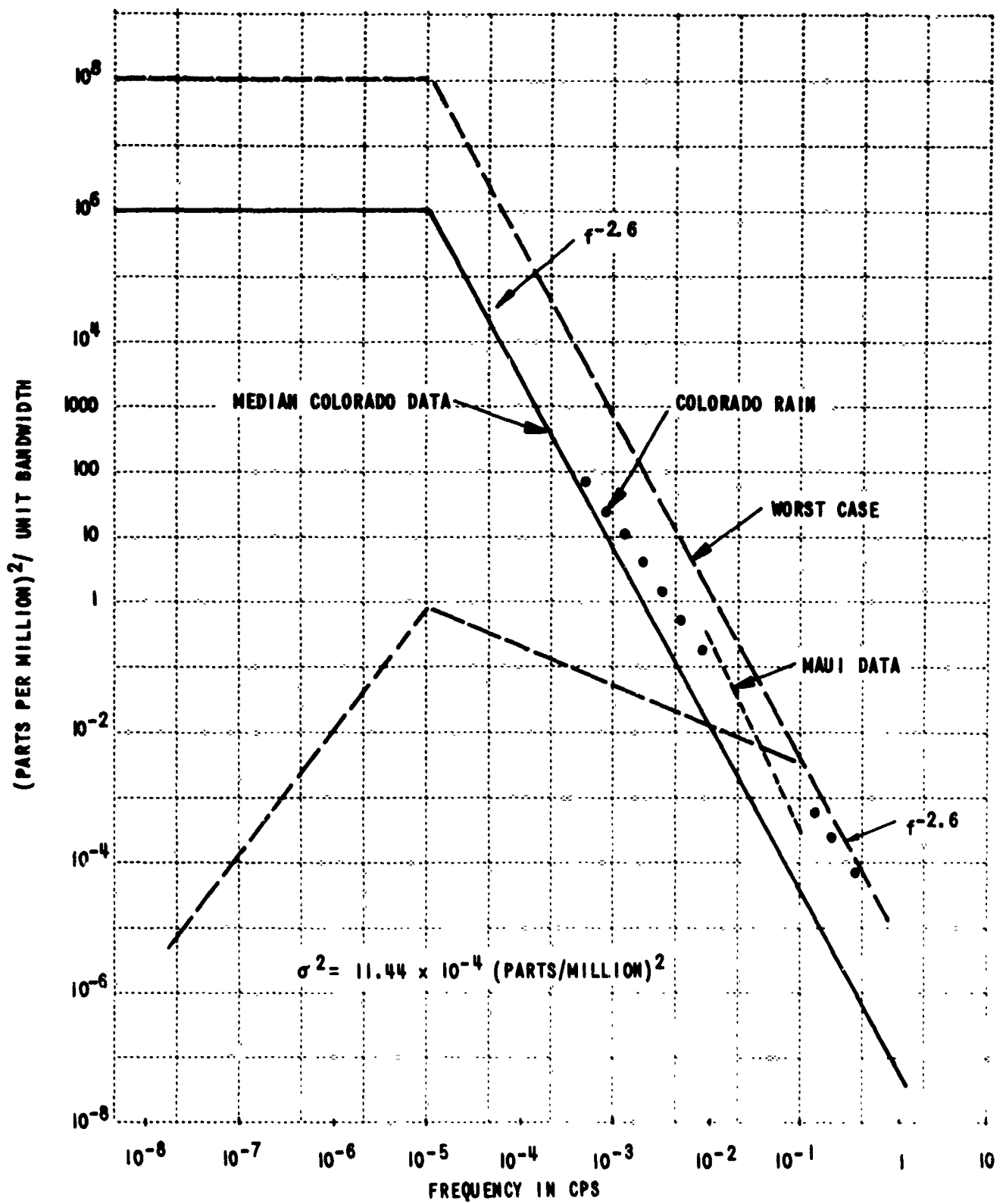
11

Figure 1 SPECTRUM OF APPARENT PATH LENGTH FLUCTUATIONS IN THE TROPOSPHERE
(THOMPSON, JANES, KIRKPATRICK)

12

spectral density estimates about this median value might very well be approximately 10 decibels. The important points to note in these data are the approximate variation of the spectral density with the inverse 2.6 power of the fluctuation frequency; the fact that the median Hawaii data are approximately 10 db greater than the median Colorado data and finally that the spectral density data pertaining to the passage of a frontal system at the Colorado site are 20 db greater than the median of the Colorado data.

In order to indicate reasonable limits to the spectral density of path length fluctuations we have drawn the dotted line in Figure 1 which encompasses all of the median experimental data and should be representative of the majority of the experimental runs. In Figure 2, we present the expected value of the spectrum based upon a five second data sample (see Appendix A). The area under this curve, the variance of the path length fluctuations is 11.4×10^{-4} (parts/million)^2. If we adopt as a model of the troposphere a statistically uniform medium extending from ground up to ten kilometers altitude and a lower limit to the elevation angle of six degrees, then the maximum tropospheric path length will be less than 100 kilometers long. Consequently we expect that the root mean square phase fluctuations on a long tropospheric path will be less than

$$\sigma = \frac{[11.4]^{1/2} \times 10^{-2}}{10^6} \left(\frac{2\pi \times 10^5}{\lambda} \right) \ radians$$

13

FLUCTUATION OF APPARENT
PATH LENGTH IN (PARTS
PER MILLION)^2/UNIT BANDWIDTH
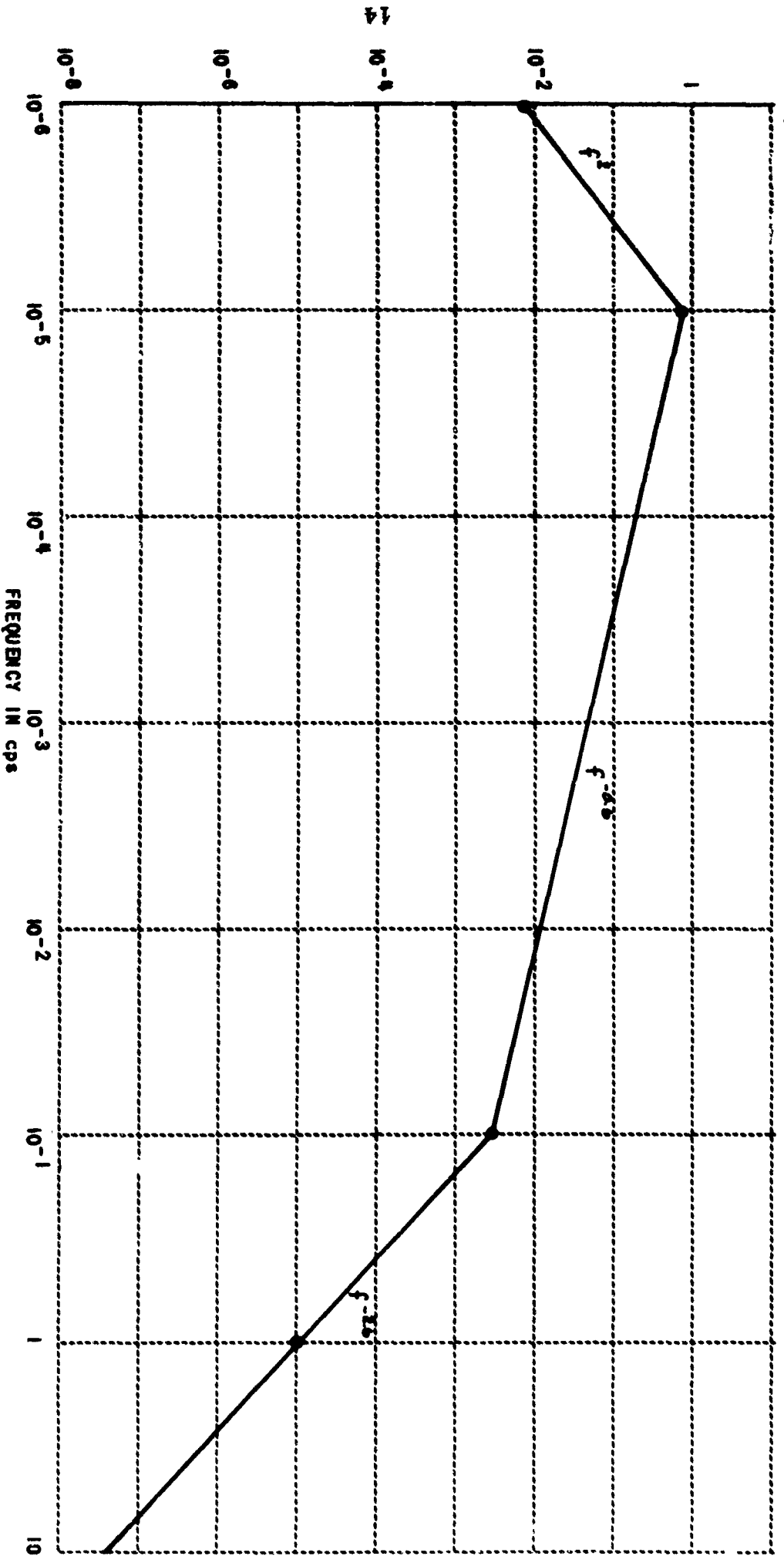
Figure 2   EXPECTED VALUE OF SPECTRUM OF SINGLE PATH PHASE FLUCTUATIONS
BASED ON A 5 SECOND DATA SAMPLE

The greater the frequency, the greater will be the rms phase fluctuations. At X-band, the highest frequency considered in this report

$$\sigma_{X BAND} \leq \frac{6\pi \times 10^{-3}}{3 \times 10^{-2}} = 8\pi \times 10^{-1} \ (radians)$$

$$\sigma^2_{X BAND} \leq 0.394 \ (radians)^2$$

Since our previous discussion of ionospheric phase fluctuations at X-band indicates that there are less than 1 square radian, we do not expect resolution to be impaired. It should be further noted that even if the phase fluctuations were larger than one square radian, the amount of beam spreading (due to the continuous portion of the angular spectrum) might be quite small. The correlation distance of the phase fluctuations (derived in Appendix A) is of the order of 30 meters. At X-band, the continuous portion of the spectrum is therefore $\frac{\lambda}{d} \leq \frac{3 \times 10^{-2}}{3 \times 10^{1}}$ = 1 milliradian.

2.4 The Wide Band Satellite and Aircraft Interferometer Experiments

It would appear therefore that tropospheric and ionospheric effects should not limit angular resolution. In order to prove these conclusions under actual field conditions an experiment utilizing satellite transmissions at 2250 Mcs was proposed. Interferometers having baselines of 100 and 1000 meters in North-South and East-West directions were installed at a field site near Buffalo, New York. The equipment is fully described in Wide Band Report No. UB-1363-P-101. The satellite transmitter was designed with both the interferometer experiment and wide bandwidth transmission experiment (to be described in Section 4 on Range Resolution) in mind.

The interferometer experiment had as its goal the measurement of the phase fluctuations incurred on a combined tropospheric and auroral-ionospheric path. In order to accomplish the auroral measurements, a polar orbiting satellite was required. Our initial plan was to include the Wide Band transmitting apparatus on an experimental Midas satellite. By the time it became apparent that a satellite experiment was not immediately forthcoming, the installation of ground equipment was complete and a system checkout program utilizing aircraft transmissions was initiated. Although the prime purpose of the aircraft program was to check out the interferometer system, it was recognized that this program would also offer an opportunity to measure the tropospheric phase fluctuations encountered on a rotating line of sight path in contrast with the NBS experiment already mentioned, which employed a path whose coordinate end points were fixed. Detailed results of this program are presented in Appendix C but the general results can be summarized as follows. On a propagation path which extended from ground level to approximately 40,000 feet and whose length was 60 nautical miles, the measured mean squared phase fluctuations were very closely approximated by the phase fluctuations associated with the uncertainty of actual aircraft position. The difference between our estimates of phase fluctuation and the phase fluctuations associated with unknown aircraft

position were far less than the estimates of the worst possible

phase fluctuation conditions illustrated in Figure 2. We conclude

therefore that Figure 2 probably represents a pessimistic estimate

(which it was designed to do) of the phase fluctuations associated with

the troposphere and therefore, at least at frequencies equal to or

less than 10,000 Mcs, the troposphere will not limit angular resolution.

3. VELOCITY RESOLUTION

The ability of a radar system to resolve two targets on the
basis of differing Doppler shifts is clearly a function of the purity
of the transmitted waveform and the duration of the observation. It
is equally a function of the stability of the propagation path. Consider
a monochromatic plane wave reflected from a target whose radial
velocity is N_r . In the absence of phase fluctuations due to the propagation
path, the returned signal is of the form

$$E(t) = \cos\left[\omega t - \phi(t) + \phi_0\right]$$

where

$$\dot{\phi}(t) = \frac{2\pi}{\lambda}\left(R_0 - r_n t\right)$$

If there are random phase fluctuations, the received signal is of form

$$E_r(t) = \cos\left[\omega_0 t - \phi(t) - \phi_n(t) + \phi_0\right]$$

where $\phi_r(t)$ is the random phase fluctuation associated with the
propagation path. The spectrum of the received signal can be obtained
from the Fourier transform of the autocorrelation function $\rho_E(\tau)$

$$\rho_E(\tau) = \overline{E_r(t) E_r(t+\tau)} = \frac{1}{2}\left\{\overline{\cos\left[2\omega_d t + \omega_d \tau + \psi_r(t) + \phi_n(t+\tau) + 2\phi_0\right]} + \overline{\cos\left[\omega_d \tau + \Delta\phi(\tau)\right]}\right\}$$

$$\rho(\tau) = \frac{1}{2}\overline{\cos\left[\omega_d \tau + \Delta\phi(\tau)\right]}$$

where $\Delta \phi(t)$ is defined by $\Delta \phi(t) = \phi(t+\tau) - \phi(t)$ and ω_d is the Doppler shifted frequency. As before, if $\phi_\tau(t)$ is normally distributed, the density function of $\Delta \phi_\tau(t)$ is given by $p(\Delta \phi)$

$$p(\Delta \phi) = \frac{1}{\left\{ 4\pi \sigma^\nu [1-\rho_\phi(\tau)] \right\}^{\frac{1}{2}}} \; \exp - \left\{ \frac{(\Delta \phi)^\nu}{4\sigma^\nu [1-\rho_\phi(\tau)]} \right\} d\Delta \phi$$

where again σ^ν is the variance of $\phi_\tau(t)$ and $\rho_\phi(\tau)$ is the normalized autocorrelation function of $\phi_\tau(t)$

$$\rho_E(\tau) = \cos \omega_d \tau \, \exp \left\{ -\sigma^\nu [1-\rho_\phi(\tau)] \right\}$$

And again, in a manner identical to that indicated in Appendix A, the spectrum of E_r is

$$S(f) = \exp \left\{ -\sigma^\nu \right\} \left[\delta(f-f_d) + \int_0^\infty \sum \frac{\sigma^{2n}}{n!} \rho_\phi^{\,n}(\tau) \cos \omega_d \tau \cos \omega \tau \, df \right]$$

Propagation phase path fluctuations abstract power from the Doppler shifted line in the received power spectrum and spread it into a continuous distribution centered around the Doppler shifted line. So long as the mean squared phase fluctuations are small (less than one square radian) the power in the "smeared" continuous spectrum will be much less than the power in the Doppler shifted line and velocity resolution

19

of two targets of equal or nearly equal cross section can be effected
to the extent permitted by signal-to-noise ratio, integration time and
other system parameters.

Consider that we desire to resolve targets whose velocities
differ by 0.1 feet per second (.03 meters/second). The differential
Doppler shift Δf_d will be

$$\Delta f_d \approx \frac{2(\Delta \nu)}{\lambda} = \frac{.06}{\lambda}$$

Table II lists the differential Doppler shift as a function of operating
wavelength. Also listed is the minimum time necessary for any
system to resolve the indicated frequency difference.

Table II

Operating Wavelength in Centimeters	30	10	3
Frequency Difference cps	0.2	0.6	2.0
Minimum Observation Time seconds	10	3.3	1

For an averaging time of 5 seconds, we have already seen
that the mean squared phase fluctuations at X-band are less than 0.394
square radians. Consequently we do not expect that tropospheric phase fluctu-
ations alone will limit the ability to achieve velocity resolution of 0.1
feet per second.

20

4. RANGE RESOLUTION

Range resolution is the ability of a radar system to distinguish
between two targets of equal cross section which differ only in the range
coordinates. If the two targets are point sources and have identical
radar cross sections, then the range resolution achievable by a radar
system is slightly in excess of $(1/2)c\tau$ where c = velocity of propagation
and τ is the duration of the radar pulse.

Radar range resolution is a function of the bandwidth of the
radar system. Increased range resolution is achieved by radiating
a narrower pulse. The narrower the radiated pulse, the broader is
the radiated spectrum and hence, the bandwidth of the radar system.

The limits to the achievable range resolution are the limits
imposed upon the usable bandwidth. The real atmosphere of the earth
will impose bandwidth limitations because the atmosphere is both
dispersive and non-uniform. These considerations will be examined in
order.

4.1   The Dispersive Atmosphere

The presence of free electrons in the ionosphere (a region
extending from approximately 60 kilometers in altitude upwards to the
limits of the earth's atmosphere) modifies the refractive index such

21

tha

$$n = \left[1 - \frac{Ne^2}{m\epsilon_0 \omega^2} \right]$$

where n = refractive index

N = local electron density (number per cubic meter)

m = mass of an electron = 9×10^{-3} kilograms

e = charge of an electron = 1.59×10^{-9} coulombs

ω = angular radio frequency

ϵ_0 = capacitivity of free space = 8.854×10^{-12} farads/meter

It is to be noted that the refractive index in the ionosphere
is a function of frequency. Consequently each of the waves (of differing
frequency) which comprise the radio frequency pulse will travel with
a different velocity. The pulse, after travelling through the dispersive
medium, will be distorted. The distortion will be evidenced by
an increase of apparent pulse length as well as a change in the general
shape of the pulse.

In the Phase I Report of Project Wide Band (CAL Report
No. UB-1363-P-3, March 1960) we reported on the results of the
effects of dispersion upon pulse shape as a function of carrier frequency,
percentage bandwidth and integrated electron density along the
propagation path. As a result of this investigation we concluded that
if dispersion alone were the limiting factor to pulse shape, then (for
frequencies in excess of 4000 Mcs) bandwidths of 500 Mcs could be
achieved without requiring corrective action. It also appeared that if
corrective filters were employed, 500 Mcs bandwidth propagation
could be accomplished at a carrier frequency as low as 2000 Mcs.

4.2   Non-Uniform Atmosphere

The fact that the refractive index in the ionosphere as well
as in the troposphere is non-uniform may limit the range resolution
at certain frequencies. To the extent that multipath propagation
(discussed in the Section on Angular Resolution) is important, it
may limit the achievable range resolution since energy travelling
over non line-of-sight paths will arrive at times later than the energy
travelling over the direct path. In the Phase 1 Report on
Project Wide Band, we indicated that we were not certain of the
multipath situation in the auroral ionosphere. As a result of the Radio

Astronomy Experiment, reported in the first Radio Astronomy Report [CAL Report No. UB-1363-P-4] and with some additional detail in Appendix B, we have concluded that range resolution of 1 foot (a bandwidth of 500 Mcs) is possible in the presence of the auroral ionosphere if the carrier frequency is well in excess of 500 Mcs.

It should be emphasized that the above conclusion is based upon a definition of resolution which implies that the target radar cross sections are identical and that the phase fluctuation statistics are not strongly frequency dependent. We shall discuss the first limitation in the next section of this report and shall indicate the extent of the resolution problem for unequal targets in greater detail. During the course of this discussion, the effects of the frequency dependence of the phase fluctuation statistics will become more clear.

5. RESOLUTION OF TARGETS OF
UNEQUAL RADAR CROSS SECTION

In the previous discussions we have been able to give our estimates of the resolution limits imposed by the atmosphere in angle, range and velocity space when resolution is defined in terms of targets of equal cross sections. In recent years, the specifications for more sophisticated radar systems have pre-supposed the existence of systems which can resolve targets whose radar cross section may differ by more than 30 db. The effects of the atmosphere upon the resolution capabilities of such systems poses a problem of quite different magnitude than for the types of system which have previously been considered. A simple example might serve to illustrate the point.

Consider the angular resolution problem treated in Section 2. We have seen that when the mean squared phase fluctuations are σ^2 , power is abstracted from the wave arising from the target direction and is spread over a range of angles of roughly $\pm \dfrac{\sigma \lambda}{2d}$.

The available data indicate that the expected value of the mean squared phase fluctuations is less than 0.394 radians and consequently the full width of the continuous spectrum is approximately one milliradian at X-band. The power associated with the continuous spectrum is ($1 - e^{-\sigma^2}$) so that for example the power in a range of angles $\triangle \Theta$, of approximately 1/10 milliradians is .032 units. The situation is depicted in Figure 3 where the resultant undiffracted wave is 13 db more intense than the power in a tenth milliradian beamwidth. Consequently it would

25

.632   UNDIFFRACTED
COMPONENT

$\sigma^2 = 0.394$

$d_o = 30$ METERS

RELATIVE POWER

.316

POWER DENSITY PER
UNIT BEAMWIDTH
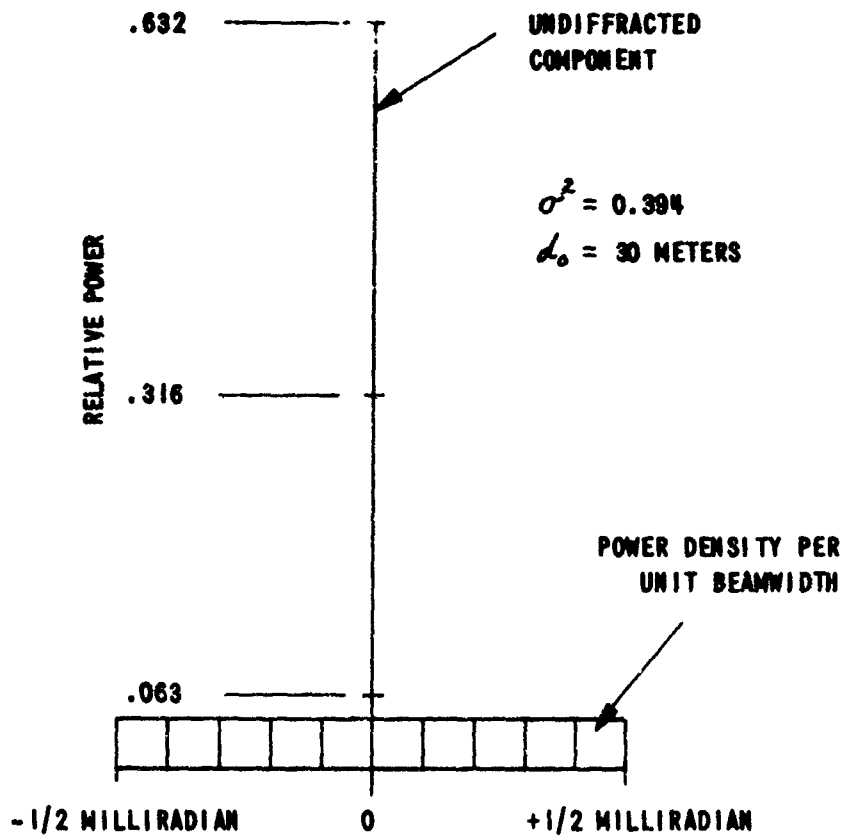
.063

-1/2 MILLIRADIAN   0   +1/2 MILLIRADIAN

Figure 3   ANGULAR SPECTRUM AT X-BAND
ANTENNA BEAMWIDTH = 0.1 MILLIRADIANS

be very difficult to resolve two targets, separated by a one-half milliradian whose radar cross sections differed by more than 13 db. The above results are dependent upon the mean squared phase fluctuations being approximately 0.394 square radians, the correlation distance being 30 meters, and the antenna beamwidth being 0.1 milliradians.

Another example may illustrate the dependence of the resolution criterion upon these parameters. If all values of the parameters are the same as before except that the correlation distance of the atmospheric phase fluctuations is increased to 100 meters, then the power density per unit 0.1 milliradian beamwidth will be three times the previous value and the width of the continuous spectrum will be one-third of a milliradian. Under these circumstances, a one-tenth milliradian system will have difficulty in resolving two targets, separated by 0.16 milliradians, when their cross sections differ by more than 15 db. If the averaging time required to make the measurements is less than the 5 seconds we have used in this report, the expected variance of the phase fluctuations will be reduced and the resolution capabilities of the system will be improved. It should also be noted that if antenna size presents no insuperable engineering problems, decreasing the operating frequency while increasing the antenna aperture will reduce (by the frequency ratio squared) the variance of the phase fluctuations and hence improve the angular resolution of a system.

27

Similar considerations hold for the velocity resolution capabilities of a radar system. In this case the "correlation time" of the phase fluctuations takes the place of the "correlation distance" used in the previous angular resolution discussion. Reducing the averaging time or the frequency of operation may improve the resolution capabilities of proposed systems.

The ability of a system to resolve two targets of vastly unequal cross section which differ only in range is a function of what has come to be called "range sidelobes". Range resolution of approximately one foot (500 Mcs bandwidths) is usually only considered for pulse compression systems. In order to achieve resolution of this order a swept frequency pulse approximately 5 or 10 microseconds is collapsed down to the desired pulse length. Rather precise shaping of the amplitude and phase characteristics of this pulse is required to achieve range sidelobe levels of perhaps 25-30 db. Strong signal-to-noise ratios are required if the phase of the signal is to be a meaningful quantity. If the phase path fluctuations are exactly governed by a relationship of the sort

$$\phi(t, \lambda) = \frac{2\pi}{\lambda} \Delta R(t) \qquad (5.1)$$

28

where $\phi(t,\lambda)$ is the instantaneous phase shift at time t and wavelength λ

$\Delta R(t)$ is the random phase path fluctuation and is independent of frequency

Then the only way in which phase path fluctuations can influence the shape of the resultant collapsed pulse is to have the random phase path fluctuation change in the time period τ of the uncollapsed pulse. It should be further noted that a linear change in phase path with time may cause a range error but cannot cause an increase in range sidelobes.

The available propagation data indicate that the changes of phase path fluctuation in time period less than 10 microseconds are very small and indeed are beyond the measurement capabilities of available equipment. We are led to believe then that if the uncollapsed pulse is less than 10 microseconds long, with the signal-to-noise ratios and linear dynamic range of available wide band radar equipment, changes in phase path fluctuations during the pulse time is of minor importance.

What may be of greater importance is the fact that the path length fluctuations at two widely separated frequencies may be uncorrelated and cannot therefore be represented by (5.1). Two possible mechanisms come readily to mind which may lead to this situation. The first mechanism involves the dispersive properties of the ionosphere which could cause two frequencies, separated by 500 Mcs, to travel two slightly different ray paths and therefore encounter two differing time histories of path fluctuation.

29

One might expect that the contribution of the very largest irregularities of refractive index might be common to both radio frequencies but that path length fluctuations of the smaller irregularities would be uncorrelated.

The second mechanism has to do with the scattering properties of the irregularities of refractive index. If there is a cutoff size in the spectrum of irregularities, the smallest irregularities will scatter the lower of the two frequencies over a slightly wider angle than they will the higher of the two frequencies. Since the resultant phase at a point on the ground is the sum of all such forward scattered wavelets, the two path length histories may be slightly different at the two different frequencies.

Both of the suggested mechanisms for uncorrelated path length fluctuations recognize that such uncorrelated path length fluctuations will be primarily due to the smaller refractive index irregularities. One would therefore expect that the higher frequency components of the phase fluctuations would be uncorrelated. The National Bureau of Standards has completed a series of measurements on a 47 kilometer line-of-sight over-water path at Eleuthera Island in the Bahamas using frequencies of 9400 and 9200 Mcs. (Janes et al. 1963). Although the presence of the sea surface as a reflector tends to obscure the applicability of the results, the data show that the phase history of the two signals is uncorrelated at spectral frequencies greater than one cycle per second. This is the only experiment instrumented to measure uncorrelated path length fluctuations as a function of frequency separation. Such path length fluctuations may set a lower limit of range sidelobe suppression.

5.1 The Wide Band Satellite Experiment

In order to measure the effects of uncorrelated phase path
fluctuations for frequencies differing by 500 Mcs on auroral ionospheric
and long tropospheric paths a satellite experiment was proposed and
initiated. The basic experiment consisted of sending a carrier and 3 pairs
of sidebands separated by 100, 200, and 300 Mcs. These signals were
to be received on the ground and the sidebands were to be separately
mixed with the carrier to obtain pairs of frequencies of 50, 100, and
150 Mcs. The phase difference between these pairs of frequencies
was to be recorded and analyzed.   The dispersive
properties of the atmosphere would cause the recorded phase difference
to vary slowly and regularly (the phase difference is proportional to the
integrated electron density along the propagation path). Measurements
of the phase fluctuations about the regular curve should lead to estimates
of the mean squared phase fluctuations as a function of frequency separation.
In this experiment the difference phase fluctuation variance would be
measured at only three frequency separations.

We believed that it was most important to make these measure-
ments through the auroral ionosphere so that the satellite vehicle should be
in a near-polar orbit. The carrier frequency of the Wide Band Satellite
transmitter was also to be used for the satellite interferometer experiment
described in Section 2 of this report.

The choice of carrier frequency and actual radiated bandwidth
of the satellite-borne transmitter was determined by the availability
of hardware which could operate in the satellite environment. A study
and evaluation of the available designs of wideband transmitters was
presented in the Phase 1 Wide Band report. On the basis of the
information then available a frequency modulated, voltage tuned
magnetron was selected for the transmitter. A subcontract was let
with Radiation, Inc. of Melbourne, Florida to furnish this transmitter in
conformance with specifications detailed in the Phase 1 Wide Band
Report. During the course of this development program difficulties
with magnetron performance were experienced and the subcontract
transmitter program was discontinued in favor of a new design making
use of TWT's that had been developed for satellite use since initiation of
this project.

When at a later time it became apparent that the Wide Band Satellite
Transmitter could not be accommodated "piggyback" on existing Air Force
satellite programs, attention was directed towards the design of a
complete satellite package including solar cells, command and control,
telemetry, and atitude stabilization. The results of this design study
are reported in CAL Report UB-1363-P-201 entitled "Spacecraft for Radar
Propagation Experiments-Design Study Report" dated 30 June 1962.
The spacecraft design was adaptable to larger launching vehicles but
it appeared that the Air Force Blue Scout launch vehicle would suffice.

The funds required for the spacecraft development program were unavailable and as a result, no active satellite experiments have been performed.

5.2   Radar Studies of Passive Satellites

The original Wide Band contract work statement called for an investigation of the feasibility of establishing the atmospheric limits on resolution from radar measurements of orbiting satellite vehicles. At that time (1960) it was apparent that existing radar systems having sufficient sensitivity to measure satellite echo strength as a function of time did not have the necessary bandwidth to enable one to estimate range resolution limitations. The cost of installing coherent transmitting and receiving systems which could utilize satellite reflections at say three frequencies separated by approximately 300 to 500 Mcs was deemed inordinately high. Consequently attention was focussed on one way propagation measurements using a satellite-borne transmitter.

ite

e

ir

33

5.3　Additional Areas of Investigation

During the course of the Wide Band program we were directed to analyze the atmospheric propagation effects upon a dispersed antenna array - satellite communication system. The final report for this preliminary investigation is submitted as Appendix D of this report.

6. SUMMARY

The limitations imposed upon radar resolution as a consequence
of propagation through the atmosphere have been defined in terms
of the ability of a radar system to discriminate between two targets of
equal radar cross section. In so doing we have attained the basic
objectives of Project Wide Band. The experimental data obtained under
the radio astronomy portion of the Wide Band program have been most
valuable in defining the limits to which the auroral ionosphere will limit
resolution as a function of frequency. The recent data on tropospheric
fluctuations, obtained by the National Bureau of Standards under a variety
of weather and climatic conditions, provides the basis for estimates of the
limits of resolution imposed by tropospheric propagation. The fact
that our estimates are pessimistic and are designed to reflect the
worst propagation conditions has been confirmed in part by our wide
baseline interferometer-aircraft experiment.

The limits to radar resolution in the case of two targets of
unequal cross section cannot be simply defined since the end results
are dependent upon the individual radar system time constants and
parameters. However, the method of evaluating the limitations of
angular and velocity resolution (for unequal targets) of a system has
been demonstrated through an example in Section 5. We also showed
that to the extent that propagation path length fluctuations are independent

35

of frequency, range resolution will not be limited by atmospheric effects. However, we noted that at least part of the path length fluctuations at two separated frequencies will be uncorrelated. If the variance of these uncorrelated phase fluctuations is small enough, the attendant increase in "range sidelobe levels" may not be noticeable in the sidelobe levels which will exist in an unperturbed system. Since there exist no measurements of the uncorrelated phase fluctuations along a complete propagation (auroral-ionospheric plus tropospheric) path we have no information on which to base an estimate of the resolution limitations which might be imposed. We feel, however, that for a 1-foot pulse-length system operating at frequencies of 4000 Mcs or greater, the resolution limitations will only be associated with targets which have grossly disparate radar cross sections, say 25-30 db.

We conclude with a list of resolution capabilities for targets of equal cross section which we feel can be obtained under the worst propagation conditions associated with the earth's atmosphere. To the extent that the auroral ionosphere is representative of the conditions to be expected as a result of a high altitude nuclear detonation, then these estimates will hold for that condition.

1. Angular Resolution - Angular resolution of 0.1 milliradians, at frequencies greater than 1000 Mcs can be attained for targets of equal cross section. Our estimates are that this degree of resolution can be obtained at X-band when the target cross sections differ by as much as 13 db.

2, Velocity Resolution - Velocity resolution of 0.1 feet per second can be attained for targets of equal cross section. We estimate that this degree of resolution can be obtained at X-band when the target cross sections differ by as much as 13 db.

3. Range Resolution - Rahge resolution of 1.0 foot at frequencies greater than 4000 Mcs can be attained for targets of equal cross section. The limitations to resolution for targets differing greatly in radar cross section cannot be well defined but   may be equal to 1.0 foot for targets whose cross sections differ by as much as 30 db.

The above estimates are based upon essentially infinite signal-to-noise ratio. The range and velocity resolution achievable with practical radar systems may very well be limited by the limits to signal-to-noise ratio and the linear dynamic range of operation inherent in any practical radar system.

db.

7. REFERENCES

Bramley, E. N., Proc. Inst. Elec. Engrs. (London) B, 102, 533, 1955

Jenkins, F. A. and H. E. White, "Fundamentals of Optics," 2nd Ed. McGraw-Hill, N. Y., 1950

Norton, K. A., J. W. Herbstreit, et al., NBS Monograph 33, Nov. 1, 1961

Thompson, Janes, and Kirkpatrick, JGR, 65, 193, 1960

CAL REPORTS

CAL Report No. UB-1363-P-3, Atmospheric Limitation to Radar Resolution, Phase I Report, March 1960.

CAL Report No. UB-1363-P-4, Radio Astronoy Report, Propagation Through a Disturbed Ionosphere: Effect Upon Range and Angular Resolution - Project WIDE BAND, January 1962

CAL Report No. UB-1363-P-101, Wide Band Receiving Installation, February 1962, Revised April 1962.

CAL Report No. UB-1363-P-201, Spacecraft For Radar Propagation Experiments Design Study Progress Report, 30 June 1962.

Appendix A

Mathematical Derivations

Phase Changing Diffraction Screen

Consider that the electric field intensity, measure along a plane, of a radio wave is given by

$$E(x_0, t) = \cos\left[\omega t + \phi_{x_0}(t)\right]$$

and that the field measured at a point $x_0 + \Delta x$ is

$$E(x_0 + \Delta x, t) = \cos\left[\omega t + \phi_{x_0 + \Delta x}(t)\right]$$

The spatial autocorrelation function of the electric field as a function of x, the distance between the measuring points is $\rho_E(x)$.

$$\rho_E(x) = \overline{E(x_0) \, E(x_0 + \Delta x)} = \overline{\cos\left[\Delta \phi_x(t)\right]}$$

If the $\phi_{x_0}(t)$ are normally distributed, it can be shown that the density function of the difference $\Delta\phi = \phi_{x_0} - \phi_{x + \Delta x}$ is normally distributed with

$$p(\Delta\phi) = \left\{\frac{1}{4\pi\sigma^2\left[1 - \rho_\phi(x)\right]}\right\}^{1/2} \exp\left\{-\left[\frac{(\Delta\phi)^2}{4\sigma^2\left[1 - \rho_\phi(x)\right]}\right]\right\} d\Delta\phi$$

where $p(\Delta\phi)$ is the probability density function of $\Delta\phi$

σ^2 is the variance of the phase fluctuations $\phi_{x_0}(t)$

$\rho_\phi(x)$ is the normalized spatial autocorrelation function of $\phi_{x_0}(t)$

$$\rho_E(x) = \frac{1}{\left\{4\pi\sigma^2\left[1-\beta_\phi(x)\right]\right\}^{1/2}} \int_{-\infty}^{\infty} \varkappa p - \left\{\frac{(\Delta\phi)^2}{4\sigma^2\left[1+\beta_\phi(x)\right]}\right\} \cos\Delta\phi \, d\Delta\phi$$

$$\rho_E(x) = \varkappa p - \sigma^2\left[1 - \beta_\phi(x)\right]$$

The angular power spectrum is the Fourier transform of the spatial correlation function of the electric field

$$\overline{|F(s)|^2} = \varkappa p\left\{-\sigma^2\right\}\left[\delta(s) + F'(s)\right]$$

where S is the sine of the angle of arrival

and

$$F'(s) = \int_0^\infty \sum_{n=1}^{\infty} \frac{\sigma^{2n}}{n!} \left[\beta_\phi(x)\right]^n \cos 2\pi s x \, dx$$

In the case considered by Bramley

$$\beta_\phi(x) = \varkappa p\left\{-\left(\frac{x}{x_0}\right)^2\right\}$$

where x_0 is the "correlation distance" measured in wavelengths, so that

$$F'(s) = \sum_{n=1}^{\infty} \left(\frac{\sigma^{2n}}{n!}\right)\left(\frac{\pi}{n}\right)^{1/2}\left(\frac{x_0}{2}\right)\varkappa p\left\{-\frac{\pi^2 s^2 x_0^2}{n}\right\}$$

When $\sigma^2 \gg 1$, terms in the series for $F'(s)$ out to approximately $n = 2\sigma^2$ must be taken. The half width of the continuous spectrum $F'(s)$ will then be

$$S \equiv \sin\theta = \frac{\sqrt{2}\,\sigma}{\pi x_0} \sim \frac{\lambda}{2d}$$

The effect of a finite length of record in computing the variance of
a random variable

Given $f(t) = \sum\limits_{n=0}^{\infty} C_n \cos[\omega_n t + \phi_n]$

we will define the autocorrelation function of a finite sample length T as

$$\rho(\tau) = \frac{1}{T}\int_0^T f(t)f(t+\tau)\,dt - \left[\frac{1}{T}\int_0^T f(t)\,dt\right]^2$$

$$\bar{f} = \frac{1}{T}\int_0^T f(t)\,dt = \sum_n \frac{2C_n}{\omega_n T}\sin\left(\frac{\omega_n T}{2}\right)\cos\left[\frac{\omega_n T}{2} + \phi_n\right]$$

$$\left(\bar{f}\right)^2 = \sum_n \frac{4C_n^2}{(\omega_n T)^2}\sin^2\left(\frac{\omega_n T}{2}\right)\cos^2\left(\frac{\omega_n T}{2} + \phi_n\right)$$
$$+ \sum_i \sum_{\substack{j \\ i \neq j}} \frac{4C_i C_j}{(\omega_i \omega_j)T^2}\sin\left(\frac{\omega_i T}{2}\right)\sin\left(\frac{\omega_j T}{2}\right)\cos\left(\frac{\omega_i T}{2} + \phi_i\right)\cos\left(\frac{\omega_j T}{2} + \phi_j\right)$$

$$\overline{f(t)f(t+\tau)} = \frac{1}{T}\int_0^T \sum_i \sum_j C_i C_j \cos(\omega_i t + \phi_i)\cos(\omega_j t + \phi_j)\,dt$$

$$\rho(\tau) = \overline{f(t)f(t+\tau)} - \left(\bar{f}\right)^2 = S_1 + S_2$$

$$S_1 = \sum_n \left[\frac{C_n^2}{2T}\int_0^T \left\{\cos[2\omega_n t + \omega_n\tau + 2\phi_n] + \cos\omega_n\tau\right\}dt - \frac{4C_n^2}{(\omega_n T)^2}\sin^2\left(\frac{\omega_n T}{2}\right)\cos^2\left(\frac{\omega_n T}{2} + \phi_n\right)\right]$$

$$S_1 = \sum_n \left[\frac{C_n^2}{2}\left\{\cos\omega_n\tau + \frac{\sin\omega_n T}{\omega_n T}\cos\left(\omega_n T + \omega_n\tau + \phi_n\right)\right\} - C_n^2 \frac{\sin^2\left(\frac{\omega_n T}{2}\right)}{\left(\frac{\omega_n T}{2}\right)^2}\cos^2\left(\frac{\omega_n T}{2} + \phi_n\right)\right]$$

$$S_2 = \sum_i \sum_{\substack{j \\ i \neq j}} \left[C_i C_j \left\{\frac{1}{T}\int_0^T \cos(\omega_i t + \phi_i)\cos(\omega_j t + \phi_j)\,dt - \frac{\sin\left(\frac{\omega_i T}{2}\right)\sin\left(\frac{\omega_j T}{2}\right)\cos\left(\frac{\omega_i T}{2} + \phi_i\right)\cos\left(\frac{\omega_j T}{2} + \phi_j\right)}{(\omega_i \omega_j)T^2}\right\}\right]$$

If we ask for the expected value of the correlation function and recognizing that in the equations the values of ϕ_i and ϕ_j are equally probable

$$\mathcal{E}(s_i) = \text{expected. value of } s_i = 0$$

$$\mathcal{E}(s_1) = \sum_n \frac{C_n^2}{2} \left\{ \cos \omega_0 \tilde{\tau} + \left\langle \frac{\sin \omega_n \tilde{\tau}}{\omega_n \tilde{\tau}} \cos(\omega_n \tilde{\tau} + \omega_0 \tilde{\tau} + \phi_n) \right\rangle \right.$$

$$\left. - \frac{\sin^2\left(\frac{\omega_n \tilde{\tau}}{2}\right)}{\left(\frac{\omega_n \tilde{\tau}}{2}\right)^2} \left[1 + \left\langle \cos(\omega_n \tilde{\tau} + 2\phi_n) \right\rangle \right] \right\}$$

$$\rho(\tilde{\tau}) = \sum_n \frac{C_n^2}{2} \left[\cos \omega_n \tilde{\tau} - \frac{\sin^2\left(\frac{\omega_n \tilde{\tau}}{2}\right)}{\left(\frac{\omega_n \tilde{\tau}}{2}\right)^2} \right]$$

$$\rho(0) \equiv \text{variance} = \sum_n \frac{C_n^2}{2} \left[1 - \frac{\sin^2\left(\frac{\omega_n \tilde{\tau}}{2}\right)}{\left(\frac{\omega_n \tilde{\tau}}{2}\right)^2} \right]$$

The variance is seen to be composed of the power in each frequency band which would exist if we had an infinite record length $\sum_n \frac{C_n^2}{2}$, but with each power density weighted by a filter function

$$g(\omega) = 1 - \frac{\sin^2\left(\frac{\omega_n \tilde{\tau}}{2}\right)}{\left(\frac{\omega_n \tilde{\tau}}{2}\right)^2}$$

For high frequencies, $\dfrac{\sin^2\left(\dfrac{\omega_h T}{2}\right)}{\left(\dfrac{\omega_h T}{2}\right)^2}$ is very small and the

high frequency spectral densities contribute their full weight to the

total variance. Computing the variance from a limited time average is

equivalent to passing the data through a high pass filter whose 3 db

cutoff occurs when

$$\frac{\sin \pi f_c T}{\pi f_c T} = 0.707$$

$$\pi f_c T = 1.396$$

$$f_c = \frac{0.44}{T} \sim \frac{1}{2T}$$

For frequencies below and up to the cutoff frequency

$$1 - \frac{\sin^2(x)}{x^2} = 1 - \left[1 - \frac{x^2}{3!} \cdots\right] \approx \frac{x^2}{3!}$$

so that the filter function behaves as f^2.

A-5

Appendix B

Radio Star Fadeouts and Radio Propagation

Interferometer records of intense radio sources have sometimes shown the loss of the interference patterns for periods of time ranging from a few minutes to several hours. This phenomenon, now called a radio star "fadeout," was first reported by Huntley (1953) and later by Koster (1956, 1958 and 1963) and was thought to be characteristic primarily of the equatorial ionosphere. More recently, similar radio star "fadeouts" have been reported by investigators viewing radio sources through the ionosphere in high northern magnetic latitudes (Little (1959), Benson (1960), Flood (1962), Moorcroft (1963), Flood (1963)). Radio star "fadeouts" have also been observed in Hawaii (to be discussed in this paper), and severe amplitude scintillations were also observed by a 400 Mcs pencil beam radiometer located in Trinidad, B.W.I.

In this discussion we review the results reported in Flood (1963), and present new results obtained from:

1. A further analysis of the data collected during 1960 - 1961

2. An analysis of radio star fadeouts observed in Hawaii

3. A period of intense scintillation of the radio sources in Cygnus and Cassiopeia as measured by a 400 Mcs radiometer in Trinidad, B.W.I.

Review of Previous Results

Phase switched interferometers operating at 52 and 147 Mcs using baselines of 300, 600 and 900 feet East-West and 1000 and 2000 feet North-South were employed to observe the radio source in Cassiopeia. At the latitude of Buffalo, New York (43°), the radio source is circumpolar and during the period September 1960 to September 1961, 24-hour recordings of the interference pattern were obtained at 52 Mcs. The 147 Mcs equipment was initially directed so that Cass A was monitored around the hours of lower culmination. After April 1961, the antennas were modified so that 24-hour recordings were obtained at 147 Mcs as well.

In Flood (1963), the results of the East-West baselines were analyzed. Radio star fadeouts were shown to be fairly common occurrences. For reference purposes, Figure B-1 is an example of the fringe pattern at 52 Mcs, taken during a "quiet" upper culmination period. An example of a radio star fadeout is given in Figure B-2. The fadeout is indicated by an arrow in the figure. Notice that the reduction in amplitude of the interference pattern is a function of the antenna baseline - the reduction in amplitude increases with increasing baseline distance. Absorption therefore cannot be a prime factor in producing a fade. Figure B-3 is a plot of the number of occurrences of fadeouts as a function of local time. Star fadeouts, while occurring uniformly thru all hours of local time, do show a distinct tendency to maximize in the evening hours.

Figure B-4 is a plot of the occurrence of radio star fadeouts as a function of local time for twelve successive months. The average time of lower culmination for each month is indicated. It is clear that while star fadeouts are most common around the time of lower culmination (which advances two hours in local time for each month), there is a secondary process clearly visible during the autumnal equinoctial periods. To better illustrate this point, Figure B-5 is a plot of the number of radio star fadeouts as a function of local time during the months of April and October. During April, when the time of lower culmination occurs during the early evening hours (2200 EST), the curve of occurrence of star fades is single-humped and centered around the time of lower culmination. The October data on the other hand show two clearly defined periods of fadeouts, centered around the time of lower culmination (1000 EST) and the early evening hour (2300 hours).

Figures B-5 & B-6 are interpreted as indicating the existence of two independent processes producing the radio star fade. The first is a zenith angle dependence such that star fades are far more common during the hours of lower culmination when the path lengths through a scintillation causing ionosphere are longest. The second process appears to be a phenomenon centered in local time in the early evening hours. Since the time of lower culmination progresses steadily through all hours of local time in the course of a year, the two processes converge to give a single temporal peak in the early evening hours in April and diverge to produce
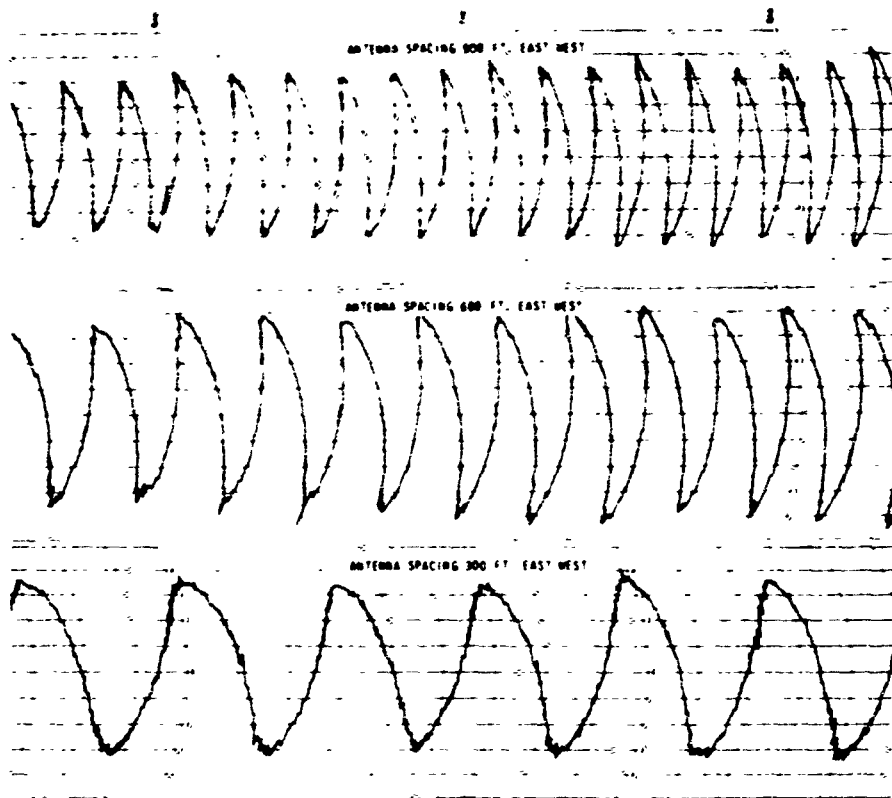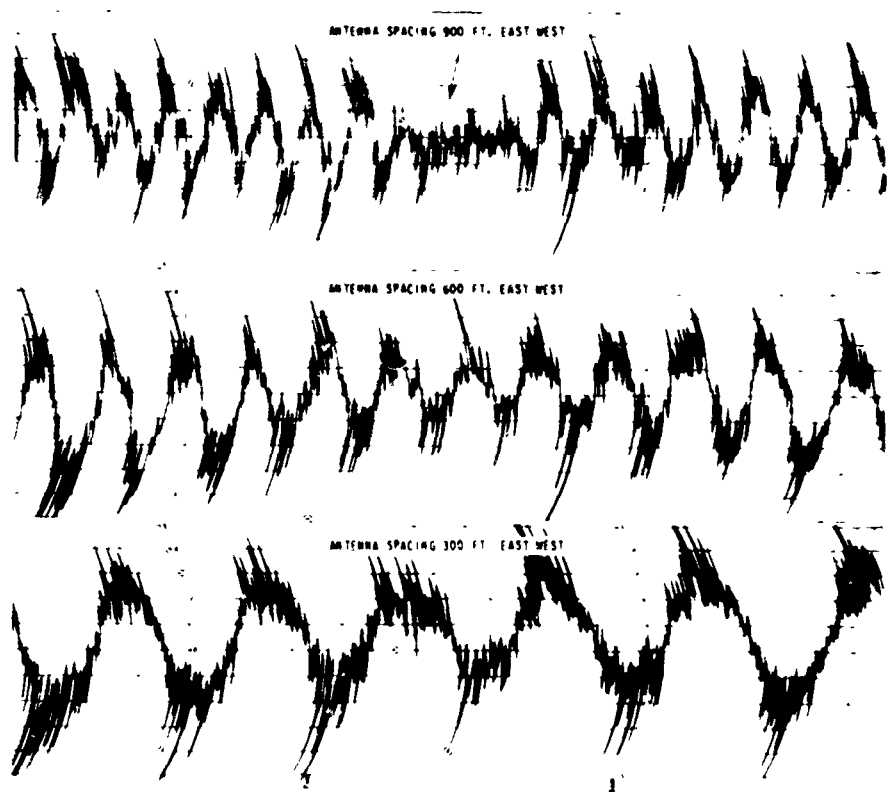
Figure B-1 QUIET DAY FRINGE PATTERN

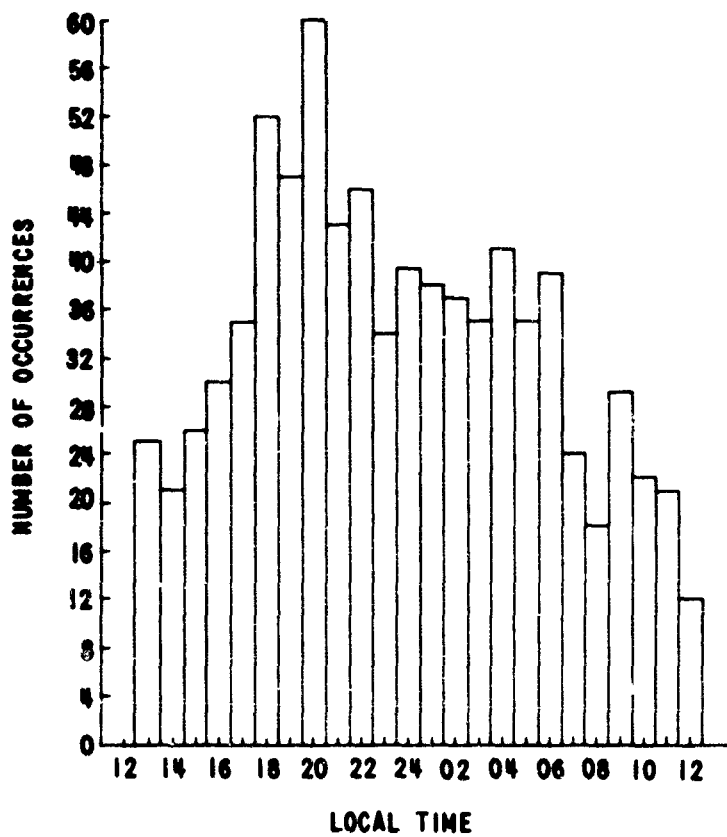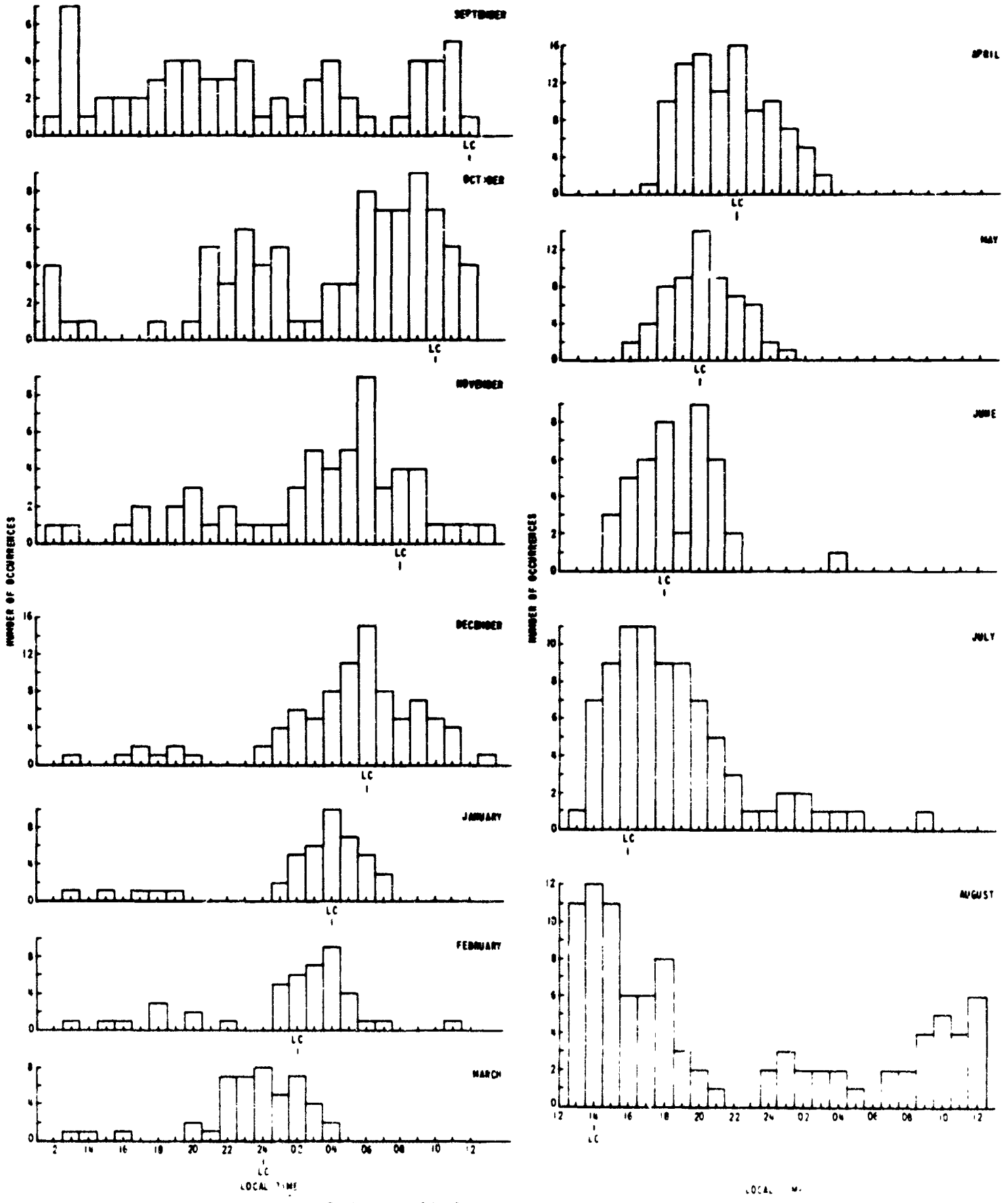FIGURE B-2 INTERFEROMETER FRINGE PATTERN INDICATING A RADIO STAR FADE

Figure B-3 OCCURRENCE OF RADIO STAR FADES OBSERVED ON 900 FOOT EAST-WEST
BASELINE AT 52 MCS SEPTEMBER 20, 1960 TO SEPTEMBER 20, 1962

B-4

Figure B-4 MONTHLY VARIATION OF OCCURRENCE OF STAR FADES
AS A FUNCTION OF LOCAL TIME

B-5

OCTOBER 1960

APRIL 1961
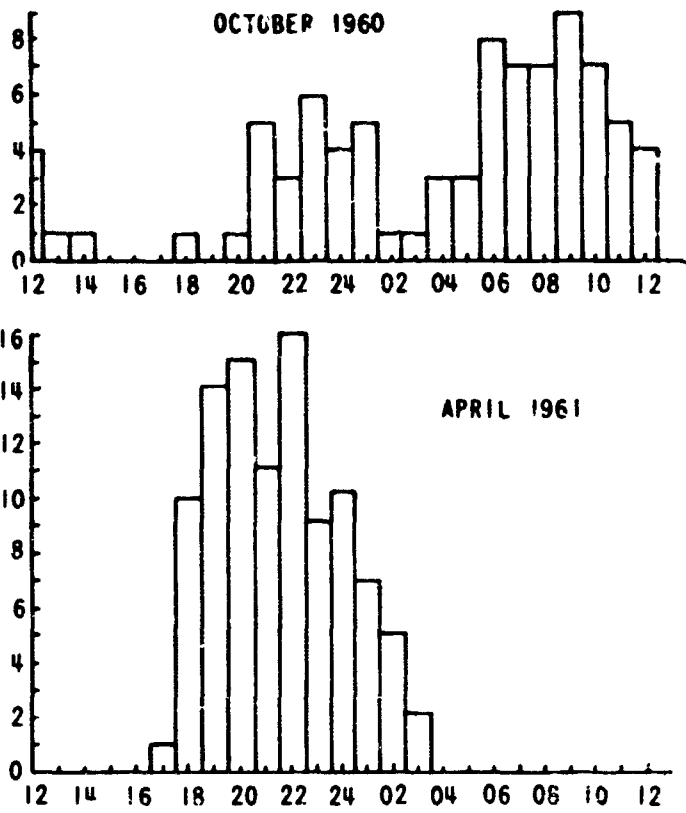
Figure B-5 DIURNAL OCCURRENCE RADIO STAR FADES IN OCTOBER AND APRIL

NUMBER OF HOURS

12 11 10 9 8 7 6 5 4 3 2 1 LC 1 2 3 4 5 6 7 8 9 10 11
HOURS BEFORE   LOWER CULMINATION   HOURS AFTER
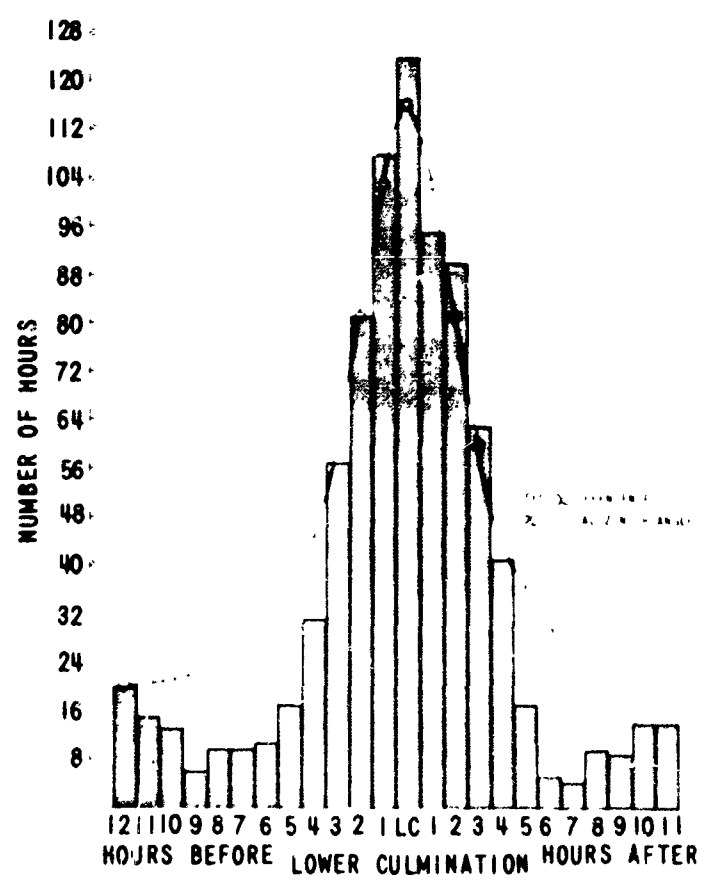
Figure B-6 NUMBER OF HOURS HAVING RADIO STAR FADEOUTS AS A FUNCTION OF STAR
POSITION, DATA TAKEN SEPTEMBER 20, 1960 TO SEPTEMBER 30, 1961

B-6

the bimodal curve of October. It is also clear that the majority of the fadeouts are produced by the first mechanism -- associated with the longest paths thru the scintillation producing region. This fact is well illustrated by Figure B-6 which is a plot of the number of star fadeouts as a function of local sidereal time. The data are quite well fitted by a secant dependence of the zenith angle.

Correlation with Other Geophysical Data

Attempts have been made to correlate the occurrence of radio star fades with other geophysical parameters. Before discussing these results it is well to keep in mind the fact that the F-region penetration point for the path Buffalo to Cassiopeia at lower culmination is at latitude 52.5°N (1000 km north of Buffalo) where the magnetic dip is 80°. The E-region penetration point at lower culmination is at latitude 47°N (450 km north of Buffalo) where the magnetic dip angle is approximately 76°. Magnetic K indices recorded at Agincourt, Ontario (approximately 100 km north of Buffalo) provide the records of magnetic activity closest to the E and F region penetration points. The ionosonde closest to the ionospheric penetration point is located in Ottawa, Ontario (45.4° N, 75.9°W), approximately 400 kilometers northeast of Buffalo, New York. Auroral backscatter radars, at 49.7, 143.5 and 226 Mcs are operated from Buffalo under a program of auroral research. The most common range of auroral echoes at Buffalo lies between 500 and 800 km north. In general, therefore, there are no geophysical data taken precisely at the ionospheric penetration points for the star at lower culmination, when radio star fadeouts are most probable.

In view of the great distance between Agincourt and the E and F region ionospheric penetration points, we attempted to correlate the occurrence of radio star fadeouts for those months when upper culmination (for which the penetration points are closest to Buffalo) occurred during the period 1800 - 2400 hours. To do this the data from the months of September, October, November and December 1960 were used. During these months, the times of lower culmination differ sufficiently from the evening maxima times so as to be resolvable -- the monthly diurnal variation curves are more or less "two-humped."

B-7

It is tempting to speculate that this secondary evening maximum is associated with auroral activity along the propagation path. If we can establish a relationship between K index at Agincourt and the presence of backscattered auroral echoes observed at Buffalo, we may be able to use the magnetic data as an index of auroral activity. To this end, film records of auroral backscattered echoes at 49.7 Mcs were examined for their correlation with Agincourt K figure. The results are plotted in Figure B-7 where, as can be seen, the probability of observing an aurora at 50 Mcs increases rapidly for K values greater than 3. There is only one data point each for K = 6 and K = 7 but the trend of the curve is clear. It is also interesting to note that backscattered auroral echoes have been observed, although infrequently, when the Agincourt K index was 0 and 1. For the purposes of this paper we shall assume that an Agincourt K Index of four or greater implies auroral conditions.

The data for the months September, October, November and December 1960 were searched for fadeout periods during the hours 1800 to 2400. The results are tabulated in Table B-I.

Table B-I

Fadeouts during 1800 - 2400 Local Time

Month	Average Agincourt K Index Non-fadeout Periods	Average K Index Fadeout Period	Total Number of Events	Number of Events with K ≥ 4
Sept.	1.97	3.1	18	6
Oct.	3.0	3.0	15	6
Nov.	3.0	6.5	7	6
Dec.	2.5	3.0	4	2

Average K for entire period (1800 - 2400 local time) = 2.6
Average K for fadeout periods   3.6
Twenty out of 44 events have K ≥ 4.

The average value of the K index is noticeably higher during the fadeout periods than it is during non-fadeout times. Approximately one half the fadeout periods may be associated with a strong probability of aurora (K ≥ 4).
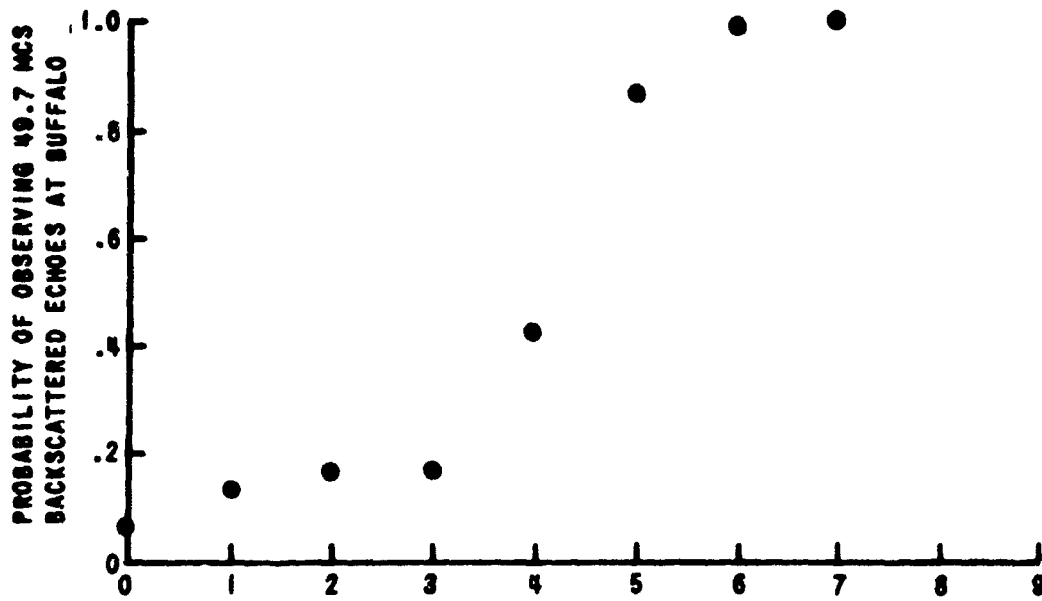
Figure B-7 PROBABILITY OF OBSERVING 50 MCS AURAL ECHOES FROM
BUFFALO, N.Y. AS A FUNCTION OF AGINCOURT K INDEX

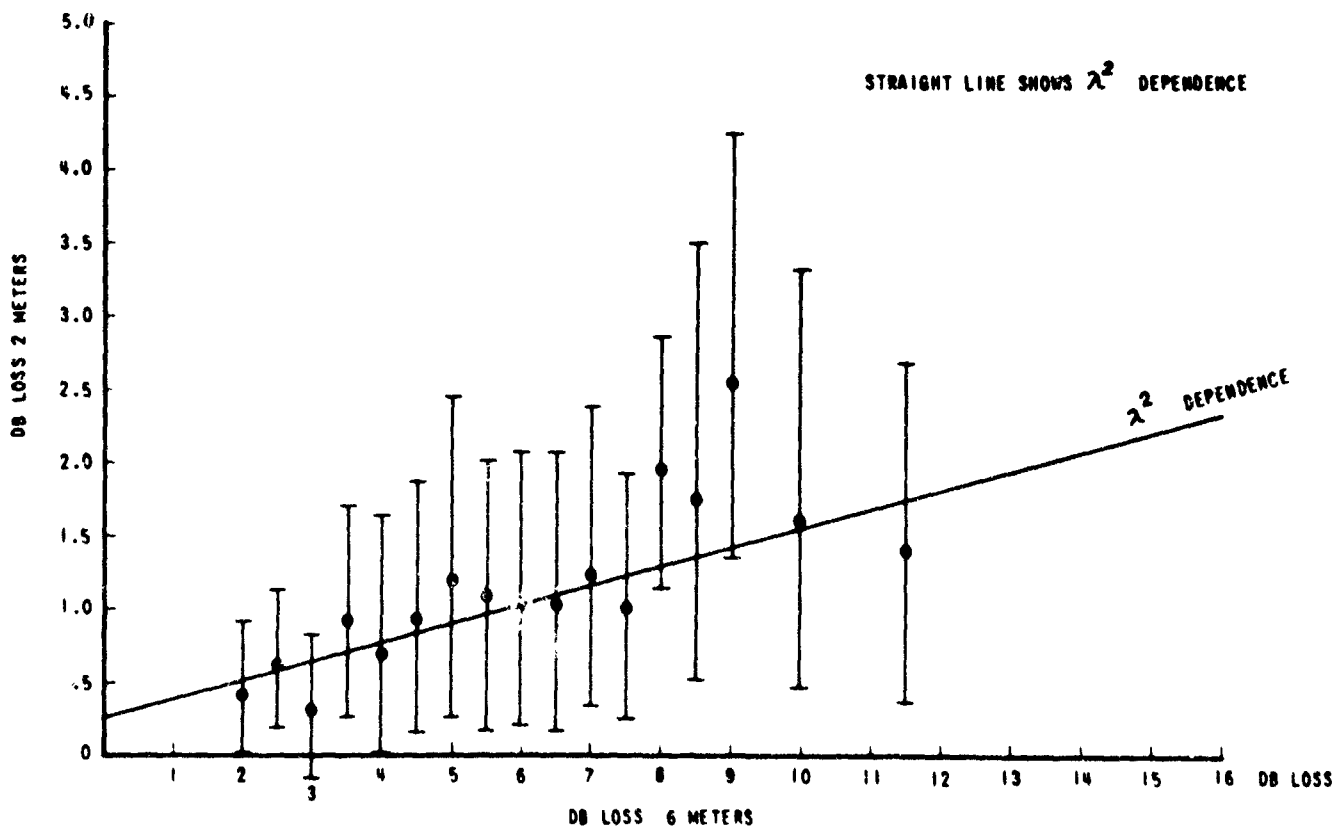Figure B-8 DB LOSS AT 6 METERS PLOTTED AGAINST DB LOSS AT 2 METERS

B-9

A substantial number of auroral backscatter film records for the month of August 1961 were available for comparison with star fadeout periods between 1800 - 2400 hours. Table B-II lists a comparison of the auroral and fadeout data.

Table B-II

A Comparison of Aurora Backscatter and Star Fadeouts

Date	Time	Fadeout	Max K Figure	Auroral Echoes
Aug. 1	1844	Yes	3	Yes
Aug. 2	1824	Yes	3	Yes
Aug. 3	1800-1900	Yes	4	Yes
Aug. 3	1900-2000	Yes	5	Yes
Aug. 4	1800-2040	No	1	No
Aug. 5	1814	Yes	3	No
Aug. 7	1800-2246	No	2	Yes
Aug. 8	1800-2300	No	3	No
Aug. 9	1800-2117	No	2	No
Aug. 10	1800-2030	No	4	Yes (2000-2015)
Aug. 11	1800-2323	Yes (1830-1930)	4	Yes (1814-1825)
Aug. 21	1800-2214	No	1	No
Aug. 22	1800-2215	No	1	No
Aug. 24	1800-2318	No	3	No
Aug. 25	1800-2400	No	4	No
Aug. 29	1830	Yes	5	Yes
Aug. 30	1800-1900	Yes	4	Yes
Aug. 30	1900-2000	Yes	5	Yes
Aug. 30	2000-2100	Yes	5	Yes (Weak)
Aug. 30	2100-2200	No	5	Yes
Aug. 30	2300-2400	Yes	4	Yes

We conclude therefore that there is a strong correlation between the presence of aurora and the occurrence of a star fadeout. We further hypothesize that the early evening maximum of star fades, present in the diurnal variation curves of the months around the autumnal equinox, is correlated with the presence of aurora. These conclusions are in substantial agreement with those of Moorcroft (1963) and Benson (1960).

Cause of Radio Star Fadeout

It can be shown (Moorcroft 1963, Flood 1963) that the fringe amplitude output of a phase-switched (or phase-swept interferometer of the type described by Lawrence and Jespersen 1961) is given by

$$E_o = \overline{A_s^2}\left\{1 - \frac{\overline{\Delta A^2}}{A_s^2}\left[1 - \rho_A(r)\right]\right\} exp\left\{-\overline{\phi_o^2}\left[1 - \rho_\phi(r)\right]\right\} \qquad \text{B-(1)}$$

where $\overline{A_s^2}$ is the power emitted from the radio source

$\overline{\Delta A^2}$ is the mean squared amplitude fluctuation of the star signal

$\rho_A(r)$ is the spatial correlation function of the amplitude fluctuations

$\overline{\phi_o^2}$ is the mean squared phase fluctuation introduced by a random ionosphere

$\rho_\phi(r)$ is the spatial correlation function of the phase fluctuations

In the derivation of the above formula, the phase fluctuations have been assumed to be normally distributed with zero mean value (a reasonable assumption) and the amplitude and phase fluctuations have been assumed to be independent (a not so reasonable assumption).

Now the most intense amplitude scintillation phenomena, usually associated with large phase fluctuations, are such that the star signal amplitudes at the two antennas are Rayleigh-distributed and totally uncorrelated. Under these circumstances

$$\frac{\overline{\Delta A^2}}{A_s^2} = .215 \text{ and } \rho_A(r) = 0$$

so that

$$E_o = .79\,\overline{A_s^2}\,exp\left\{-\overline{\phi_o^2}\left[1 - \rho_\phi(r)\right]\right\} \cdots\cdots \qquad \text{B-(2)}$$

The maximum reduction in interference fringe visibility due to amplitude scintillations alone is 21 percent or roughly 1 db. Since the fadeouts which form the subject of this report show reductions in fringe amplitude of 2 db to greater than 18 db, it is clear that fadeouts are primarily caused by phase fluctuations. The relationship between the depth of the star fade and the mean squared phase fluctuations observed on a baseline of length r is approximately

$$\text{db decrease} = 4.3 \, \overline{\phi_r^2}(r) = 4.3 \, \overline{\phi_\bullet^2}\left[1 - \rho_\phi(r)\right] \qquad \text{B-(3)}$$

Further evidence that phase fluctuations are the prime cause of fadeouts can be adduced from Figure B-8 where simultaneous observations at 52 and 147 Mcs of star fades between 2 and 10 db (the limit of good accuracy is reading the data) are plotted. The mean values of the data are seen to be fitted with a λ^2 law which is just what one would expect for phase fluctuations due to electron density fluctuations in the ionosphere (Booker 1958).

Anisotropy of the Irregularities Producing the Phase Fluctuations

The analysis so far has dealt with data from the East-West baselines. The simultaneous operation of North-South and East-West baseline offers the opportunity to examine the anisotropy of the correlation function.

By restricting the analysis to those fadeouts which occur within one hour of the meridian passage of the radio source, one can compare the db loss on the North-South baseline with the db loss on the East-West baseline. In making these comparisons, the effective North-South baseline length is the physical length multiplied by the sine of the elevation angle (10° and 74° respectively, for lower and upper culmination respectively).

Not all fadeouts occurring during meridian passage are included in the analysis which follows. These cases of total star fadeout obviously could not be analyzed. Decisions regarding the relative strengths of the fadeouts on the two baselines were possible in 124 cases. Of these, 85 cases showed

B-12

the fadeout to be stronger on the East-West baseline and 39 cases indicated that the fadeout was equal or stronger on the North-South baseline. Almost all of the 124 cases analyzed occurred during the time of lower culmination when the line of sight from the interferometers to the radio source is nearly perpendicular to the earth's magnetic field. The fact that 39 events imply a shorter correlation distance along the direction of the magnetic field is most surprising since all reports of star scintillation experiments indicate that the correlation distance (of the electron density fluctuations causing the star scintillations) measured along the magnetic field is something like five times the correlation distance measured transverse to the magnetic field (Spencer 1955).

A partial explanation of the apparent discrepancy between our results and previous reports of the anisotropy of the correlation function may lie in the fact that the normal scintillation measurements apply to F-region irregularities. The auroral dependence previously indicated might imply that some of the fadeouts here reported may actually be caused by the auroral E region where the anisotropy of the large scale irregularities is not well developed.

Correlation of this anomalous anisotropy of the phase fluctuations with K figures from Agincourt has been attempted. The average K figure for those fadeouts which showed a greater signal loss on the East-West baseline was 2.39, while for those fadeouts which showed a greater loss on the North-South baselines the average K figure was 2.47. It would appear that magnetic activity has no strong correlation with the anisotropy of the phase fluctuations. It should be noted however that only six instances of a fadeout at upper culmination were considered in this analysis (all of which were stronger on the East-West baseline) so that the other 95% of the data corresponds to lower culmination when the E and F-region ionospheric penetration points are 350 and 900 kilometers north of Agincourt, the source of the K figure determinations.

Correlation with Spread-F Activity

The F plots published by the Defense Research Communications Establishment (Canada) for the ionosonde in Ottawa, Ontario have been examined for the diurnal variation of Spread-F at Ottawa during the period September 1, 1960 through August 31, 1961. All half hourly readings indicating a spread were tabulated and the results are plotted in Figure B-9. As expected, Spread-F is a nighttime phenomenon, occurring 88 percent of the nights at 0300 local time. The location of the maximum of Spread-F occurs approximately six hours after the evening maximum of star fades. The fact that the maximum in the diurnal variation of star scintillations precedes the Spread-F maximum has been reported by numerous investigators and the time lag between the two phenomena is sometimes ascribed to the shielding of higher altitude irregularities which presumably cause star scintillations by the lower ionosphere.

The fact that two processes indicate a nighttime maximum may introduce a correlation into processes which are otherwise independent. With only one year's data on hand we do not have a sufficient number of cases to look for correlation in the fluctuations of each process from their own average diurnal variation. It is interesting to note, however, that the 300 kilometer penetration point at the time of lower culmination is above James Bay and just south of the permanent maximum of Spread-F reported by Penndorf (1962) for the Foxe Basin.

Size of Irregularities

The size of the irregularities producing star fades can be deduced from experimental data and Equation B(3). It should be noted that in order to plot the phase correlation function, the magnitude of $\overline{\phi_0^2}$, the mean squared phase fluctuations for two totally uncorrelated paths. must be known. The experimental data on hand are limited to a maximum signal-to-noise ratio of approximately 20 db and since a loss of 20 db on a 900 foot East-West baselines is not uncommon, the estimates which follow are only order of magnitude. It would appear from our analysis that a maximum scale size
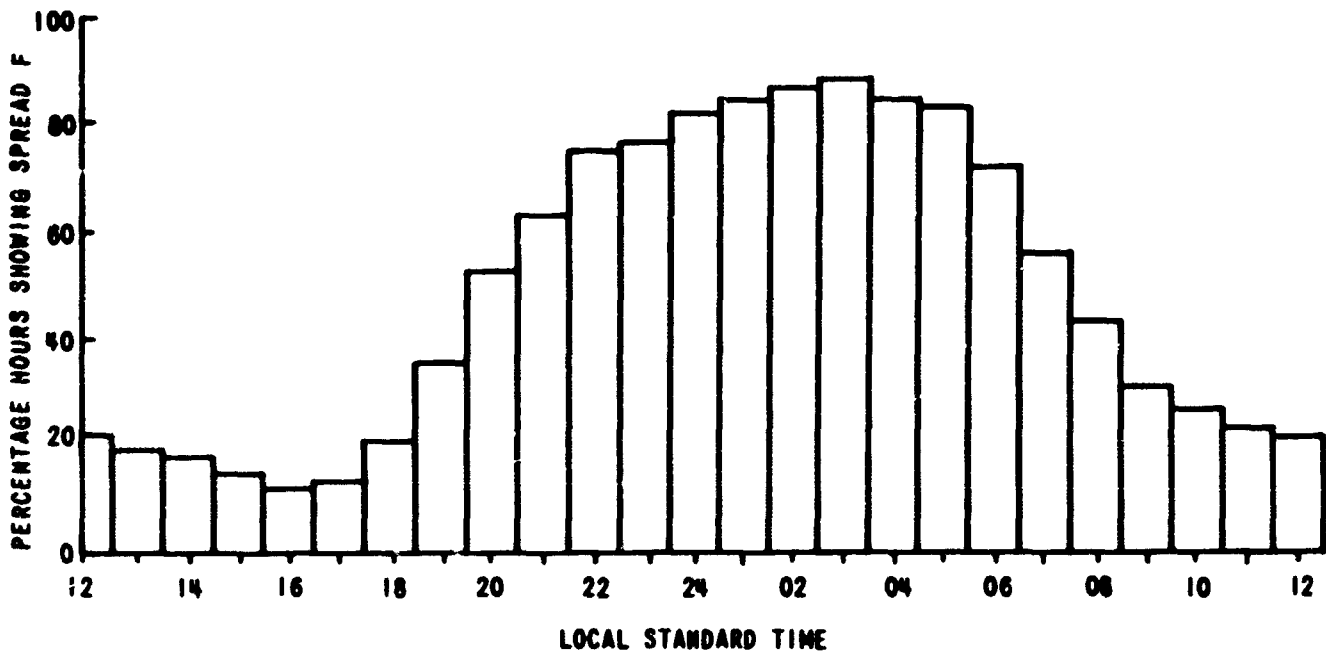
Figure B-9 PER CENT OF HOURS SHOWING SPREAD F AT OTTAWA, ONTARIO
SEPTEMBER 1, 1960 - AUGUST 31, 1961

of 200-300 meters is not inconsistent with data taken during intense star
fades. This figure is deduced by noting that the star fade loss increases
rapidly between the 600 and 900 foot spacings implying that there is a
rapid decrease in the correlation function evaluated at spacings of 600 and
900 feet. It is recognized that an estimate of this sort probably tends to
underestimate the size of the irregularities. We have not attempted to
estimate the correlation distance in the North-South direction since we
have only two baselines and therefore two data points. In addition, since
the vast majority of the fadeouts occur near lower culmination, our effective
baseline dimensions in the North-South direction are only 190 and 380 feet.

Radio Star Fadeouts in Hawaii

Interferometer recordings of the radio sources in Cygnus and Cassiopeia
were obtained on the island of Maui (latitude 21°N) during the period May 15,
1962 through November 5, 1962. Baselines of 150, 300 and 600 feet East-West
were used at 52, 147 and 253 Mcs while 300 and 600 foot North-South baselines
were used on the two lower frequencies. During this period, one definite
radio star fadeout was recorded, beginning at 1020 hours GMT on July 19, 1962
and lasting until roughly 1800 hours GMT.

The field site was almost unsuitable for scintillation work. Quasi-
continuous power line arcing created a very serious interference problem
so that the exact magnitude of the fadeout could not be measured. However,
the significant features of the records are as follows:

1. The intensity of the signal loss was greater, the lower the
   operating frequency and the greater the baseline line lengths;

2. The duration of the radio star fadeout increased with increasing
   baseline length and decreasing operating frequency;

3. The duration and intensity of fadeout on the North-South baselines
   was smaller than the duration and intensity on the East-West
   baselines,

4. The fadeout was complete - that is, the signal dropped to the
   noise level for at least ten minutes on the 253 Mcs 600 foot
   East-West baseline.

During this time period, H. F. signals from Midway Island were monitored. The quality of the signals was characterized by an unusual flutter fade. The available data suggest that this was an instance of the equatorial F-region flutter fade reported by Koster (1963). The fact that there was only one instance of this fairly common equatorial phenomenon may well be explained by the geomagnetic latitude of Maui (21°N). It is also worth noting that the data are consistent with field aligned irregularities having a high axial ratio.

400 Mcs Scintillation in Trinidad

A 400 Mcs radiometer employing an eighty-five foot diameter paraboloid monitored the radio sources in Cygnus, Cassiopeia and Centaurus during the night of July 15, 1960. (These data were taken by the General Electric Company and were made available by the Rome Air Development Center.) Prior to 2107 hour EST, the signals from Cygnus were normal, indicating a 0.1 db rms fluctuation. An abrupt start of scintillation activity was noticed at 2107 hours; there is an uncertainty of the exact time of the start of scintillation activity due to a minor equipment malfunction. Figure B-10 example of the scintillation of the source in Cygnus. The zero signal level is at an ordinate value of 1.4 and the mean signal level during undisturbed periods has an ordinate value of 5. (The ordinate scale is linear in power.) Figure B-11 taken some time earlier, is a drift plot of the Cygnus source through the radiometer beam.

During the course of these observations, the antenna was also turned to observe the radio source in Centaurus in the South-West and Cassiopeia in the North-East. The Centaurus signals were normal -- no pronounced scintillation activity was discernible. The Cassiopeia signal on the other hand fluctuated strongly.

Since the recordings are linear in power, scaling of the records for the fluctuation of the power ΔP from the mean value of the power, P, was straightforward. Table B-III lists some of the values of the root mean square of $\Delta P / \bar{P}$ which were measured.
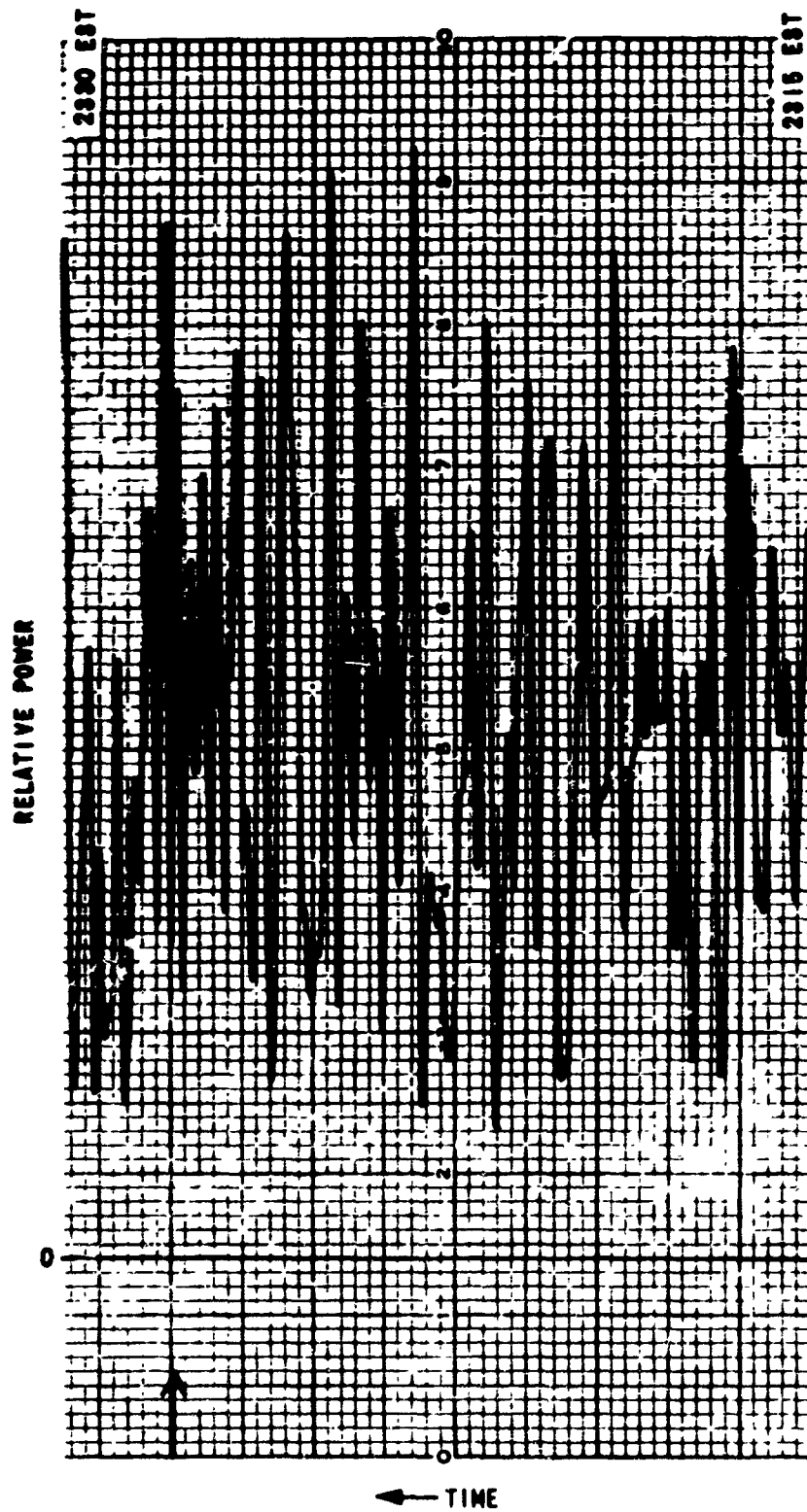
Figure B-10 SCINTILLATION OF RADIO SOURCE IN CYGNUS, OBSERVED AT 400 MCS
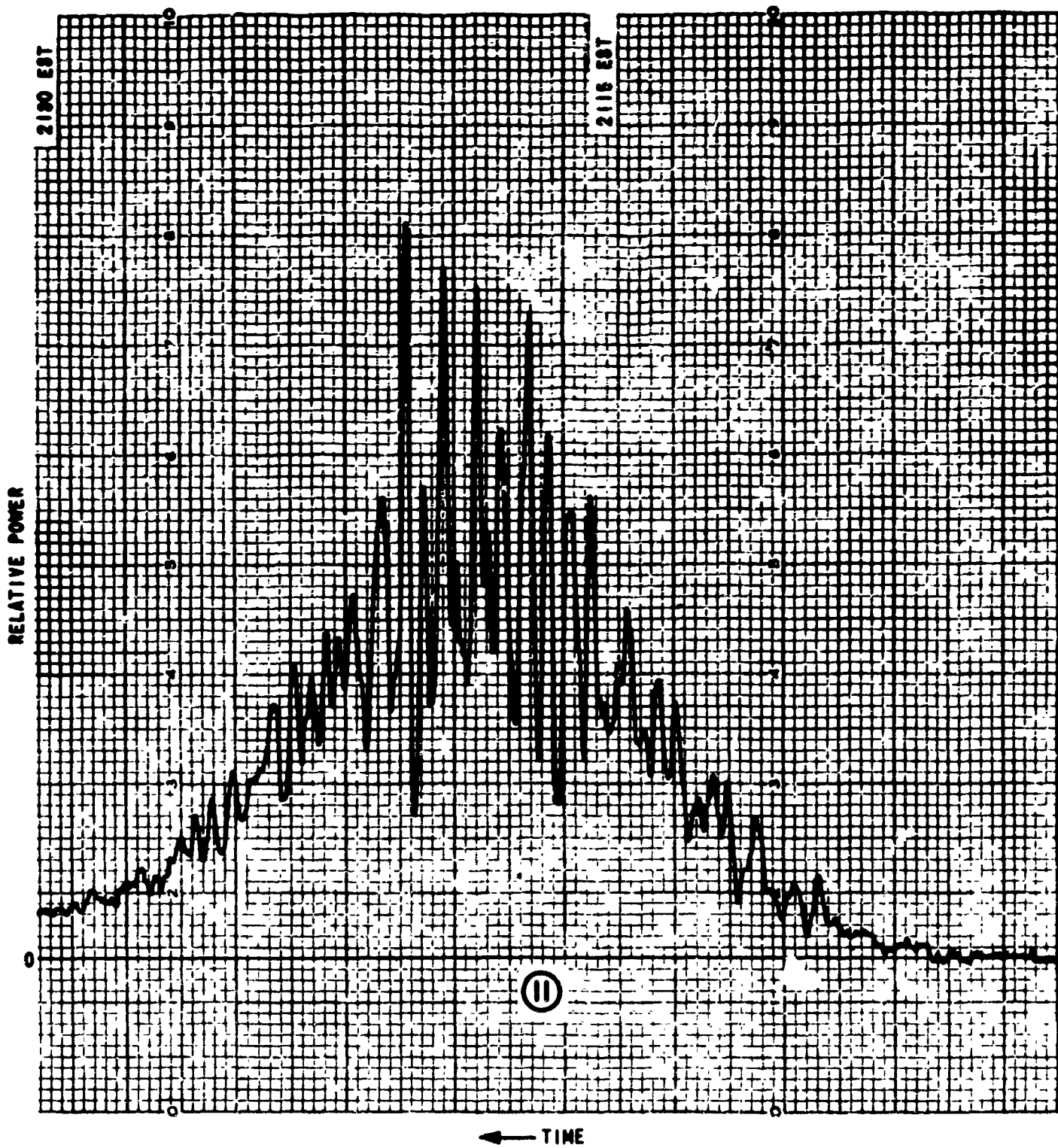FROM TRINIDAD B.W.I. - JULY 15, 1960

Figure 3-11 DRIFT PATTERN OF RADIO SOURCE IN CYGNUS
JULY 15, 1960 — 400 MCS — TRINIDAD

B-19

Table B-III
RMS Fluctuation in Power   15 July 1960

Time	Radio Source	$(\Delta P/P)_{rms}$
2204-2213	Cassiopeia	0.24
2239-2249	Cygnus	0.16
2315-2330	Cygnus	0.39
2400-0010	Cygnus	0.52

The highest percentage fluctuation measured was 0.52. It should be noted the percentage fluctuation of power for a Rayleigh distribution of amplitudes, which would imply the absence of an undiffracted specular wave, is 100%. Clearly, then, under the circumstances of July 15, 1960, multiple scattering was not complete and an undiffracted component of the signal was present.

These Trinidad data are decidedly different from the usual data obtained at this site and are not meant to be "typical." The planetary K index for this particular period was at the 8+ level and we are not sure whether the data pertain to an aurorally disturbed E or F region. Nevertheless, the data are pertinent in that they; along with the Maui data, represent unusually high values of phase and amplitude scintillations measured at low latitudes. There is reason to believe that the Trinidad data may refer to auroral irregularities but the Maui data most probably refer to F-region irregularities.

The Effect of Sunspot Activity on Radio Star Fadeouts

In an attempt to estimate the effects of solar activity upon the occurrence of radio star fadeouts, the 52, 147, and 253 Mcs interferometers were operated from Buffalo, N. Y., during the period December 1, 1963 through May 31, 1964. The intensity and duration of radio star fadeouts is apparently much less now than during a comparable period in 1960-61. It would appear, therefore, that the number as well as strength of the radio star fadeouts is associated with solar activity.

Star Fadeouts and Resolution

To obtain a semimaximum value for $\overline{\phi_o^2}$, we have to examine the data carefully. There have been a large number of occasions when the 52 Mc/s interferometers showed a complete loss of star signal on all base lines. Since the maximum signal-to-noise ratio is of the order of 20 db, an 18- to 20-db star fade is analogous to complete equipment saturation. All we can say is that the loss exceeds 18 db and therefore that the mean squared phase fluctuations are in excess of 4.2 square radians at 52 Mc/s. However, on at least three occasions, a 147 Mc/s star fadeout of greater than 11 db has been recorded. This would imply an 88-db loss at 52 Mc/s on these occasions.

Radio star fadeout observations in the auroral zone have been made by Little (1959) who reported that a 7-db loss was measured at a frequency of 223 Mc/s on an interferometer baseline of 100 meters. Using the λ^2 law, we would predict a loss of 16 db at 147 Mc/s rather than the 11 db used in the preceding paragraph. Since the 11 db was not an absolute maximum and we would expect stronger auroral disturbances at the Alaskan location of Little, his observations are in accord with the basic auroral nature of the phenomenon as well as the validity of the λ^2 dependence. From Equation B-3

$$\overline{\phi^2}_{(r)} = (\frac{1}{4.3})\text{db less}$$

$$\overline{\phi_o^2} \approx 30 \text{ square radians } \textit{at 50 mcs} \qquad \text{B-(4)}$$

(using Little's data). The mean squared phase fluctuations at any other frequency will therefore be assumed to have a "maximum" (in view of the λ^2 dependence).

$$\phi_o^2 = \left(\frac{30}{36}\right) \lambda^2 \approx \lambda^2 \text{ square radians} \qquad \text{B-(5)}$$

As typical examples of the variance of the phase fluctuations, we would expect 36×10^{-4} and 9×10^{-4} square radian at frequencies of 5000 and 10,000 Mcs respectively. That these values will not be uncommon can be

Star Fadeouts and Resolution

To obtain a semimaximum value for $\overline{\phi_o^2}$, we have to examine the data carefully. There have been a large number of occasions when the 52 Mc/s interferometers showed a complete loss of star signal on all base lines. Since the maximum signal-to-noise ratio is of the order of 20 db, an 18- to 20-db star fade is analogous to complete equipment saturation. All we can say is that the loss exceeds 18 db and therefore that the mean squared phase fluctuations are in excess of 4.2 square radians at 52 Mc/s. However, on at least three occasions, a 147 Mc/s star fadeout of greater than 11 db has been recorded. This would imply an 88-db loss at 52 Mc/s on these occasions.

Radio star fadeout observations in the auroral zone have been made by Little (1959) who reported that a 7-db loss was measured at a frequency of 223 Mc/s on an interferometer baseline of 100 meters. Using the λ^2 law, we would predict a loss of 16 db at 147 Mc/s rather than the 11 db used in the preceding paragraph. Since the 11 db was not an absolute maximum and we would expect stronger auroral disturbances at the Alaskan location of Little, his observations are in accord with the basic auroral nature of the phenomenon as well as the validity of the λ^2 dependence. From Equation B-3

$$\overline{\phi^2}_{(r)} = (\frac{1}{4.3})\text{db less}$$

$$\overline{\phi_o^2} \approx 30 \text{ square radians } at \text{ } 50 \text{ } mcs \qquad \text{B-(4)}$$

(using Little's data). The mean squared phase fluctuations at any other frequency will therefore be assumed to have a "maximum" (in view of the λ^2 dependence).

$$\phi_o^2 = \left(\frac{30}{36}\right) \lambda^2 \approx \lambda^2 \text{ square radians} \qquad \text{B-(5)}$$

As typical examples of the variance of the phase fluctuations, we would expect 36×10^{-4} and 9×10^{-4} square radian at frequencies of 5000 and 10,000 Mcs respectively. That these values will not be uncommon can be

ascertained from the fact that estimates of a "typical" strong fade at 147 Mc/s are approximately 7 db. This would reduce the above "maximum" values by a factor less than 2.

The above estimates of the variance of the phase fluctuations at the S and X bands are surprisingly large and indicate that for some long propagation paths which traverse the auroral ionosphere, the ionospheric contributions to the short term variance of the phase fluctuations are of the same order as the tropospheric contributions.

Effect of Ionospheric Phase Fluctuations on Angular Resolution

The lack of phase correlation at two points implies a loss of antenna gain and angular resolution. If we define the maximum antenna dimension D as that dimension which would result in a mean squared phase fluctuation of 1 radian squared, then estimates of the maximum resolving power (based on a Rayleigh criterion of λ/D) can be made from the experimental data.

Following Ratcliffe's (1956) usage, we will take $\overline{\phi_o^2}$ greater than one squ radian to imply multiple scatter, indicating that the intensity of the undiffracted wave is not much larger than the intensity of the waves arriving over a variety of angles. For the case $\overline{\phi_o^2}$ small compared to 1 radian squared, the scattered waves are small compared to the zero-order wave, and the angle of arrival is "perfectly" defined.

From B(5) we conclude that for frequencies in excess of 300 Mc/s the angular resolution will be determined by the size of the antenna aperture. At frequencies less than 300 Mc/s, the limits to angular resolution will be determined by the ionospheric phase path irregularities. The cone angle of arrival for frequencies less than 300 Mc/s is determined by λ/D. where D is as defined above.

If the phase fluctuations $\overline{\phi_o^2}$ are defined by

$$\overline{\phi_{(r)}^2} = \overline{\phi_o^2} \left[1 - \rho(r) \right] \qquad \text{B-(6)}$$

where $\rho(r)$ is the normalized autocorrelation function of the phase fluctuations, and we assume that

$$\rho(r) = exp\left\{-\frac{r^2}{L^2}\right\} \qquad \text{B-(7)}$$

where L is the "correlation distance," then combining B-(5), B-(6) and B-(7) we obtain

$$\overline{|\phi(r)|^2} \approx \frac{\lambda^2 r^2}{L^2} \qquad \text{B-(8)}$$

The maximum effective antenna dimension D will therefore be

$$D = \frac{L}{\lambda} = \frac{L}{\phi_0} \qquad \text{B-(9)}$$

Equation B-(9) is analogous to the result of Ratcliffe (1956) who points out that, in diffraction from an irregular screen, when the mean squared phase fluctuations $\overline{\phi_0^2}$ exceed 1 radian squared, the effective correlation distance measured on the ground is equal to the true correlation distance divided by ϕ_0 .

The cone angle of arrival θ is defined by

$$\theta = \frac{\lambda}{D} = \frac{\lambda^2}{L} \qquad \text{B-(10)}$$

It is clear that to predict the amount of beam broadening to be expected at frequencies less than 300 Mc/s, a knowledge of the correlation distance L is required. For ionospheric phase path fluctuations at least, L is generally greater than 100 meters, since the mean squared phase fluctuations generally increased at distances greater than 300 feet at 147 Mc/s. To put a pessimistic limit to the degree of resolution that can be achieved, we take L to be 100 meters and $\overline{\phi_0^2}$ to be equal to λ^2 square radians (equation B-(5)) Table B-IV lists the limitations to angular resolution as a function of frequency.

B-23

Table B-IV

Limitations to Angular Resolution as a Function of Frequency

Frequency, Mc/s

	50	150	300
θ In milliradians	360	40	10

Bandwidth Limitations as a Consequence of Phase Path Fluctuations

The observed relationship between radio star fadeouts and auroral back-scattering at closely allied frequencies suggests that, on occasion at least, the source of the fluctuations is in the auroral E region. Under these circumstances, the geometry in Figure B-12 is appropriate for estimating the multipath bandwidth limitations imposed by propagation through the auroral ionosphere. Consider the worst possible case: a source at an infinite distan e from the scattering screen. Radiation received on the ground over a cone angle θ arrives with a time delay (referred to the ray arriving in the line-of-sight direction) of τ

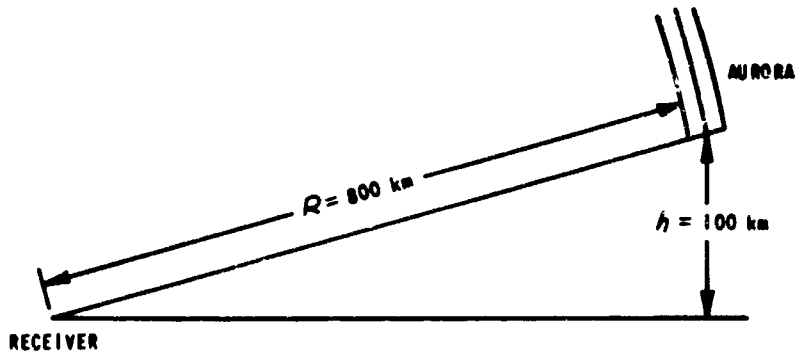$$\tau = \frac{R\theta^2}{8c} \qquad \text{B-(11)}$$

Equation B-(11) implies that a very narrow pulse would be broadened into a pulse length τ. Such pulse broadening would limit the range resolution of a pulse radar to an amount $\frac{c\tau}{2}$,

$$\frac{c\tau}{2} = \frac{c}{2}\left(\frac{R\theta^2}{8c}\right) = \frac{R\theta^2}{16}$$
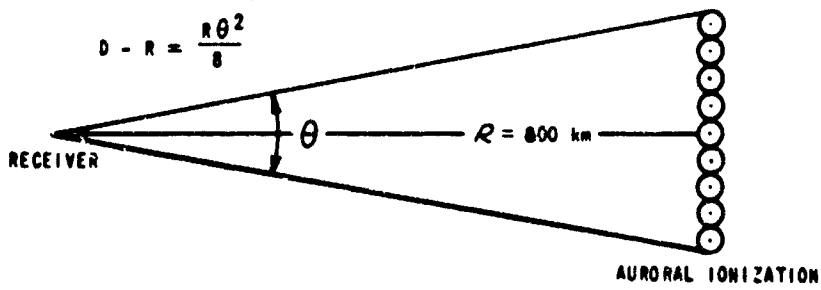
and from B-(10)

$$\frac{c\tau}{2} = \frac{R\lambda^4}{16L^2} \qquad \text{B-(12)}$$

ELEVATION VIEW OF AURORAL GEOMETRY

$$D^2 = R^2 \left(1 + \frac{\theta^2}{4}\right)$$

$$D - R = \frac{R\theta^2}{8}$$

PLAN VIEW OF AURORAL GEOMETRY

Figure B-12 AURORAL MULTIPATH GEOMETRY

Taking R to be of the order of 8×10^5 meters and L to be 100 meters (minimum), we obtain a pessimistic limitation to range resolution:

$$\frac{c\tau}{2} = 5\lambda^4 \qquad \text{B-(13)}$$

Range resolution of better than 1 foot (approximately 0.3 meter) can be achieved at all wavelengths less than 0.5 meter if multipath alone is the limiting factor in range resolution.

Acknowledgements

References

Benson, R. F.:   The Effect of Line of Sight Aurora on Radio Star Scintillations, J. Geophys. Res. 65, 1981, 1960.

Booker, H. G.:   The Use of Radio Stars to Study Irregular Refraction of Radio Waves in the Ionosphere, Proc. IRE, 46, 298, 1958.

Flood, W. A.:   Paper presented to URSI Commission III, Wash., D. C., May 1962.

Flood, W. A.:   A Study of Radio Star Fadeouts and Their Application to Radar Resolution, J. Geophys. Res. 68, 4129, 1963.

Huntley, H. E.:   Radio Astronomy in the Tropics, Nature 172, 108, 1953.

Koster, J. R.:   Radio Star Scintillations at an Equatorial Station, J. Atmos. & Terr. Phys. 12, 100, 1958.

Koster, J. R.:   Some Measurements of the Irregularities Giving Rise to Radio Scintillation at the Equator, J. Geophys. Res. 68, 2579, 1963.

Koster, J. R.:   Some Measurements of the Sunset Fading Effect,
    J. Geophys. Res. 68. 2571. 1963.

Lawrence, R. S., Jespersen, J. L , and Lamb. R. C.   Amplitude and
    Angular Scintillations of the Radio Source Cygnus A Observed at
    Boulder, Colorado,   J. Res. of NBS Section D, 65. 333, 1961.

Little, C. G.:   Final Report Radio Properties of the Auroral Ionosphere,
    Geophysical Institute. College Alaska,   February 1959,   Contract
    AF 30(635)-2887.

Moorcroft, D. R.:   Radio Star Fadeouts on Phase Switching Interferometer
    Records,   J. Geophys. Res. 68, 111, 1963.

Moorcroft, D. R., and Forsyth, P. A.:   On the Relation between Radio Star
    Scintillations and Auroral and Magnetic Activity,   J. Geophys. Res. 68,
    117, 1963.

Penndorf, R.:   Geographic Distribution of Spread F in the Arctic,   J. Geophys.
    Res. 67, 2279, 1962.

Penndorf, R.:   Diurnal and Seasonal Variation of Spread F in the Arctic,
    J. Geophys. Res. 67, 2289, 1962.

Ratcliffe, J. A.:   Some Aspects of Diffractive Theory and Their Application
    to the Ionosphere,   Rep. Prog. Phys. 19, 188, 1956.

Spencer, M.:   The Shape of Irregularities in the Upper Ionosphere,
    Proc. Phys. Soc. B. 68, 493, 1955.

Wright, R. W., Koster, J. R., and Skinner, N. J.:   Spread-F Layer Echoes
    and Radio Star Scintillation,   J. Atmos. & Terr. Phys. 8, 240, 1956.

3.

APPENDIX C
TROPOSPHERIC PHASE PATH FLUCTUATION EXPERIMENT

Late in 1962 it became evident that shifts in Air Force planning
would preclude the availability of a suitable satellite vehicle for the
WIDE BAND experiments. Therafter, a short-term contract (AF 30(602)-
2840) was opened to permit preliminary examination of the question: what
portion of the satellite-ground propagation path behavior can be ascribed
to tropospheric influences? Under this contract, a B-57 airplane was
fitted with an S-band beacon transmitter and there were begun a series
of flights during which transmissions were made over an approximately
50-mile long, constantly varying tropospheric path from air to the inter-
ferometer ground stations. The aircraft speed was typically 400 knots
and its altitude 42,000 feet.

A report summarizing the results from the tropospheric propagation
experiment was issued at the termination of contract AF 30(602)-2840,
and the experimental effort was resumed under contract AF 30(602)-2077.
Specific goals for the continued program were the investigation of
tropospheric phase path fluctuations under a variety of different meteor-
ological conditions, and in particular during thunderstorms. Because
of the large quantity of data collected during the Spring of 1963, the
additional data to be collected during the continuation of the program were

intended to represent the many different weather conditions encountered
in the Buffalo area rather than just more data for the average good weather
day. Because of weather conditions prevailing during July and August
1963, only two flights were conducted during disturbed (thunderstorm)
weather. The remaining data represent meteorologically "quiet"
conditions.

EXPERIMENTAL PROCEDURE

The tropospheric phase path fluctuation experiment was conducted
at the CAL Sand Hill receiving site[5] located approximately 20 miles
northeast of Buffalo, New York. The purpose of the program was to
obtain experimental data that could be used to determine the limitations
on angular radar resolution at S-band imposed by random fluctuations of
refractive index in the troposphere.

In order to obtain a bng propagation path through the troposphere,
the S-band (2250 mc) beacon transmitter was carried on board a B-57
aircraft in the altitude range of 39,000 ft to 42,000 ft. The flight plan
followed by the B-57 is shown in Figure C-1. This pattern was flown
twice during each experiment, and required approximately one hour per
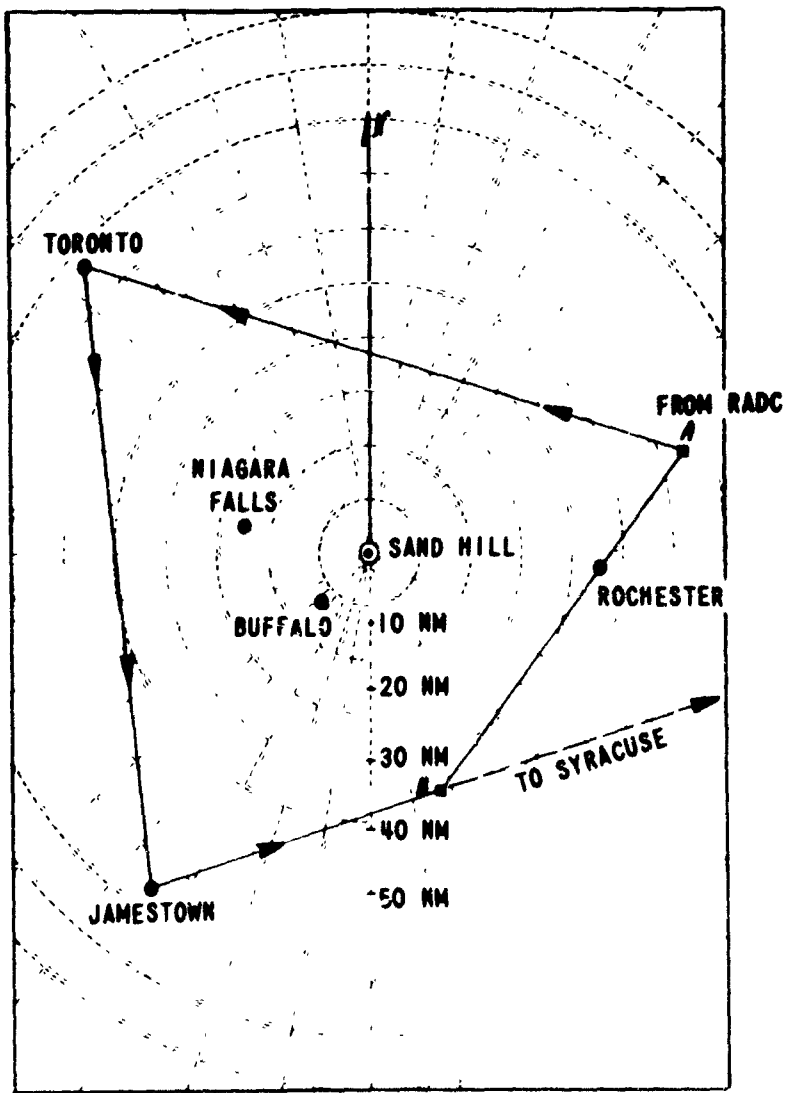lap at an average ground speed of 400 knots.

Figure C-1 FLIGHT PLAN USED FOR TROPOSPHERIC EXPERIMENT

The beacon transmitter carried by the B-57 consisted of a cavity oscillator capable of delivering 2 watts of c,w. power to its antenna. The transmitter and associated solid-state power supply circuitry were thermally stabilized by means of a temperature controlled heat sink. Using a Freon-evaporation cooling system plus shock mounting of all transmitter components, resulted in long-term (2 hours) frequency stability of about 10 parts per million and an incidental frequency modulation spectrum that was about 4 kilocycles wide at the halfpower points. The transmitting antenna, a quarter wave stub against a groundplane, was mounted on the under side of the fuselage, near the tail, with the stub extending downward. Occasional tracking difficulties were experienced when the antenna was shielded by the aircraft body during a heavily banked turn. These did not result in serious loss of data.

The receiver-interferometers were arranged on two lengths of orthogonal baselines, lying north-south and east-west, and of lengths 100 and 1000 meters. Because of the very large (relative to the operating wavelength) baseline lengths used in this experiment, all local oscillators in the interferometer complex were phase locked to a common reference signal so that phase fluctuations due to mechanical expansion or contraction of the interconnecting cables were removed. The details of the phase locking arrangement used are documented in a report[5] entitled, "WIDE BAND Receiving Installation."

The analog data from the interferometers, proportional to the
cosine of the R.F. phase difference between the interferometer antennas,
were recorded on magnetic tape at 30 in/sec. A sample of the analog
interferometer output, reproduced from the magnetic data tape, is
shown in Figure C-2.

Whenever the aircraft flew a course parallel to one of the 1000-meter
baselines, very high differential phase rates were observed, occasionally
reaching a value of 190 radians per second. In order to obtain a least
count of 2° in phase, we digitized the analog data at a rate of 5000 words
per second into six-bit binary words. The digital data points were
stored on magnetic tape in a format compatible with the requirements
of the CAL IBM 704 computer. This computer was used to perform all
of the subsequent data processing.

In addition to the four interferometers, the receiving site contained
a tracking receiver, the purpose of which was to follow the S-band
beacon transmitter and transmit azimuth and elevation information to
the antennas in the interferometer complex. The tracker antenna was
a 16 foot paraboloid with a conical-scanning feed. Tracking accuracy
was 10 milliradians with wind speeds up to 20 mph. Continuous tracking
information (sine and cosine of the azimuth angle and the sine of the
elevation angle), and WWV-time, were recorded on a four-channel
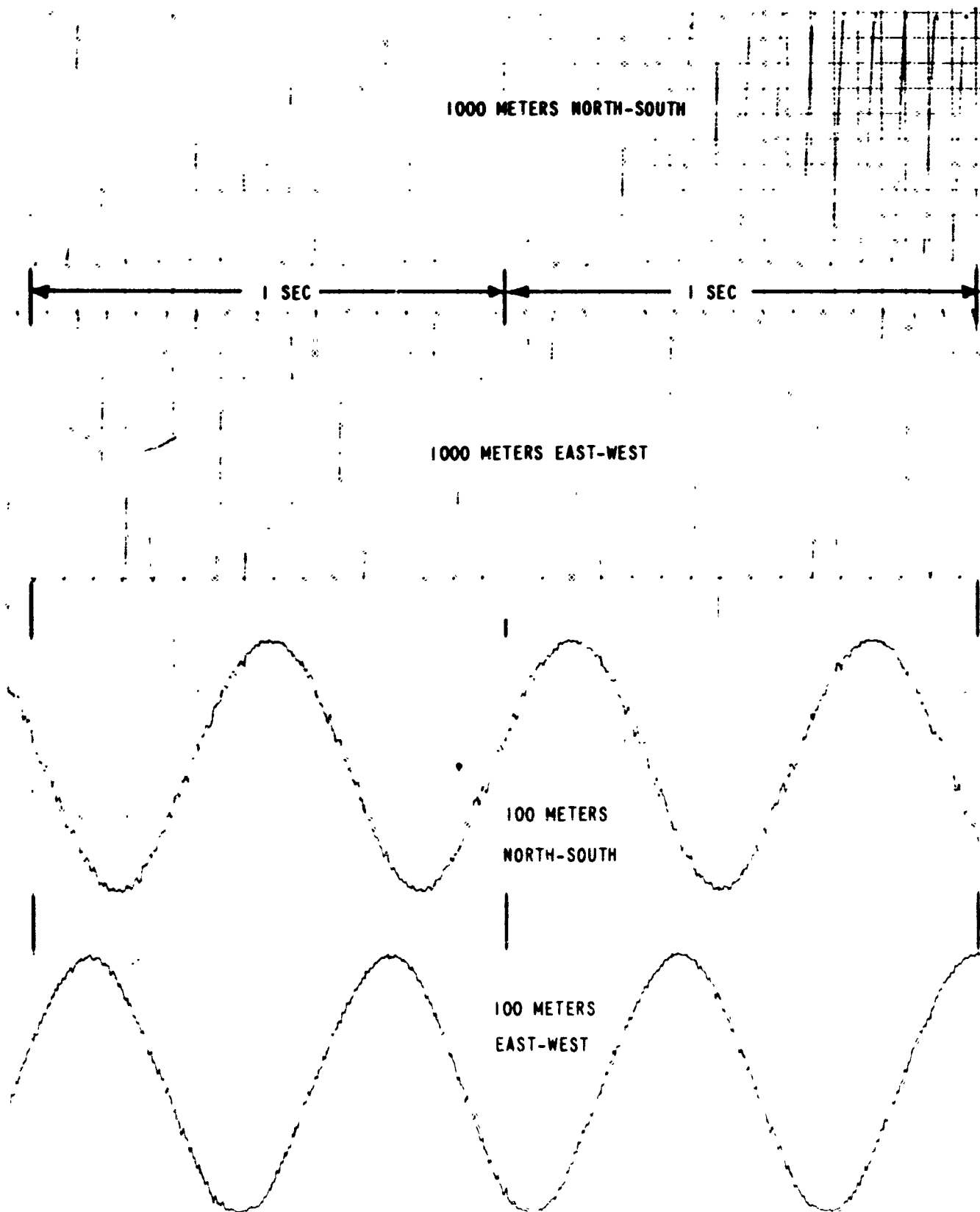Sanborn recorder during each experiment.

17 JULY 1963, 1500 EST

1000 METERS NORTH-SOUTH

|←——————— 1 SEC ———————→|←——————— 1 SEC ———————→|

1000 METERS EAST-WEST

100 METERS
NORTH-SOUTH

100 METERS
EAST-WEST

Figure C-2 INTERFEROMETER SAMPLE DATA

C-6

DATA ANALYSIS AND RESULTS

Theoretical Approach

The purpose of the CAL experiment was to investigate the magnitude and the spectrum of S-band phase fluctuations caused by random refractive index fluctuations in the troposphere. Because our experiment was conducted with the transmitter on board an aircraft, the phase path between transmitter and receivers was constantly changing, a fact which made data analysis extremely difficult. The major problem encountered was separating the phase changes due to aircraft motion from those produced by tropospheric phase path fluctuations. In the discussion that follows the time dependence of the phase changes due to the unperturbed (i.e., constant velocity, no vibration, etc.) aircraft motion will be derived in terms of aircraft velocity, range, and the angle between the direction vector to the aircraft and the interferometer baseline. The difference between such a deterministic expression for the aircraft motion and the raw phase data must constitute the desired random phase data due to propagation through the troposphere.

Figure C-3 represents the static geometry of our experiment. The transmitter is located at T, a distance R from the interferometer.
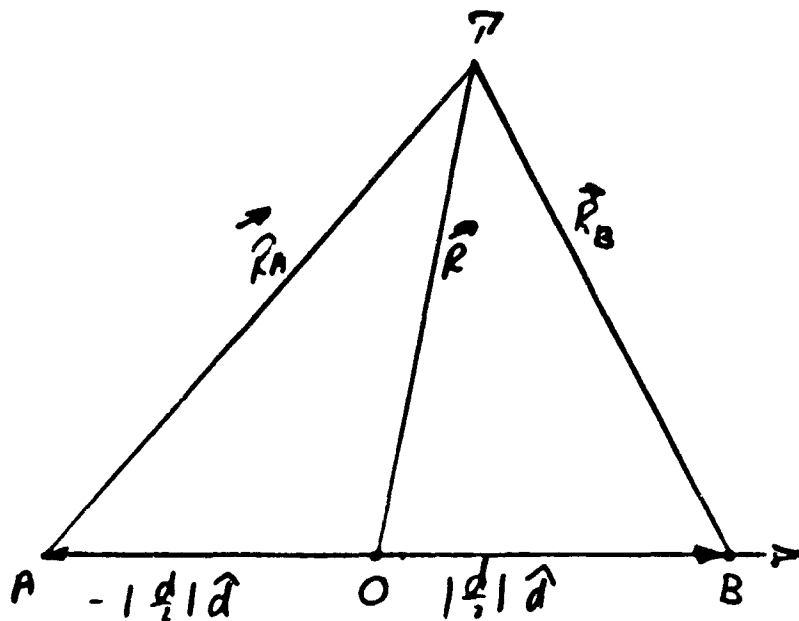
Figure C-3 - Geometry representing transmitter and receivers

The interferometer antennas are located at points A and B on a baseline that is (d) long and oriented along the y-axis. (The y-axis coincides with the north-south baseline of our experiment.) The data collected during our experiment was a function of the phase difference ϕ_{AB} between antennas A and B, where

$$\phi_{AB} = \frac{2\pi}{\lambda}\left[|R_A| - |R_B|\right] - \Delta\phi_R \tag{C4}$$

and $\Delta\phi_R = \phi_{R_A} - \phi_{R_B}$. The quantities ϕ_{R_A} and ϕ_{R_B} are the random phases incurred because of random variations in the refractive index along the paths T-A and T-B.

C-8

We will next examine the difference in magnitude ΔR between vectors $\vec{R}_A$ and $\vec{R}_B$.

$$|R_A|^2 = \left(R^2 + \frac{d^2}{4} + \vec{R} \cdot \vec{d}\right) \qquad \text{(a)}$$

$$\text{(C-2)}$$

$$|R_B|^2 = \left(R^2 + \frac{d^2}{4} - \vec{R} \cdot \vec{d}\right) \qquad \text{(b)}$$

The solution to ΔR from equation (C-2) involves expanding the quantities $|R_A|$ and $|R_B|$ in a power series. This results in the following expression for ΔR :

$$\Delta R = |R_A| - |R_B| = |R|\left[a - \frac{ab^2}{2} + \frac{a^3}{8} + \frac{3ab^4}{16} + \cdots \right] \qquad \text{(C-3)}$$

where $a = \left|\frac{d}{R}\right|\left(\hat{R} \cdot \hat{d}\right)$ and $b = \left|\frac{d}{2R}\right|$. Note that in equation (C-3) all the even powers of $\left|\frac{d}{R}\right|$ are missing. Thus if $\left|\frac{d}{R}\right|$ is a small compared to unity, the power series converges rapidly to zero. In our experiment the baseline lengths were equal to, or smaller than, 1000 meters, and the range to the aircraft was never less than 50 km. Consequently, by neglecting all terms containing $\left|\frac{d}{R}\right|$ to powers greater than unity, our error will be less than 1 part of 10,000 in the determination of ΔR : an error less than 5 milliradians when ΔR is multiplied by $\frac{2\overline{\pi}}{\lambda}$. ($\frac{2\overline{\pi}}{\lambda}$ is equal to 15 $\overline{\pi}$ radians/meter in our experiment.) A phase error of this magnitude is estimated to be at least a factor of ten smaller than the rms value of $\Delta\phi_R$ in equation (C-1) and can, therefore, be neglected.

To account for our moving aircraft we must examine the same geometry, but let the range vector $\vec{R}$ be time dependent so that

$$\vec{R(t)} = \vec{R_0} + \vec{V}\Delta t \qquad \text{(C-4)}$$

Neglecting parallax, the range difference ΔR becomes

$$\Delta R(t) = |R(t)| \, a(t) \qquad \text{(a)}$$

$$\text{(C-5)}$$

where

$$a(t) = |d| \frac{(\vec{R_0} + \vec{V}\Delta t) \cdot \hat{d}}{|R(t)|^2} \qquad \text{(b)}$$

The subscript (0) denotes the value of R at time t_0; Δt is the difference between time t_0 and time t.

It should be evident, that the solution of $a(t)$ will once more involve a power series, this time in powers of Δt. Thus, we obtain

$$\Delta R(t) = |d| \left[(\hat{R}_0 \cdot \hat{d}) + \left| \frac{V\Delta t}{R_0} \right| (\hat{v} \cdot \hat{d}) \right] \left[1 - \left| \frac{V\Delta t}{R_0} \right| (\hat{P}_0 \cdot \hat{v}) \right.$$

$$\text{(C-6)}$$

$$\left. - \frac{1}{2} \left| \frac{V\Delta t}{R_0} \right|^2 \left\{ 1 - 3(\hat{R}_0 \cdot \hat{v}) \right\} + \frac{1}{2} \left| \frac{V\Delta t}{R_0} \right|^3 \left\{ 3(\hat{R}_0 \cdot \hat{v}) - 10(\hat{R}_0 \cdot \hat{v})^3 + \cdots \right] C_3 = -\frac{1}{2}$$

The expansion can be carried out to powers of Δt higher than the cubic; the choice of how far to carry this process will depend on the magnitude of Δt which is the time over which the aircraft can reasonably be expected to fly a straight and unperturbed course. In general, we will neglect parallax and write $\Delta R(t)$ as a power series in time with coefficients C_n so that

$$\Delta R(t) = \sum_{n=0}^{N} C_n \Delta t^n = C_0 + C_1 \Delta t + C_2 \Delta t^2 + C_3 \Delta t^3 + \cdots \quad \text{(C-7)}$$

where, for the approximations made here, the first four coefficients are:

$$C_0 = |d|(\hat{R} \cdot \vec{d}) \qquad \text{(a)}$$

$$C_1 = -|d|\left|\frac{v}{R_0}\right|\left[(\hat{R}_0 \cdot \vec{d})(\hat{R} \cdot \vec{v}) - (\hat{v} \cdot \vec{d})\right] \qquad \text{(b)} \qquad \text{(C-8)}$$

$$C_2 = -\frac{1}{2}|d|\left|\frac{v}{R_0}\right|^2\left[(\hat{R}_0 \cdot \vec{d}) - 3(\hat{R} \cdot \vec{d})(\hat{R}_0 \cdot \vec{v})^2 + 2(\hat{R}_0 \cdot \vec{v})(\hat{v} \cdot \vec{d})\right] \qquad \text{(c)}$$

$$= -\frac{1}{2}|d|\left|\frac{v}{R_0}\right|^3\left[-3(\hat{R}_0 \cdot \vec{d})(\hat{R}_0 \cdot \hat{v}) + 10(\hat{R}_0 \cdot \vec{d})(\hat{R}_0 \cdot \vec{v})^3 + (\hat{v} \cdot \vec{d}) - 3(\hat{v} \cdot \hat{d})(\hat{R}_0 \cdot \vec{v})^2\right] \qquad \text{(d)}$$

C-11

It should be noted that this power series expansion for $\Delta \ell$ contains the unit vector $\hat{d}$ which, in Figure C-3, coincides with the y-axis. Thus, in this analysis the power series coefficients C_n are correct for the north-south and east-west baselines when the unit vectors $(\hat{j})$ and $(\hat{c})$ respectively, are substituted for $\hat{d}$.

Machine Computations

Analog data obtained from the experiment were reco. ded on magnetic tape and subsequently quantized into six-bit binary words. Even though the function of interest to us is $\phi_{\beta\beta}$ the raw data collected at our field site were of the form (See Figure C-2):

$$F(t) = K \cos[\phi_{AB}] \qquad \text{(a)}$$

(C-9)

$$F(t) = K \cos[f(t) + \Delta\phi_p(t)] \qquad \text{(b)}$$

where $f(t) = \dfrac{2\pi}{\lambda}\Delta R(t) = a + bt + ct^2 + \ldots$

and $\Delta\phi_p(t)$ are the random phase data that we wish to isolate and examine. Designate the times at which $F(t)$ is zero as t_ℓ. Then

C-12

$$F(t_k) \equiv 0 \qquad \text{(a)}$$

$$f(t_k) + \Delta f_R(t_k) = \left(\frac{2k+1}{2}\right)\pi \qquad \text{(b)} \qquad \text{(C-10)}$$

$$\Delta f_R(t_k) = k\pi - a' - b t_k - c t_k^2 - \cdots \qquad \text{(c)}$$

where $\quad a' = a - \dfrac{\pi}{2}$

If, in equation (C-10c), the aircraft position were known
exactly at time t_k , then we could evaluate the polynomial for $f(t_k)$
and thus solve for $\Delta f_R(t_k)$, the desired data from this experiment.
Because the airplane's position could not be determined to the accuracy
commensurate with other data,[*] we estimated values for the coefficients
in the polynomial for $f(t)$ by computing a least-squares fit for the
raw phase data. In so doing, we assumed that, over a five-second time
interval, a polynomial of the form $A + B t_k + C t_k^2$ would adequately
account for the phase changes due to aircraft motion. It must be noted
that the coefficients A, B, and C will differ from the coefficients
a', b, and c in equation (C-10c) because the least-squares

---

[*] See Appendix C-2 for a derivation of the exactness requirements.

p:ocess does not differentiate between contributions to the total phase ϕ_{AB} due to the aircraft and due to the atmosphere. Within the limitations of the assumptions and approximations made, the difference between the total phase $\phi_{AB}(t_k)$ and the polynomial $\left[A + Bt_k + Ct_k^2\right]$ is a phase that is caused by random variations of the refractive index along the propagation path.

Specific computations performed were as follows:

1. Compute the average time between consecutive zero crossings of $F(t)$. This average half period is $\tilde{\tau}$ and is defined as

$$\tilde{\tau} = \frac{t_N - t_1}{(N-1)}$$

where t_1 is the time of the first zero crossing, and t_N is the time of the last zero crossing in the data interval of 5 seconds.

2. Compute the difference P_k between the time interval $(t_k - t_1)$ and $(k-1)\tilde{\tau}$. Normalize this difference to the average half period $\tilde{\tau}$. Then

$$P_k = \frac{1}{\tilde{\tau}}\left[\tilde{\tau}(k-1) - (t_k - t_1)\right] \qquad \text{(a)}$$

(C-12)

$$P_k = (k-1) - \left(\frac{t_k - t_1}{\tilde{\tau}}\right) \qquad \text{(b)}$$

C-14

3. The values of P_ℓ were next fitted with the polynomial $\left(A' + B' t_\ell + C' t_\ell{}^\nu\right)$ by the method of least squares. The difference between the polynomial (evaluated at time t_ℓ) and P_ℓ was the remainder R_ℓ which constitutes the output from the computer program. The relationship between the polynomials $\left(A' + B' t_\ell + C' t_\ell{}^\nu\right)$ and $\left(A + B t_\ell + C t_\ell{}^\nu\right)$ as well as the similarity of πR_ℓ to $\phi_\rho(t_\ell)$, are developed in the following identities:

$$R_\ell = P_\ell - A' - B' t_\ell - C' t_\ell{}^\nu \qquad\qquad \text{(a)}$$

Substitute (C-12b) for P_ℓ :

$$R_\ell = P_\ell - \left(1 - t_1 + A'\right) - \left(1 + \frac{B'\,\tilde{\tau}}{\tilde{\tau}}\right) t_\ell - C' t_\ell{}^\nu \qquad \text{(b)} \qquad \text{(C-13)}$$

multiply both sides by π :

$$\pi R_\ell = P_\ell \pi - A - B t_\ell - C t_\ell{}^\nu \qquad\qquad \text{(c)}$$

Discussion of Results

On the basis of the foregoing discussion, and on the assumption that phase changes due to aircraft motion over a time interval of five seconds can adequately be represented by a quadratic, one would expect that the coefficients a, b, and c in equation (C-10c) are fairly well

approximated by the coefficients A, B, and C in (C13c).[*] Recognizing

the limitations inherent to our analysis technique, we computed values

for πR_ℓ from six consecutive five-second long data sections, i.e.,

every five seconds new coefficients of fit (A, B, and C) were computed.

Data collected on four different days were analyzed. Of these, two days

represented meteorologically "quiet" days, while shower and thunder-

storm activity prevailed in the Buffalo area on the other two.[**] Power

spectra were computed from the πR_ℓ values. These are presented

in Figures C-4, C-5, C-6, and C-7. Each of these four figures is a

composite of six 40 point spectra; each spectrum was computed from

5 seconds of interferometer data from which the polynomial $A + B t_\ell + C t_\ell{}^{\vee}$

had been removed.

The only data available for comparison with our results were

obtained with fixed propagation paths. Under the assumption that

spectral densities obtained on fixed paths will scale directly with the

length of the propagation path and with the square of the frequency, the

spectral in Figures C-4, C-5, C-6 and C-7 are in agreement (order of

magnitude) with the L-band results presented by Herbstreit and Thompson[1]

in 1955. In comparing their spectrum with ours, we have made the

additional assumption that the frequency dependence of $f^{-2.5}$ continues

---

[*] See Appendix C-3

[**] See Appendix C-4 for weather synopses and aircraft positions at
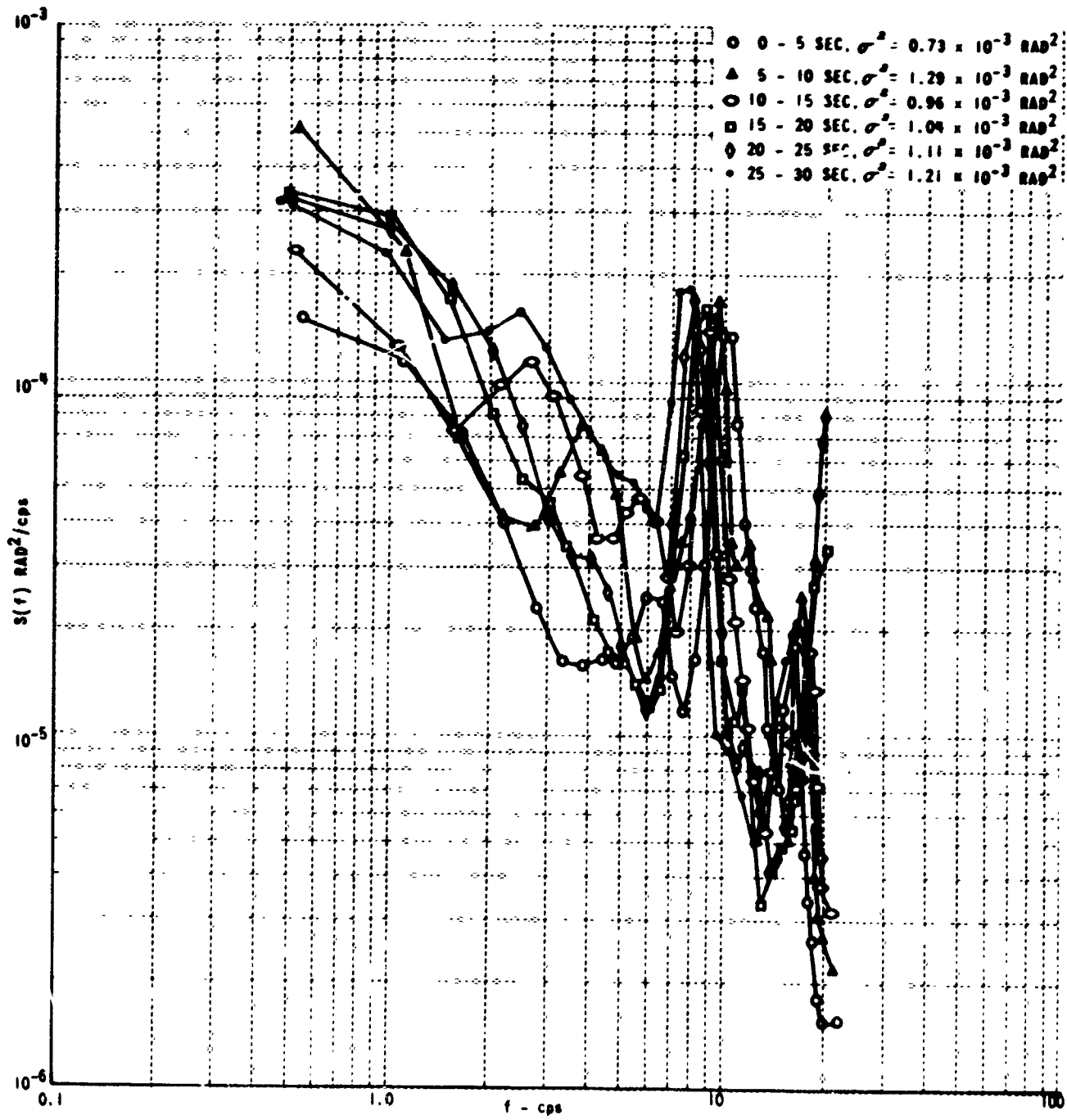the times represented by the data.

Figure C-4 PHASE FLUCTUATION SPECTRUM 1 AUGUST 1963, 1607 EDT
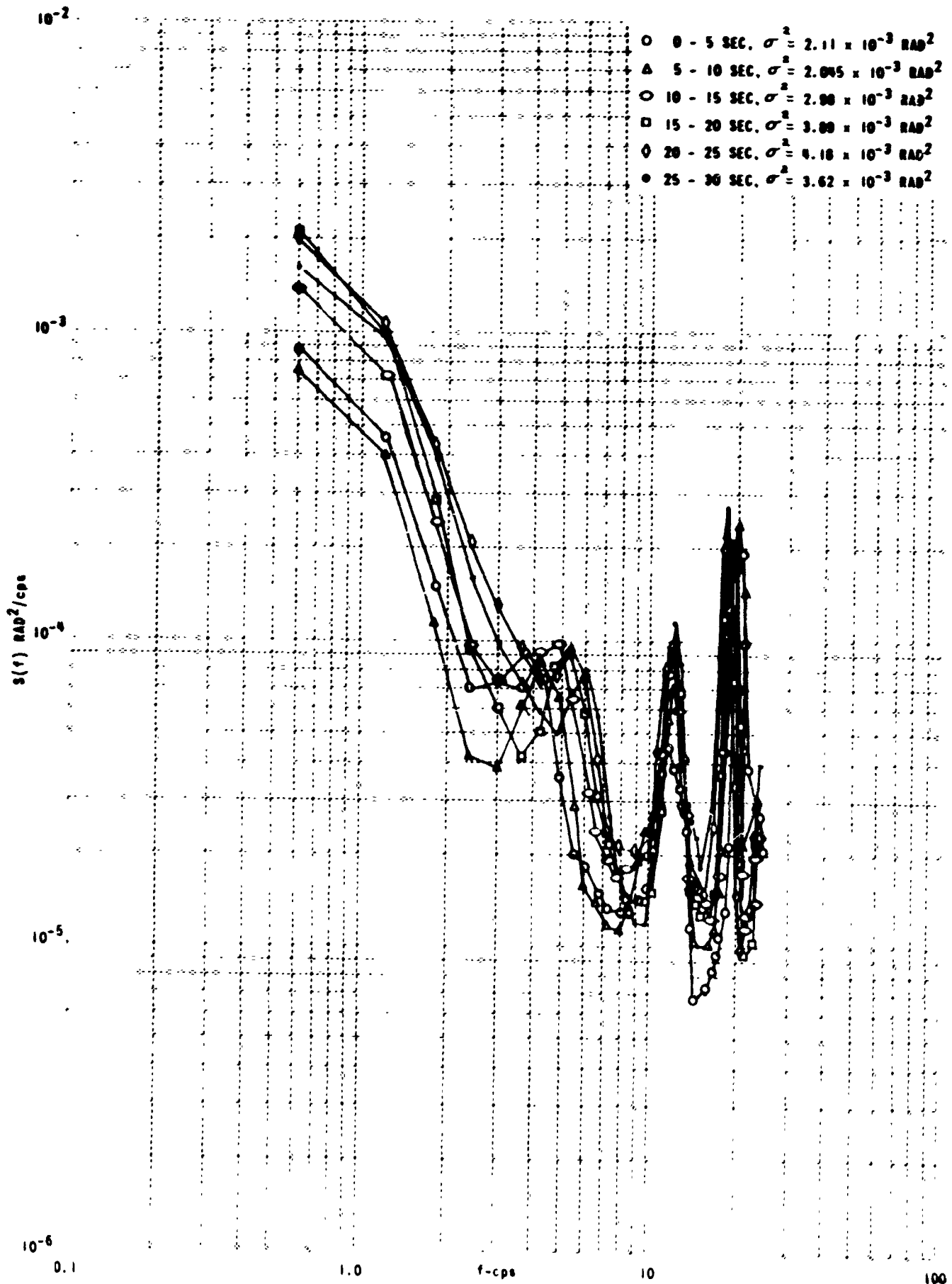1000 METER NORTH-SOUTH BASELINE

C-17

Figure C-5 PHASE FLUCTUATION SPECTRUM 22 AUGUST 1963. 1554 EDT
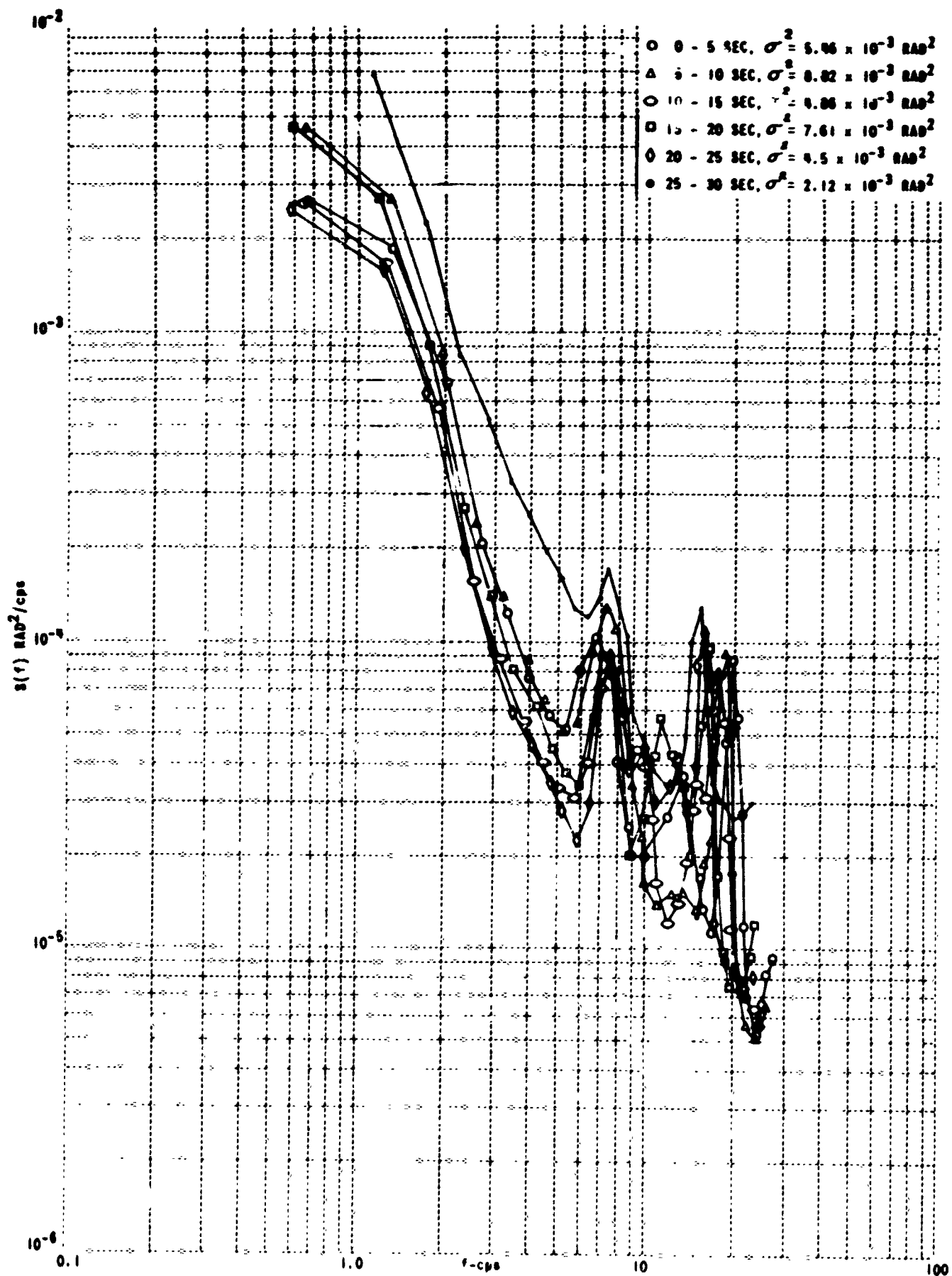1000 METER EAST-WEST BASELINE

C-18

Figure C-6 PHASE FLUCTUATION SPECTRUM 27 AUGUST 1963, 1454 EDT
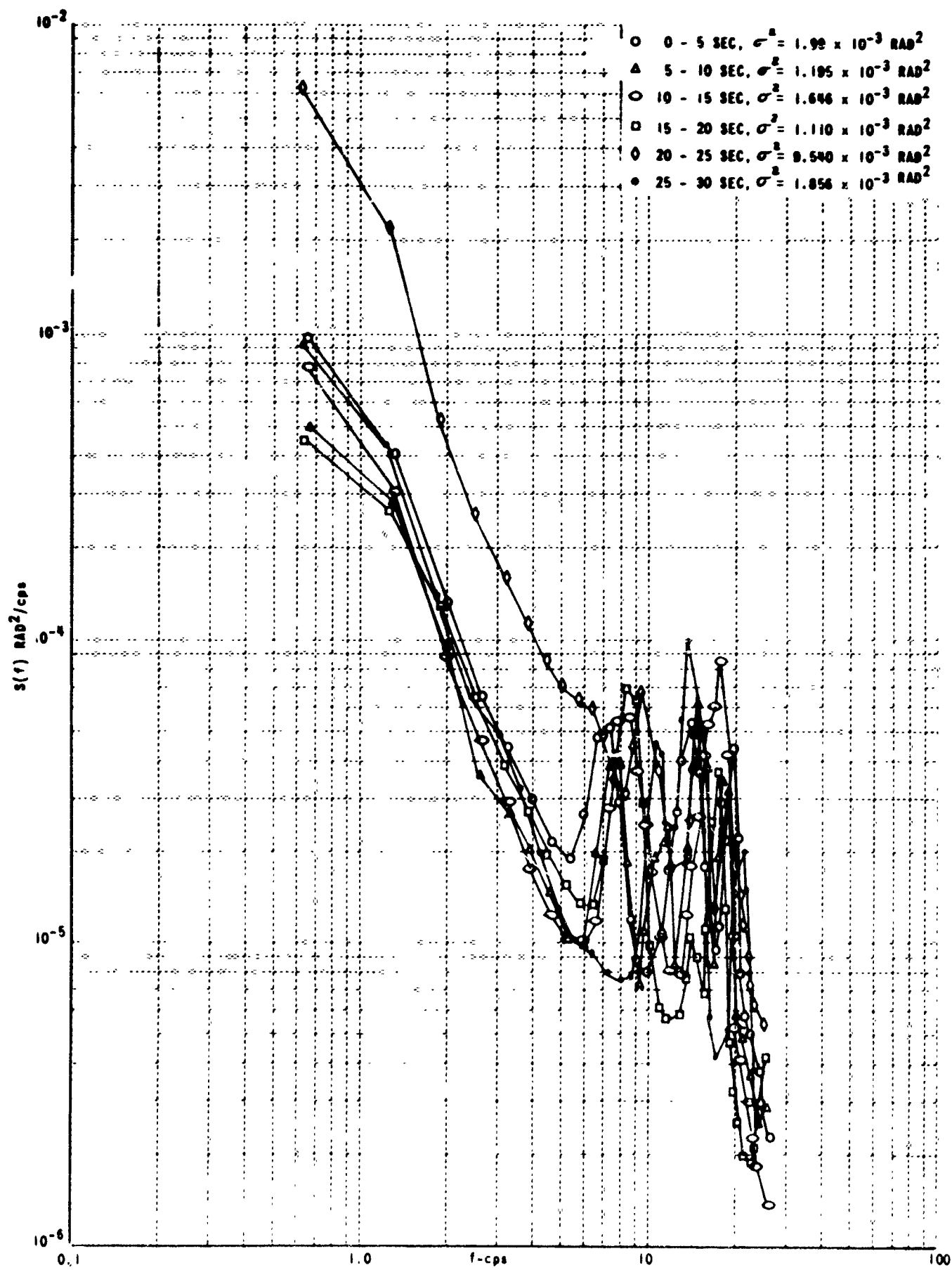1000 METER EAST-WEST BASELINE

C-19

Figure C-7 PHASE FLUCTUATION SPECTRUM 28 AUGUST 1963, 1623 EDT
1000 METER NORTH-SOUTH BASELINE

beyond the data points presented by them. The validity of this assumption is substantiated by the 9,400 mc phase-variation spectrum published by Thompson and Janes [6] in 1959.

There are several features common to all of the curves presented here. Probably the most striking one is the occurrence of large, isolated spectral densities at frequencies near 10 cps, 15 cps, and 20 cps. We do not believe that these spikes are caused by propagation through the atmosphere; the most likely explanation for their existence is that of wind-induced, natural resonant vibration of either the antenna towers, dishes, feed supports or a combination of all of these. These spikes, therefore, should be thought of as defining the system noise level.

A second feature common to practically all of the spectra obtained from our data is their similarity to the spectrum of the time function $g(t) = at^3$.[*] This similarity is particularly noticeable on meteorologically "quiet" days (See spectra for August 22 and 27). Why this parallelism should exist and what significance should be attached to it, is not well understood. It should be pointed out, however, that for power spectra to be alike, the only requirement is that their autocorrelation functions be alike. This statement implies nothing concerning the similarity of the time functions giving rise to these spectra. To illustrate this point, we have plotted in Figure C-8 the time history of $\pi \mathcal{R}_{\ell}$ (equation (C13c)) for a 5-second time interval on 28 August 1963, from $16^h 23^m 38^{sec}$ to $16^h 23^m 43^{sec}$. In the same figure appears a dotted curve which represents the time function at^3 from which the mean value has been removed, and which, over a 5-second time interval has the same variance as the time function $\pi \mathcal{R}_{\ell}$. There is no readily apparent similarity between these two time functions.

In general, our spectra over the frequency range from 0.6 cps to 20 cps are in qualitative agreement with extrapolated spectra obtained from fixed propagation paths and different operating frequency [1, 3, 4]. However, we have shown in Appendix C-3 that the cubic term (in the polynomial which accounts for phase changes due to aircraft position), also gives rise to a spectrum having the expected spectral densities and the expected frequency dependence. Therefore, our results must be treated as inconclusive as far as determination of the true magnitude and spectrum of the phase path fluctuations is concerned.
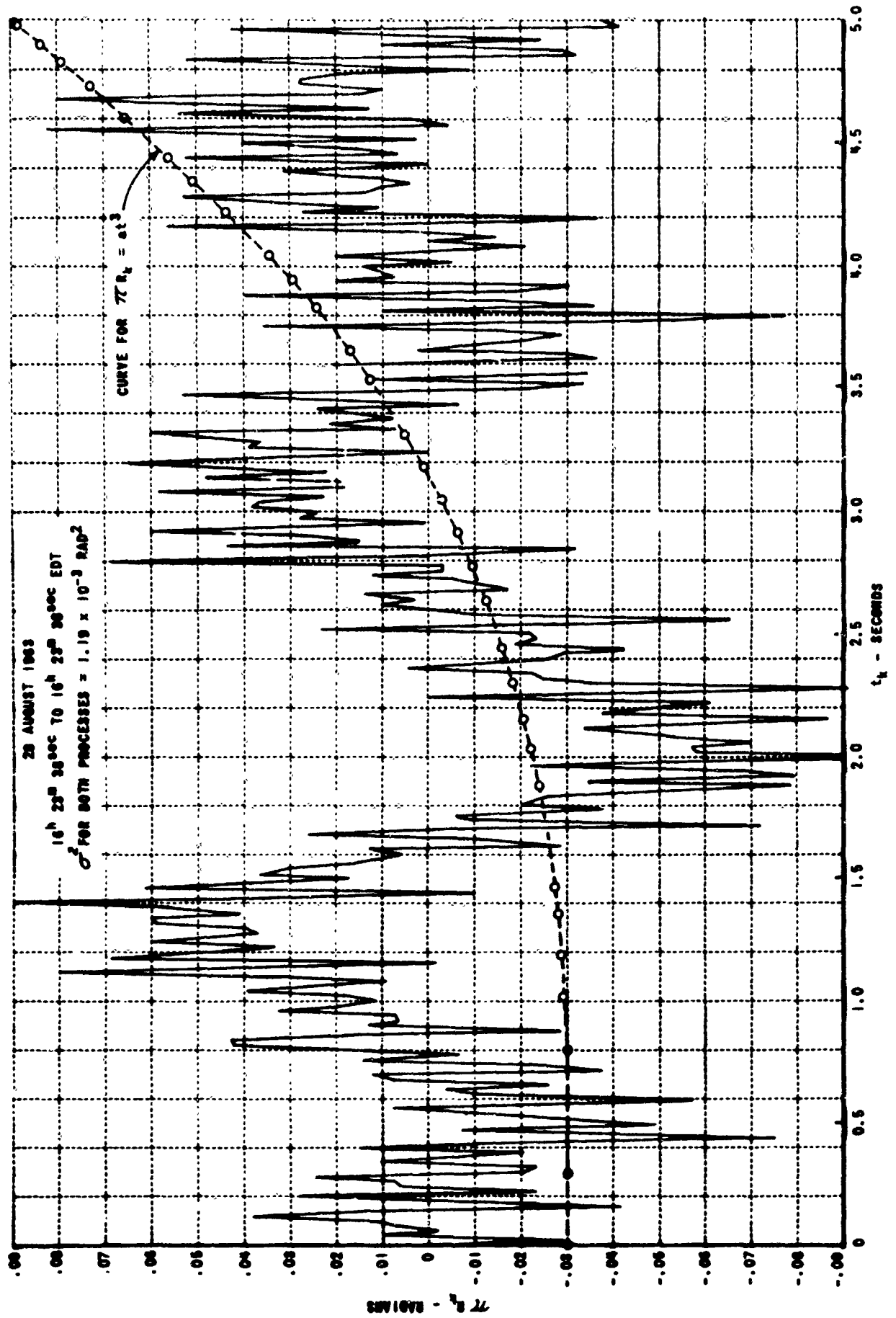
---

[*]See also Appendix C-3

Figure C-8 PLOT OF REMAINDER AFTER POLINOMINAL HAS BEEN REMOVED AS A FUNCTION OF TIME

CONCLUSIONS AND RECOMMENDATIONS

The tropospheric experiment conducted by this Laboratory was intended to yield data from which the mean square phase error and the power spectrum of phase fluctuations due to tropospheric inhomogeneities could be computed. It was expected that the mean-squared phase error caused by S-band propagation through turbulent media (such as thunderstorms) would be appreciably larger than the mean-square phase errors arising from a meteorologically quiet medium. This expectation is not supported by our data. We find, however, that the total mean-square phase error due to the combination of atmosphere, aircraft motion, antenna vibration and thermal noise is never larger than 10^{-2} square radians over a time interval of five seconds. We can safely conclude, therefore, that the phase error due to atmospheric inhomogeneities alone is smaller than this value. One of the goals of the experiment was to ascertain the limitations imposed by the troposphere on angular resolution at S-band. We can positively state that at all times angular resolution of better than 6×10^{-5} radians is achievable while propagating through the troposphere. This estimate constitues a pessimistic bound, and actual resolution limits should be finer.

Our experimental spectra are in qualitative agreement with extrapolated results obtained by the National Bureau of Standards. Because these spectra also have the same form as would be expected from residual aircraft motion effects, i.e., the at^3 term, we must treat our results as being inconclusive.

Because the achievement of maximum system accuracy necessitates that angular value of line of sight be known to 10^7 radians, there should be no further pursuit of such propagation problems by airborne experiments in which that precision cannot be realized. This recommendation is pessismistic in that it relates to phase determination within 0.5 degree. Relaxation of that limit would be accompanied by relaxation of system precision requirements.

REFERENCES

1. Herbstreit and Thompson: "Phase Measurements over Paths of Varying Lengths," Proc. IRE, 43, 1391 (1955).

2. Deam and Fannin: "Phase Difference Variations in 9350 mc Radio Signals," Proc. IRE, 43, 1402 (1955).

3. Norton, K. A., J. W. Herbstreit, et al., National Bureau of Standards Monograph 33, November 1, 1961.

4. Thompson, M. C., H. B. Jones and A. W. Kirkpatrick, JGR 65, 193, 1960.

5. CAL Report No. UB-1363-P-101. Wide Band Receiving Installation, Contract No. AF 30(602)-2077.

6. Thompson, M. C., and H. B. Janes: "Preliminary Measurements of Phase Stability over Low-Level Tropospheric Paths," NBS Report 6010, NBS Project 8300-11-8805, September 1959 (Figure 17).

Appendix C-1

**Details of Data Analysis Program Initially Used
in an Effort to Separate Vehicle Motion From the
Atmospheric Effects on the Phase of a Radio Wave**

During the early stages of the data collection and anal·sis program

it was recognized that, in order to accurately assess the effects that

the atmosphere has on the phase of a radio wave, the distance between

the radio source and the receiving instrumentation would have to

be extremely well known. In fact, the precision to which one has to

know this distance is such as to be almost unattainable even by the

most modern methods. In an attempt to circumvent these extreme

requirements, we stipulated that over the time interval required for

the phase path to change by one wavelength, the aircraft must follow

a straight-line path for which perturbations in motion would cause

phase fluctuation errors that are negligible compared to the propagation

effects. On the basis of this assumption alone, we proceeded to analyze

the phase fluctuations data along the following lines of reasoning.

The phase difference between two antennas separated by a

distance (d), both receiving a signal from a transmitter a distance ρ

away, will be (see Figure C-1-1)

$$\phi_{AB} = \frac{2\pi}{\lambda} \left(R_A - R_B \right) - \phi_{\rho_{AB}} \qquad \text{C-1(1)}$$

where $\phi_{rAB} = \phi_{rA} - \phi_{rB}$

and where ϕ_{rA} and ϕ_{rB} are the random phase fluctuations incurred along paths R_A and R_B because of random fluctuations in the refractive index along these paths.
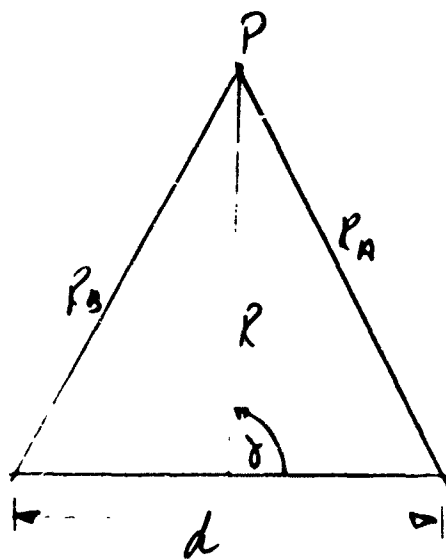

Figure C-1-1

In the interferometer experiment performed the point P was in constant motion, and the analog output from the interferometer was of the form

$$F(t) = K \sin(\phi_{AB}) \qquad \text{(a)}$$

$$F(t) = K \sin\left[f(t) + \phi(t)\right] \qquad \text{(b)}$$

where $f(t) \doteq \frac{2\pi d}{\lambda} \cos \gamma(t)$ and $\phi(t) = \phi_{r\,AB}$ and

where it has been assumed that $R \gg d$. The purpose of the data analysis program is separate the effect of the aircraft motion represented by $f(t)$ from the random phase $\phi(t)$.
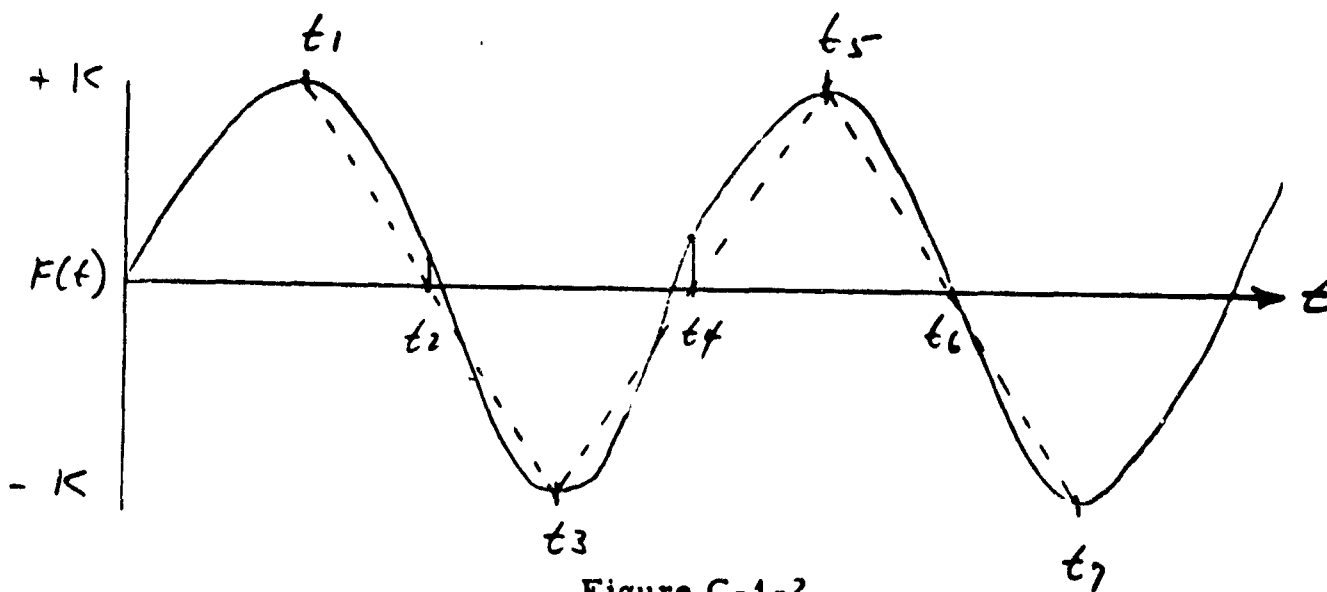

Figure C-1-2

In the interferometer experiment performed the point P was in constant motion, and the analog output from the interferometer was of the form

$$F(t) = K \sin (\phi_{AB}) \qquad \text{(a)}$$

$$F(t) = K \sin \left[f(t) + \phi(t) \right] \qquad \text{(b)}$$

where $f(t) \doteq \frac{2\pi d}{\lambda} \cos \gamma(t)$ and $\phi(t) = \phi_{r AB}$ and

where it has been assumed that $R \gg d$. The purpose of the data analysis program is separate the effect of the aircraft motion represented by $f(t)$ from the random phase $\phi(t)$.
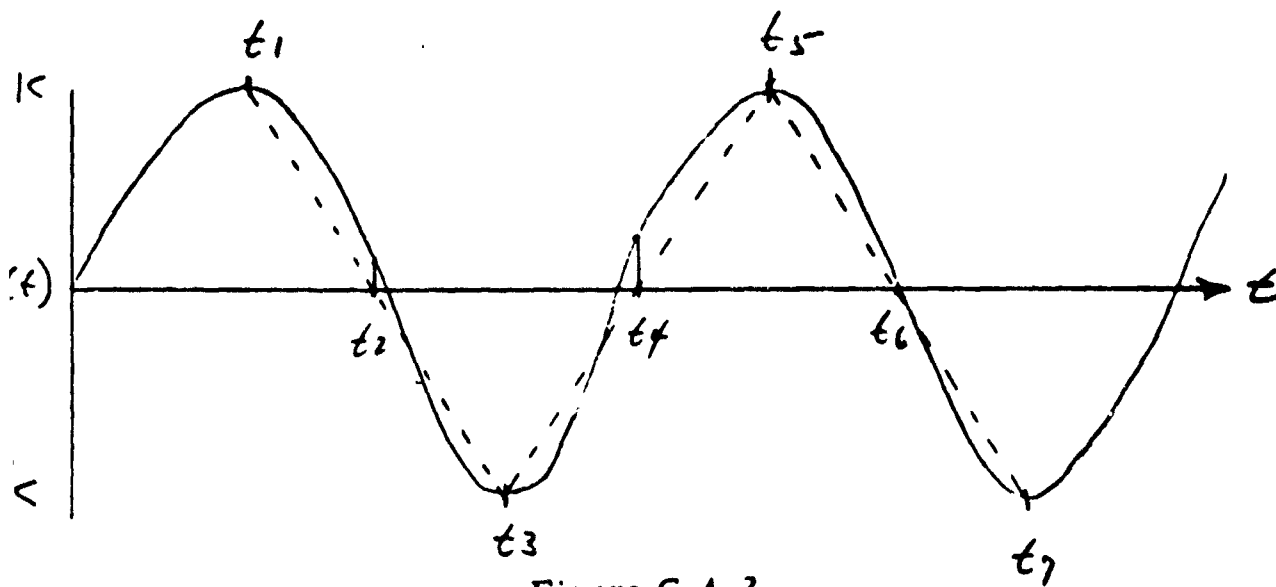

Figure C-1-2

If the value of $\phi(t)$ is small, then equation (C-12b) can be expanded to yield

$$F(t) = K \left[\left(1 - \frac{\phi^2(t)}{2}\right) \sin f(t) + \phi(t) \cos f(t) \right] \qquad \text{(a)}$$

which, for $\phi(t) \ll 1$ becomes

C-4(3)

$$F(t) \approx K \sin f(t) + K \phi(t) \cos f(t) \qquad \text{(b)}$$

One can reason, therefore, that when $f(t)$ is an odd multiple of $\frac{\pi}{2}$, then $F(t)$ is at its peak value. This occurs at times $t_1, t_3, t_5, t_7 \cdots$ If one can next assume that $f(t)$ varies linearily with time over a half period, then at time $t_2 = \frac{t_1 + t_3}{2}$, $f(t)$ should equal a multiple of π radians, and $F(t_2) = \pm K \phi(t_2)$. Consequently, the desired phase fluctuation data should be available when the functional value of $F(t)$ is evaluated at a time that is halfway between the occurrence of the peak values of $F(t)$.

C-30

We will next re-examine this data analysis procedure and show that the conclusions reached are not correct.

Again, let $F(t) = K \sin\left[f(t) + \phi(t) \right]$. At time t_1 (Figure C-1-2),

$$F(t_1) = K \tag{a}$$

$$f(t_1) + \phi(t_1) = \frac{\pi}{2} \tag{C-1(4)}$$

(b)

At time t_3

$$F(t_3) = -K \tag{a}$$

$$f(t_3) + \phi(t_3) = \frac{3\pi}{2} \tag{C-1(5)}$$

(b)

At time $t_2 = \dfrac{t_1 + t_3}{2}$

$$F(t_2) = K \sin\left[f\left(\frac{t_1 + t_3}{2}\right) + \phi\left(\frac{t_1 + t_3}{2}\right) \right] \tag{C-1(6)}$$

Now assume that $f(t)$ varies linearily with time.   Then

$$f\left(\frac{t_1+t_3}{2}\right) = f(t_2) = f\left(\frac{f(t_1)+f(t_3)}{2}\right) = \pi - \left[\frac{\phi(t_1)+\phi(t_3)}{2}\right] \qquad \text{C-1(7)}$$

and

$$F(t_2) = K\sin\left[\frac{\phi(t_1)+\phi(t_3)}{2} + \phi\left(\frac{t_1+t_3}{2}\right)\right] \qquad \text{(a)}$$

which for $\phi(t) \ll 1$

becomes

$$\text{C-1(8)}$$

$$F(t_2) \approx \frac{K}{2}\left[\phi(t_1)+\phi(t_3)-2\phi\left(\frac{t_1+t_3}{2}\right)\right] \qquad \text{(b)}$$

Let the half period be $\dfrac{T}{2} = t_3 - t_1$. Then

$$\frac{t_1+t_3}{2} = t_1 + T/4 \qquad \text{(a)}$$

$$\text{C-1(9)}$$

$$t_3 = t_1 + T/2 \qquad \text{(b)}$$

Let the component of the phase at angular frequency (ω) be given by $\exp j\omega t = \phi(t)$ and rewrite equation C-1(8b) as

$$F(t_2) = \frac{K}{2}\left[\exp j\omega t_1 + \exp j\omega t_1 \exp j\omega \frac{T}{2} - 2 \exp j\omega t_1 \exp j\omega \frac{T}{4}\right] \qquad \text{(a)}$$

$$F(t_1) = -2K \sin^2\left(\frac{\omega T}{8}\right) \exp j\omega(t_1 + T/4) \qquad \text{(b)}$$

$$F(t_2) = -2K \sin^2\left(\frac{\omega T}{8}\right) \phi(t_2) \qquad\qquad \text{C-1(10)}$$

(c)

$$F(t_2) = K \phi(t_2)\left[\cos\left(\frac{\omega T}{4}\right) - 1\right] \qquad\qquad \text{(d)}$$

Equation C-1(10d) is the actual output from the data analysis program. It differs from the desired result in that it contains a filter function proportional to $2\sin^2\left[\frac{\pi}{4}\, f/f_0\right]$, where f_0 is the frequency of the analog data (interferometer output). This filter function severely attenuates the low frequency components contained in $\phi(t)$. Its crossover frequency occurs at $f = 0.805 f_0$ and full transmission occurs at the data frequency f_1 . The frequency component of $\phi(t)$ at $0.29 f_0$ is 20 db attenuated by this function.

C-33

Consequently, data analyzed in the manner outlined can be used only over a very small frequency interval near the maximum frequency components. Because the magnitude of the random phase fluctuations at frequencies near the interferometer fringe frequency is expected to be negligibly small, the output from this data program is not considered to be satisfacrory, and the technique was discarded.

Appendix C-2

Accuracy Requirements for Aircraft Positions Data

The phase difference ϕ_{AB} between two antennas of an interferometer of baseline (d) is given (when parallax is neglected) by

$$\phi_{AB} = \frac{2\pi d}{\lambda} \left(\hat{R} \cdot \hat{d} \right) + \phi_N \qquad \text{C-2(1)}$$

where $\widehat{R}$ is the unit direction vector from the antennas to the source, and ϕ_N is the total random phase noise in the system, which includes phase path fluctuations, source vibrations, thermal noise, etc. If ϕ_N were zero, then the measured phase difference ϕ_{AB} would be exactly equal to $\frac{2\pi d}{\lambda} \left(\hat{R} \cdot \hat{d} \right)$. In the presence of phase noise, however, we will make an error $\widehat{\triangle}$ in the determination of the position vector so that

$$\phi_{AB} = \frac{2\pi d}{\lambda} \left[\vec{R} \cdot \hat{d} + \hat{\triangle} \cdot \hat{d} \right] + \phi_N \qquad \text{C-2(2)}$$

where $\hat{R}$ is the true unit position vector and $\widehat{\triangle}$ is the "unit angular error" vector, i.e. $\widehat{\triangle}$ is a vector normal to $\hat{R}$, so that $|\triangle|$ is the angular error in the determination of $\widehat{R}$. The error term in Equation C-2(2) is $\frac{2\pi d}{\lambda} \left(\hat{\triangle} \cdot \hat{d} \right)$ and this term must be equal to,

or smaller than, $|\hat{\triangle}|\dfrac{2\bar{\pi}d}{\lambda}$. Consequently we can estimate

an upper bound for the $|\hat{\triangle}|$ required so that $\phi_{N}{}^{\prime}$ may be

determined to an accuracy $\triangle\phi_{N}$. Then

$$|\hat{\triangle}| = \dfrac{\triangle\phi_{N}}{2\pi d/\lambda} \quad RADIANS$$

In our experiment, we wish to determine $\triangle\phi_{N}$ to an accuracy

of $0.5^{o} \approx 10^{-2}$ radians. Also for our experiment $\dfrac{2\bar{\pi}d}{\lambda} = 15\pi \times 10^{3}$ so

that

$$|\hat{\triangle}| \doteq 10^{-7} \qquad radians.$$

Appendix C-3

Comparison of Polynomial Coefficients to be
Expected from Aircraft Position Data with
Coefficients of Fit to the Interferometer Phase Data

In our discussion of results we have implied that the coefficients

of fit A, B, and C are representative of the coefficients a, b, and c in

the polynomial that describes aircraft motion. To verify this contention,

we calculated the linear, quadratic and cubic coefficients in equation (C-10c)

from aircraft tracking data recorded during the flight test on 28 August 1963.

These data, of course, are not sufficiently accurate for determining

aircraft position to the extent required for this experiment, but are

adequately precise to illustrate the magnitudes of the coefficients

involved here.

On 28 August 1963, at 16^h 23^m 40 sec EDT, the initial-position

vector $\vec{R}_0$ had a magnitude of 35 N miles and an inclination to

the north-south interferometer-baseline of 110°. The aircraft velocity

vector $(\vec{V})$ had a magnitude of 428 kts and an inclination to the north-south

interferometer baseline of 191° (see diagram). We estimate that the

confidence attached to these position data is as follows:

a) velocity error of $\pm 10\%$

b) aircraft course relative to baseline $\pm 7^o$

c) range error of $\pm 7\%$

d) angle between baseline and position vector $\pm 0.5^o$

From these data we calculate a linear term   (equal to $\frac{2\bar{\pi}}{\lambda} C_1$)[*]

of 144 rad/sec, a quadratic term   (equal to $\frac{2\bar{\pi}}{\lambda} C_2$) of 0.17 rad/sec^2

and a cubic term (equal to $\frac{2\bar{\pi}}{\lambda} C_3$) of 6.3 x 10^{-4} rad/sec^3. The

linear and quadratic terms (B and C in equation (C-13c))obtained

from a least-squares fit to 5 seconds of analog phase data (from 16^h 23^m

38 sec to 16^h 23^m 4⁻ sec) were found to be 164 rad/sec and 0.16 rad/sec^2,

respectively. A cubic term was not computed in our machine program;

however, it can be shown that, due to inadequate knowledge of the exact

aircraft position the cubic term $\frac{2\bar{\pi}}{\lambda} C_3$ computed above will be in

error by ±2.2 x 10^{-4} rad/sec^3. In Figure C-3-2 we have plotted the

spectrum of πP_ℓ along with the spectrum of $\frac{2\bar{\pi}}{\lambda} C_3 t^3$.

The two spectra are very similar to one another, particularly when the

limitations on C_3 are included. However, the uncertainty in

determining aircraft velocity, course, and range is too great to state

positively that the spectrum of πR_ℓ is primarily due to either

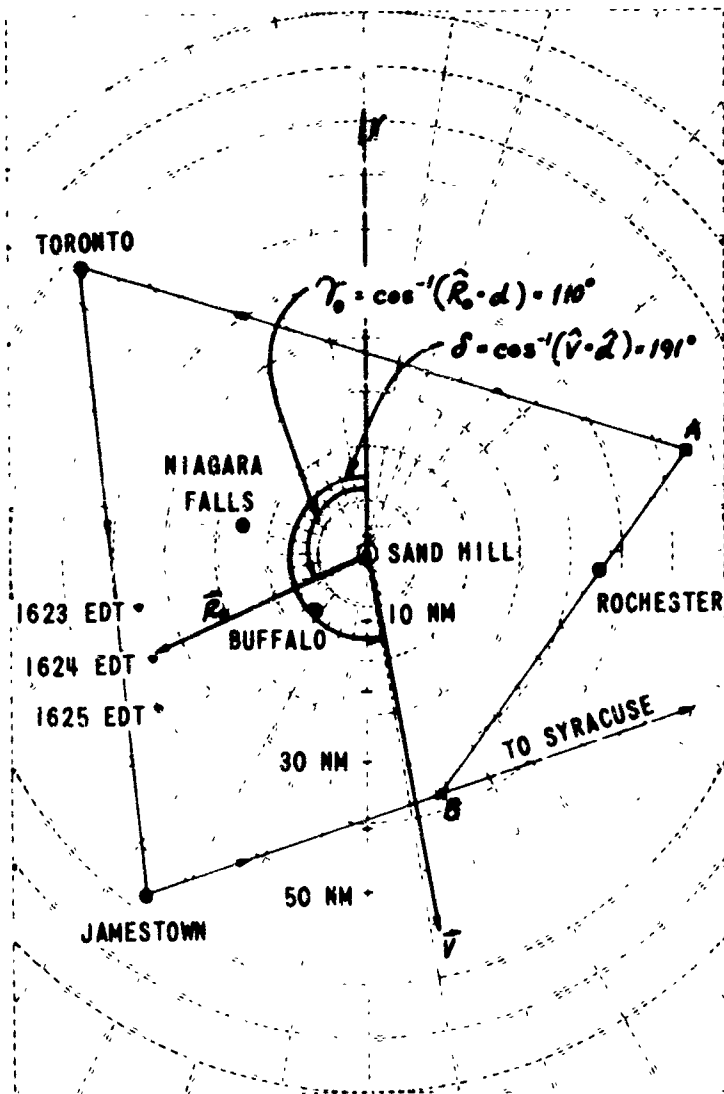aircraft motion or to atmospheric effects.

---

[*]See Equation (C-8).

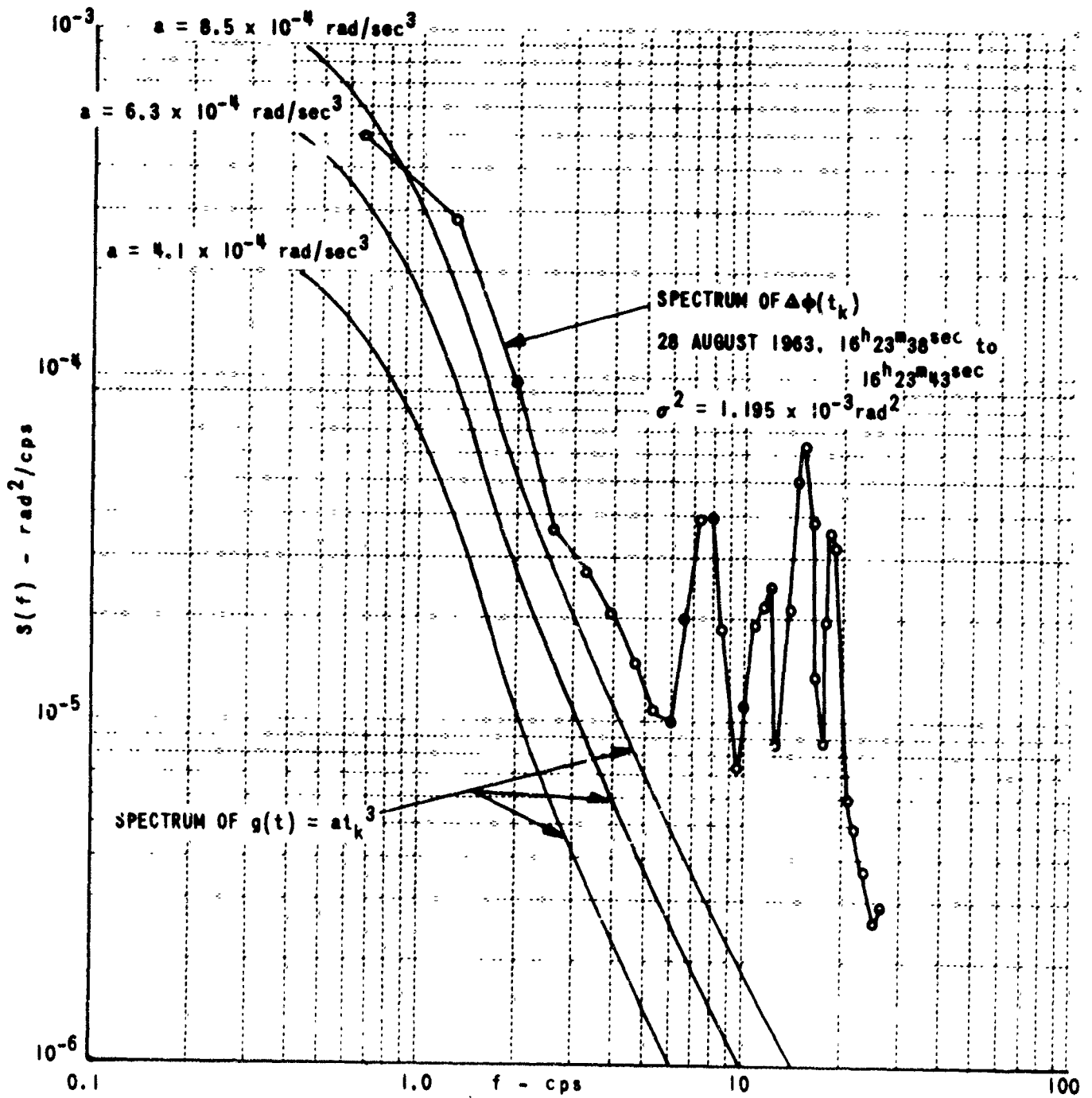Figure C-3-1 AIRCRAFT POSITION DATA FOR 28 AUGUST 1963

Figure C-3-2

C-40

Appendix C-4

Weather Summaries and Aircraft Position Data

August 1, 1963 (Figure C-4-1)

A low pressure trough passed Western New York during the morning hours inducing west to west-northwest winds at the surface and aloft during the afternoon. Showers and thunderstorms dominated the weather picture over Western New York, Southern Ontario, and Lakes Erie and Ontario all afternoon. These storms moved generally eastward to east-southwestward at about 30 mph.

At 1300 EST a line of storms was oriented from Rochester, N. Y. south-southwest through Olean, N. Y. with the strongest cells near Olean. This line of storms continued eastward to lie along a line from about Auburn, N. Y. to Wellsville, N. Y. by 1545 EST.

Thunderstorms covered most of the area north and northwest of Buffalo all afternoon. The southern edge of this group of storms extended from Port Colbourne, Ontario to Lyndonville, N. Y. at 1300 EST. At this time the strongest cells were located near Toronto, Ontario. The southern edge of the area of thunderstorms extended from Hilton, N. Y. west to Welland, Ontario at 1345 EST and extended south to State Highway 33 by 1445 EST. By 1545 EST the southern extreme of the thunderstorms was about where it had been two hours earlier.
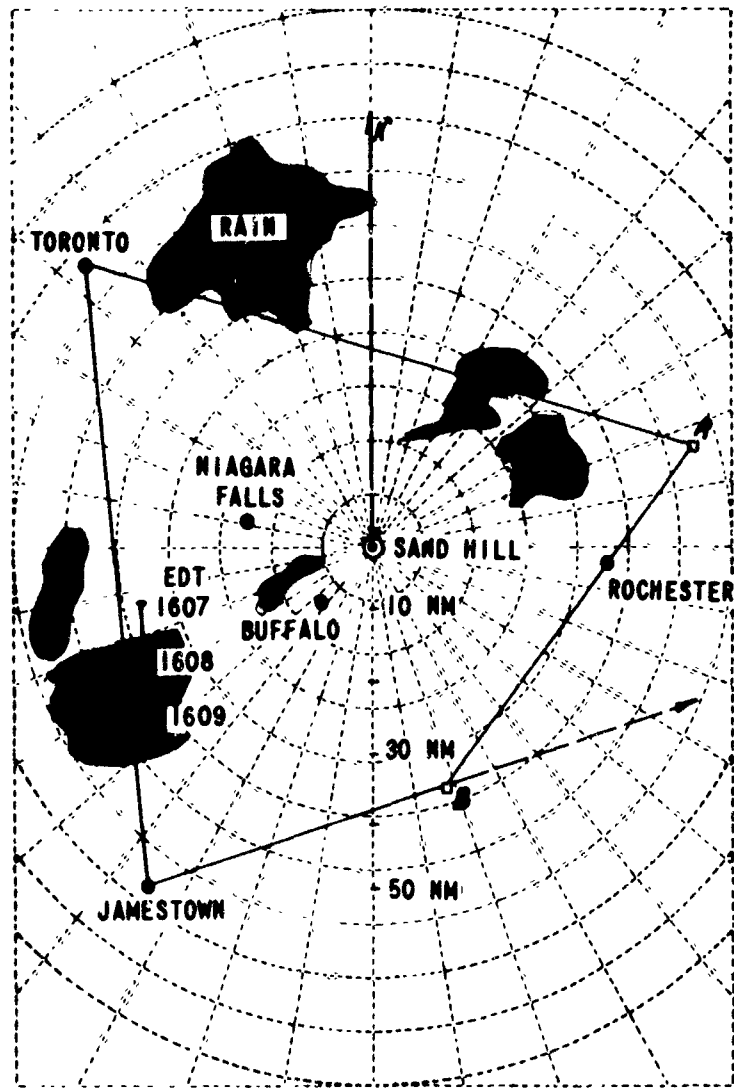
Figure C-4-1 AIRCRAFT POSITION DATA FOR 1 AUGUST 1963

C-42

Throughout this two-hour period the heaviest activity continued along a line south of Lake Ontario from Hilton, N.Y. west almost to Niagara Falls.

Scattered thunderstorms and showers persisted most of the afternoon over Eastern Lake Erie. Little or no activity occurred to the southwest toward Jamestown during the afternoon.

August 22, 1963 (Figure C-4-2)

The same high pressure system that dominated the weather pattern on the 21st persisted but weakened. A few scattered thundershowers developed over Southern Ontario prior to 1545 EST. At 1545 EST a line of showers extended from Bowmansville, N. Y. northwestward to Shelbourne, Ontario and an isolated thundershower was located about ten miles west of Niagara Falls. These storms moved eastward at about 15 mph and dissipated. By 1745 EST there were only a few showers in the vicinity of Toronto, Ontario, and a weak line of showers north of Kingston, Ontario between Peterborough, Ontario and Ogdensburg, N. Y.
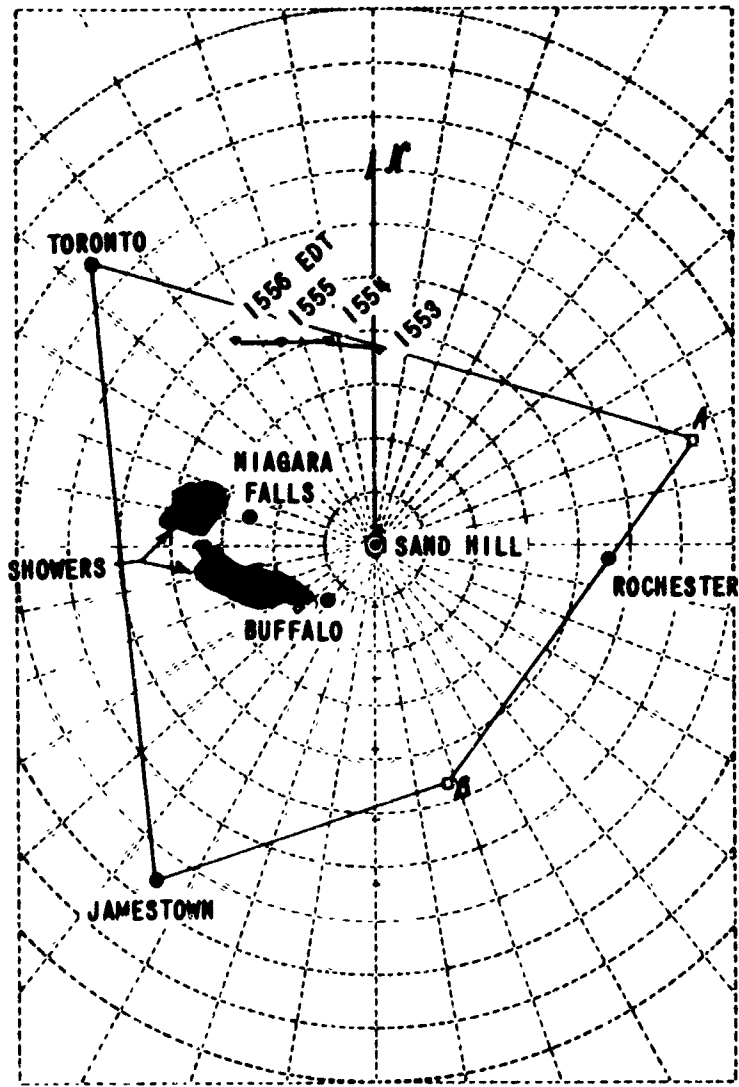
Figure C-4-2 AIRCRAFT POSITION DATA FOR 22 AUGUST 1963

August 27, 1963 (Figure C-4-3)

A Continental Polar high pressure system was centered over Western New York supressing the formation of clouds and precipitation. No significant precipitation was observed within 100 miles of Buffalo.

August 28, 1963 (Figure C-4-4)

The eastward retreat of a Continental Polar high pressure system and the approach of a low from the southwest coupled to produce wide spread showers over Western New York State during ; e afternoon and evening. At 1050 EST, rain showers were ; eported across Southern Ontario moving eastward at about 30 mph.

By 1450 EST a large area of precipitation aloft was spreading across Western New York State and into Central New York. Dry surface air prevented much of the precipitation from reaching the ground until about 1600 EST. By 1645 EST light showers generally extended to the ground and covered the area northwest of a line from Rochester, N. Y. to Erie, Pa. Somewhat heavier showers were then occurring over southern Ontario. Precipitation occurred at Buffalo between 1232 EST and 1248 EST, and from 1610 EST until 1910 EST.
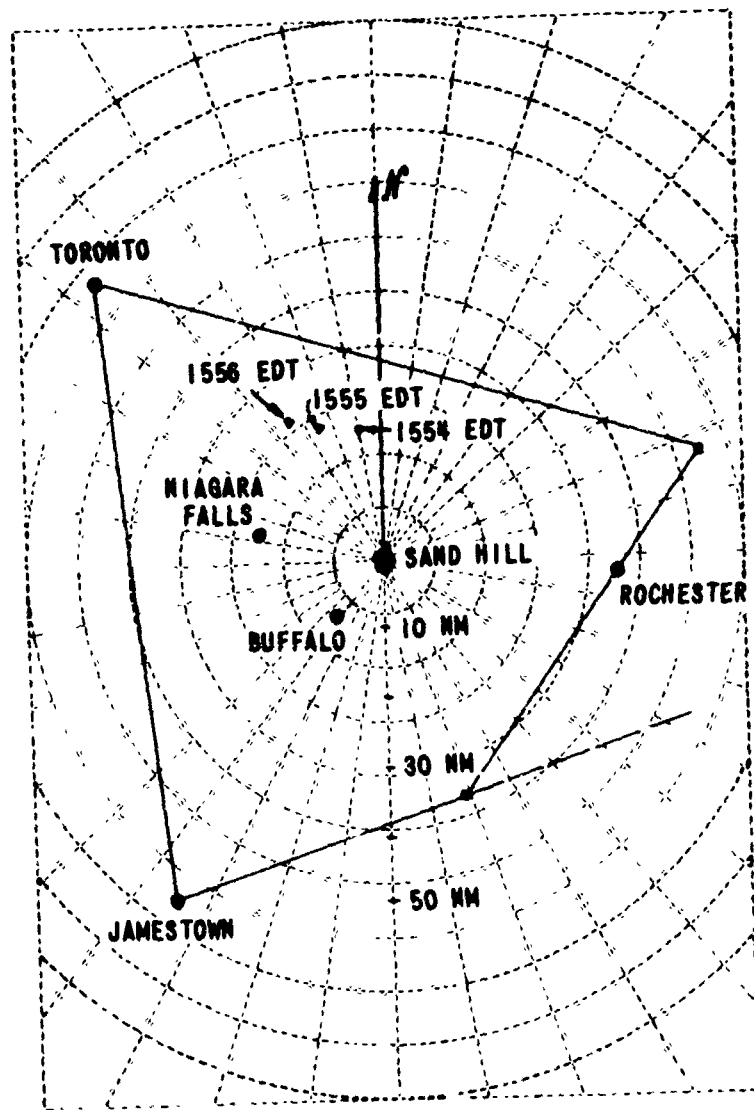
C-45

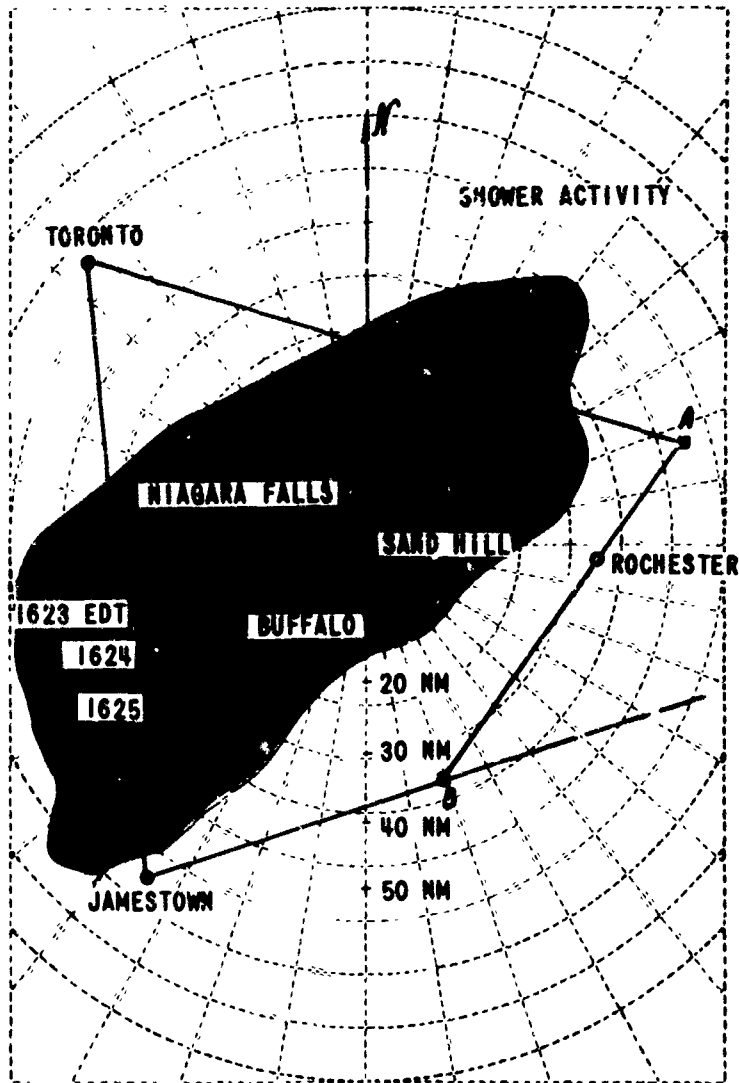Figure C-4-3 AIRCRAFT POSITION DATA FOR 27 AUGUST 1963

Figure C-4-4 AIRCRAFT POSITION DATA FOR 28 AUGUST 1963

C-47

APPENDIX D

Atmospheric Propagation Effects on a
Focussed, Multiple Antenna, Communications System

A complex of four thirty-foot X-band antennas has been proposed for the terminal equipment of a satellite communication system. The four antennas, positioned at the corners of a square 10 miles on a side, will be phased to obtain coherent illumination of the satellite. A passive or semi-active satellite at an altitude of 2200 miles is envisioned and communication between ground terminals is desired whenever the satellite is more than six degrees above the horizon of both terminals.

The purpose of this document is to indicate the nature of the propagation problem and show how the proposed system will be affected by propagation anomalies.

Ground Rules of Study

For the purpose of this study it is assumed that the effective gain of a 60 foot parabola is required at X-band (9000 Mcs). If four thirty-foot antennas are to be used to achieve full gain, they must be continuously phased so that the satellite "rides" the maximum of the interference pattern - the phase of each of the four transmitters must be such that the individual fields at the satellite are in phase. We shall call this phasing operation "focusing" the antenna system.

It should be noted that if a single thirty-foot parabola for transmitting and receiving were used in place of a 60-foot antenna, the system loss would be increased by 12 db. If the transmitter power is divided equally among four 30 foot transmitting antennas, and four phased 30 foot antennas are used for reception but the phasing control is so poor that all phases (between 0 and 2π radians) are equally probable for the transmitting and receiving complexes, then not only will the system loss be increased by 12 db but the received signal will also exhibit deep and quasi-Rayleigh fading. The "Rayleigh" fading will degrade the resultant signal to the point that it would be better to transmit full power into a single 30 foot dish, and receive with a single 30 foot dish. Overall phase control of the transmitting and receiving antennas is clearly important.

Propagation Effects

The refractive index of the earth's atmosphere is a point by point random variable. Experiments conducted by the National Bureau of Standards, among others, indicate that even on a fixed geometrical path, the phase of the received signal is a random variable. When transmissions from a single antenna are received at two other separated antennas and the instantaneous phase difference between the two received signals is recorded, the phase difference is found to be a random variable.

Figure D-1 is a plot of the power spectrum of the random phase difference measured between antennas separated by approximately one mile (NBS Hawaii Data). The length of the propagation path was 15.5 miles with the transmitter situated on a 10,000 ft. peak and the receivers located at an altitude of 100 feet along a baseline perpendicular to the prop.gation path. The spectral density estimates shown are based on 15 minute sample lengths and the spread in the ordinate values is indicative of the variability of the data.

Figure D-2 is a plot of the power spectrum of the phase fluctuation measured along a single path during the NBS Hawaii program (Ref. 1). If $\overline{\phi_0^2}$ is the variance of the phase fluctuations measured along a single path and σ^2 is the variance of the difference of phase between two antennas, then one would expect.

$$\sigma^2(n) = 2\,\overline{\phi_0^2}\,\left[1 - \rho_\phi(n)\right] \tag{D4}$$

where ρ_ϕ is the normalized cross correlation coefficient of the phase fluctuations at the two antennas.

As the separation between the antennas increases, one would expect the variance of the phase fluctuation data to increase until the limiting value of $2\,\overline{\phi_0^2}$ was reached.
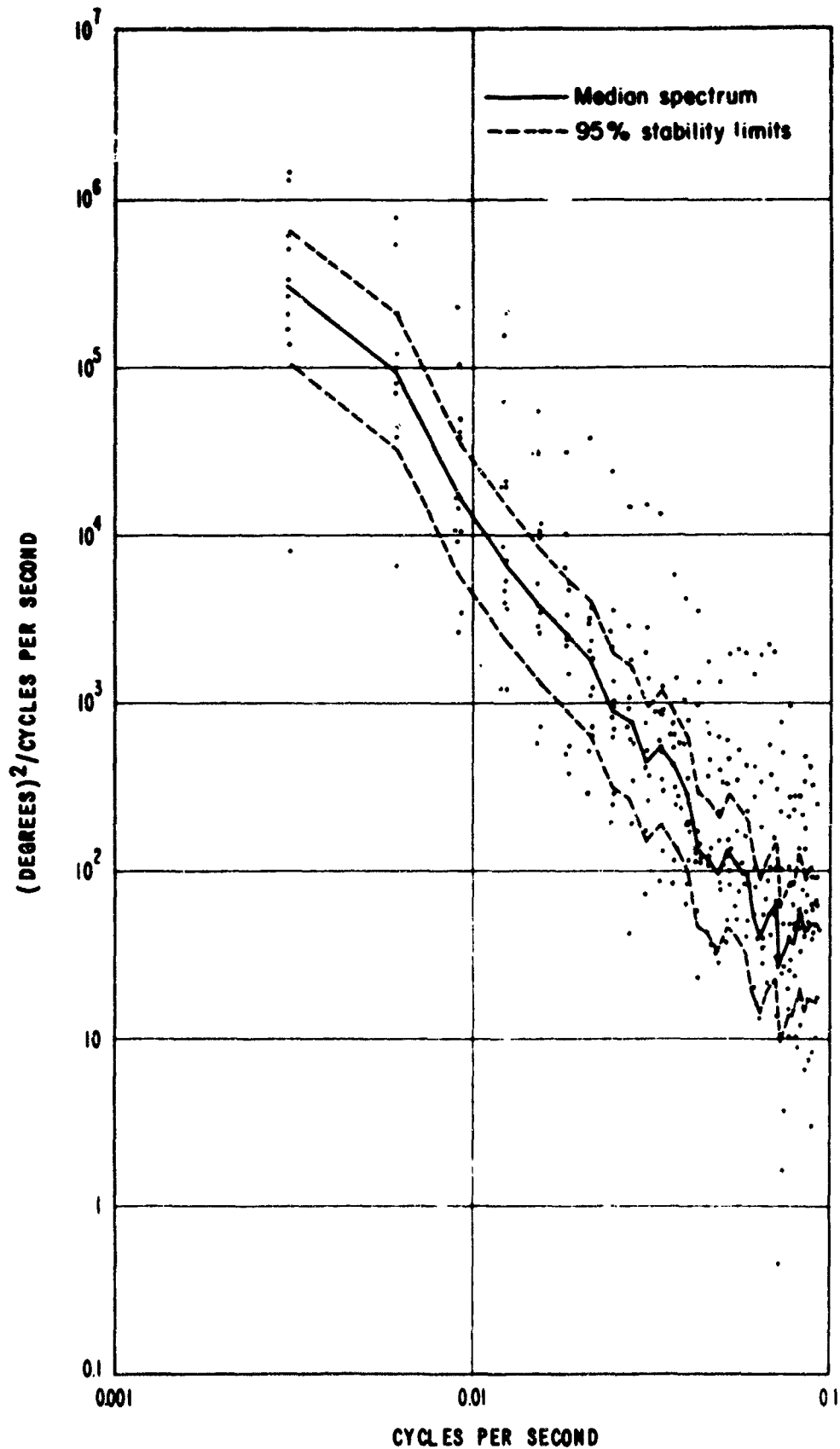
D-3

Figure D-1 HALEAKALA - PUUNENE PATH: POWER SPECTRA OF 9,414 Mc/s
PHASE DIFFERENCE VARIATIONS. BASELINE LENGTH 4847 FT(A-H)
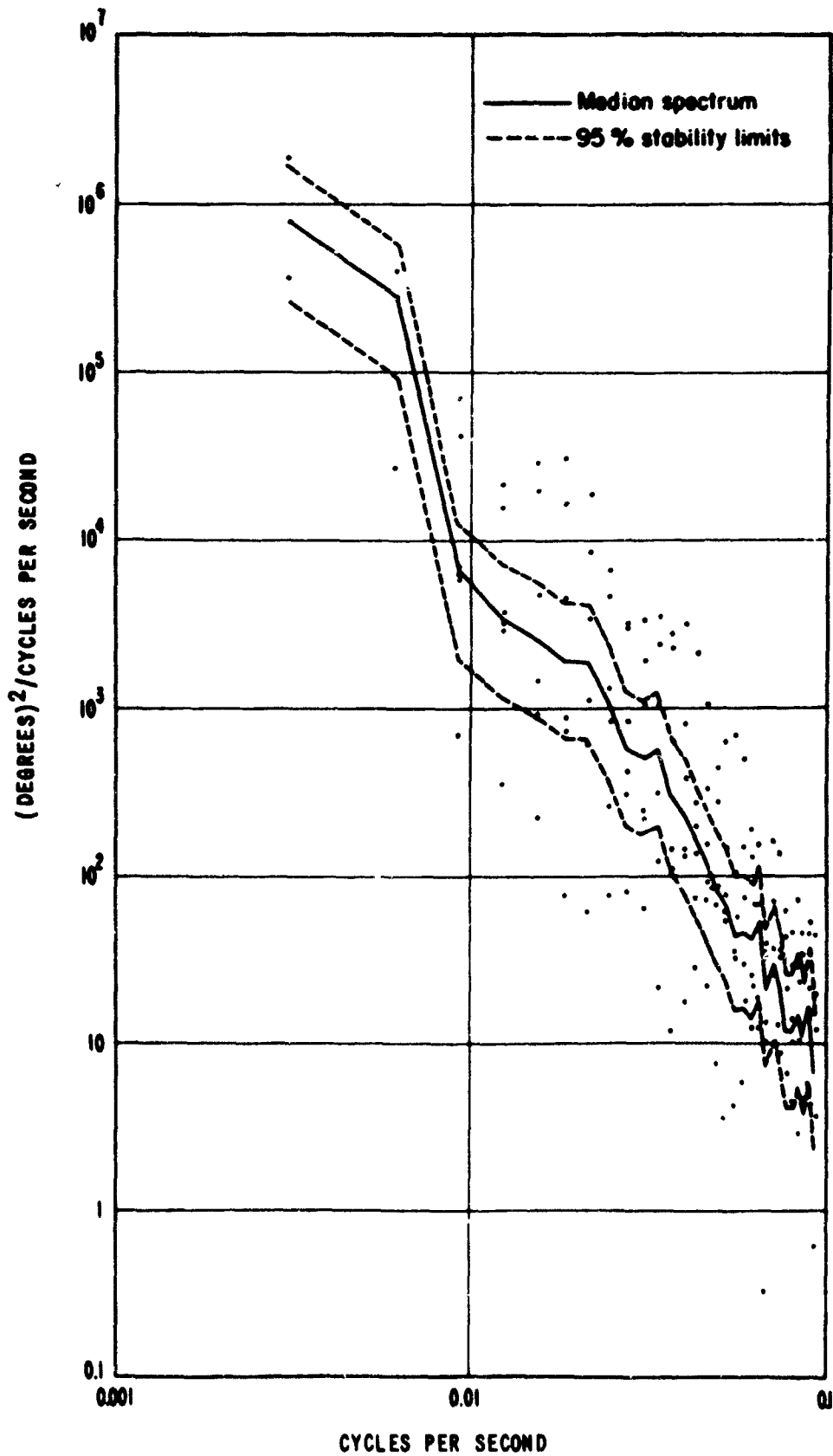
D-4

Figure D-2 HALEAKALA - PUUNENE PATH: POWER SPECTRA OF 9,414 Mc/s
SINGLE-PATH PHASE VARIATIONS

D-5

Figure D-3 is a plot of the variance of the phase difference between two antennas, plotted as a function of base length (also NBS data Ref. 1). There is a general increase in the variance as the baseline length is increased until at something like 1000 feet the curve levels off near the single path value. It should be noted that the data presented are not simultaneous (which accounts for the large spread of variances) and Figure D-3 is presented only to show the trend of the data.

Figure D-4 is a compilation the available single path phase fluctuation data (Thompson, Janes & Kirkpatrick 1960) normalized for frequency and path length.

It should be noted that the median Hawaii data indicate spectral densities an order of magnitude greater than the median of the Colorado data. It should be further noted that during a period in Colorado when a frontal rain storm occurred over the propagation path, an apparent increase in spectral density above the median density of some 20 db was observed and these data are indicated by the circled data points.

As a model of the troposphere, assume that the troposphere extends to 30,000 feet. If we take as a reference tropospheric path, a path at an elevation angle of six degrees extending from ground level to 30,000 feet, our reference tropospheric path length will be 300,000 feet or 3,000,000 wavelengths at X-band. The ordinate value of Figure D-4
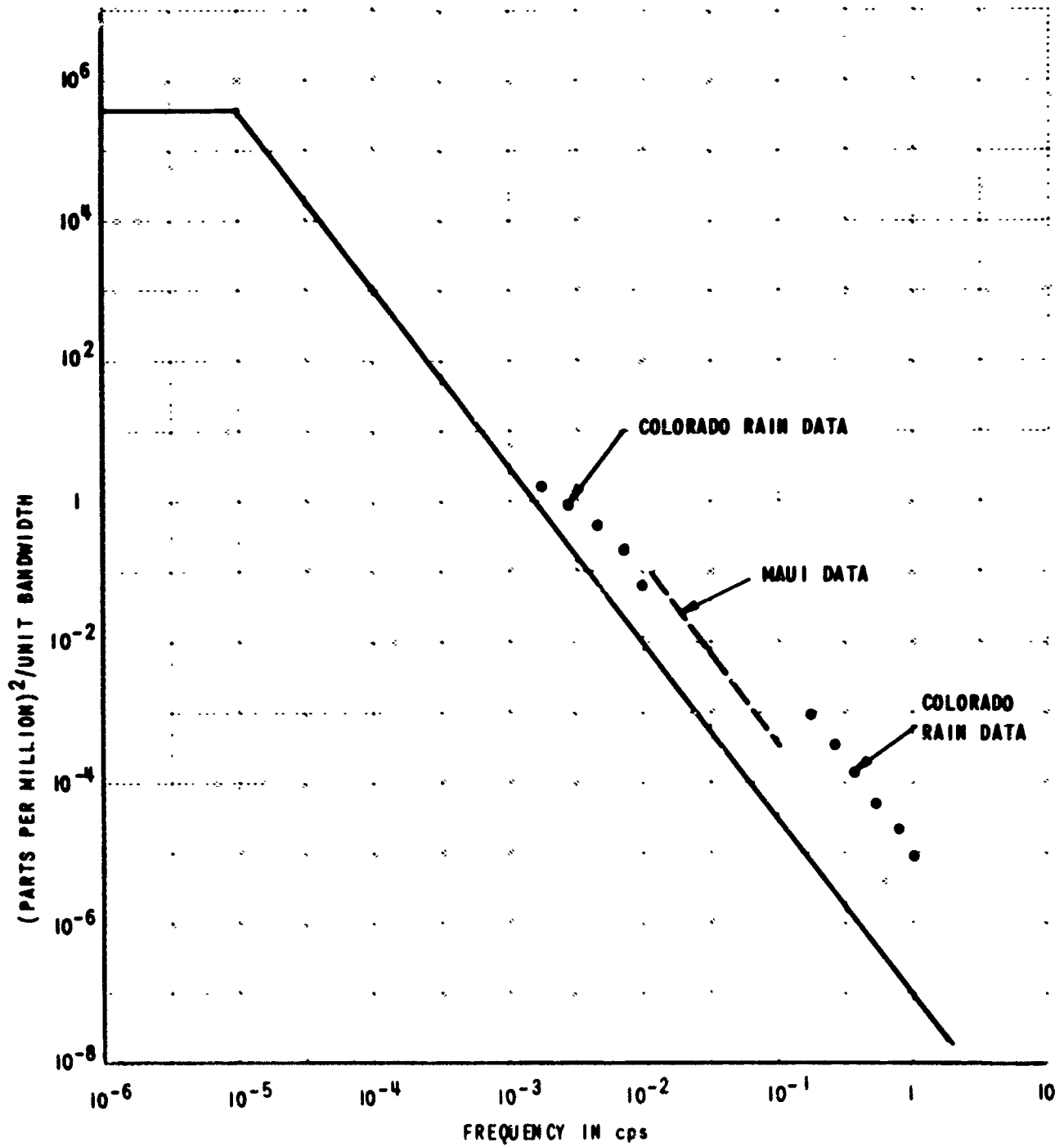
Figure D-3   HALEAKALA-PUUNENE PATH: VARIANCE OF PHASE DIFFERENCE
VERSUS BASELINE LENGTH

D-7

Figure D-4   SPECTRUM OF APPARENT PATH LENGTH VARIATIONS
DUE TO THOMPSON, JANES AND KIRKPATRICK

can then be renormalized to our reference path by multiplying the ordinate by 355 $(2\pi \times 3)^4$ to convert it to square radians/unit bandwidth. This has been done in Figure D-5.

Figure D-5 should now be viewed as the long term power spectrum of the range fluctuations to be expected on a single path for a fixed transmitter and receiver location. We will first derive the phase difference spectrum for an interierometer with a ten mile baseline. If one identifies the temporal fluctuations of phase on a single path with the drift of a turbulent refractive field across the propagation path, it is possible to use single path spectra to deduce the phase difference spectra as follows:

A wind speed of 10 feet per second (appropriate to Maui) would cause spatial irregularities of 10 feet to create a one cycle per second fluctuation. A scale relating frequency to irregularity size is indicated in Figure D-6. Also on Figure D-6 is the estimate of spectral density we shall use in our calculations. As can be seen, it is approximately 25 db more pessimistic than the median Colorado spectral density and approximately 5 db more pessimistic then the Colorado rain data. It is expected that our estimates cf system performance will therefore reflect the worst possible performance. If the system can perform under these circumstances, it should perform well most of the time.

D-9
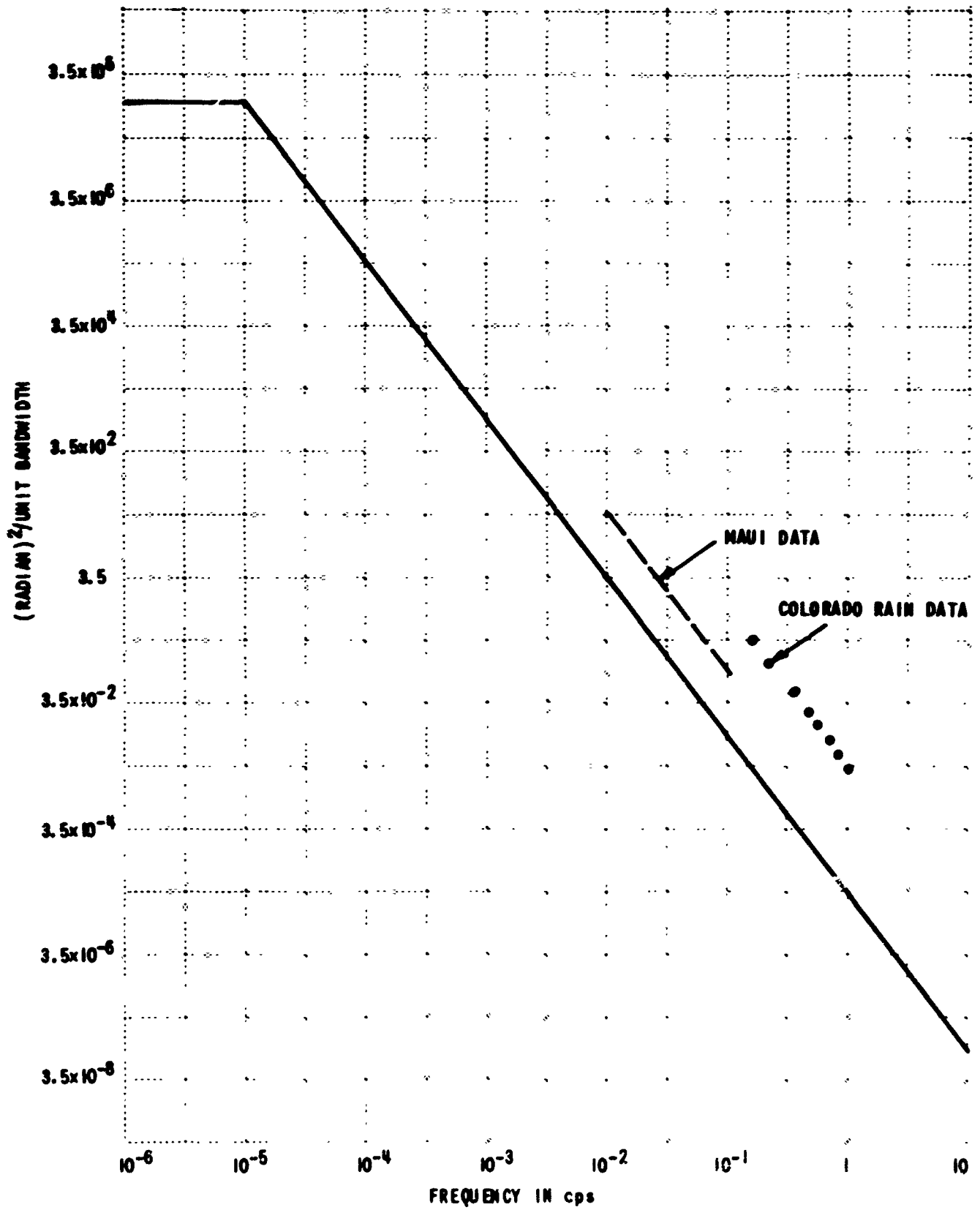
Figure D-5 EXPECTED POWER SPECTRUM OF PHASE FLUCTUATIONS
AT X-BAND FOR A 300,000 FT TROPOSPHERIC PATH

Y-axis: $(RADIAN)^2/UNIT$ BANDWIDTH

X-axis: FREQUENCY IN cps
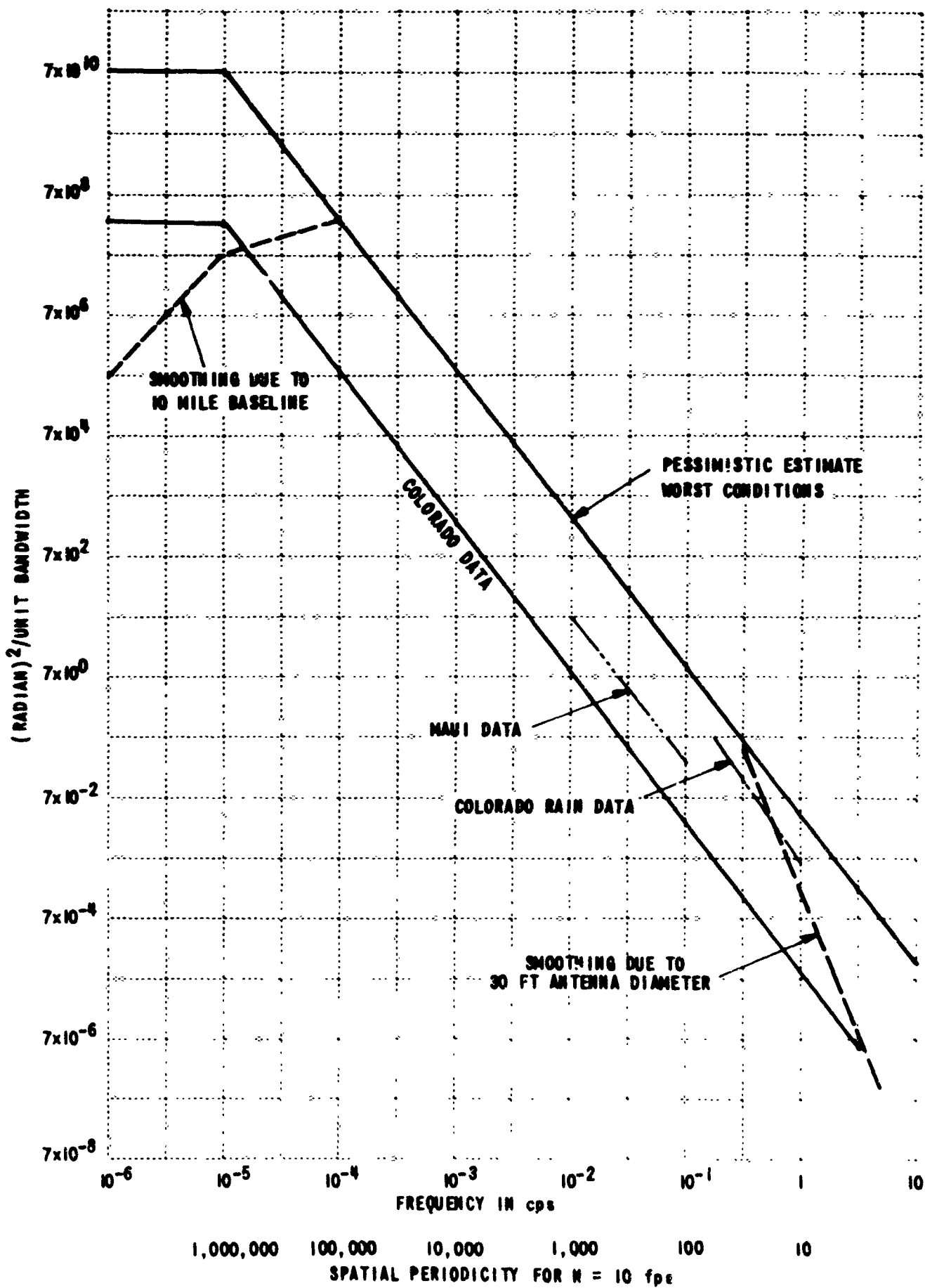
MAUI DATA

COLORADO RAIN DATA

Figure D-6 PHASE DIFFERENCE SPECTRA FOR 10 MILE BASELINE, 300,000 FT PATH IN TROPOSPHERE AT X-BAND - 30 FT ANTENNAS

The spectrum of Figure D-6 has been further modified to account for the finite baseline length. It is clear that irregularities smaller than 10 miles will cause uncorrelated phase fluctuations at the two antennas. Irregularities much larger than 10 miles would cause correlated phase fluctuations at both antennas such that the phase difference between the two antennas would be zero. It can be shown that the effect of the finite baseline can be accounted for by multiplying the single path spectrum with a filter function such that all spatial frequencies greater than twice the baseline length are attenuated with an f^2 slope. The effect of the finite baseline is indicated in Figure D-6 by the labelled dotted line.

We expect that the major contribution to the fluctuation spectrum will be dominated by the altitude region 2000-5000 feet. A wind speed of 20 feet per second appears to be representative of this altitude. Accordingly, the spectrum in Figure D-6 has been modified to take account of a 20 fps wind speed by multiplying the abscissa values by 2 and dividing the ordinate values by 2. The resulting spectrum is presented in Figure 7 and represents the expected rate of the spectrum of phase difference fluctuations experienced by a 10-mile baseline system operating in the U. S. at X-band using 30-foot antennas. It should be noted that this spectrum strictly
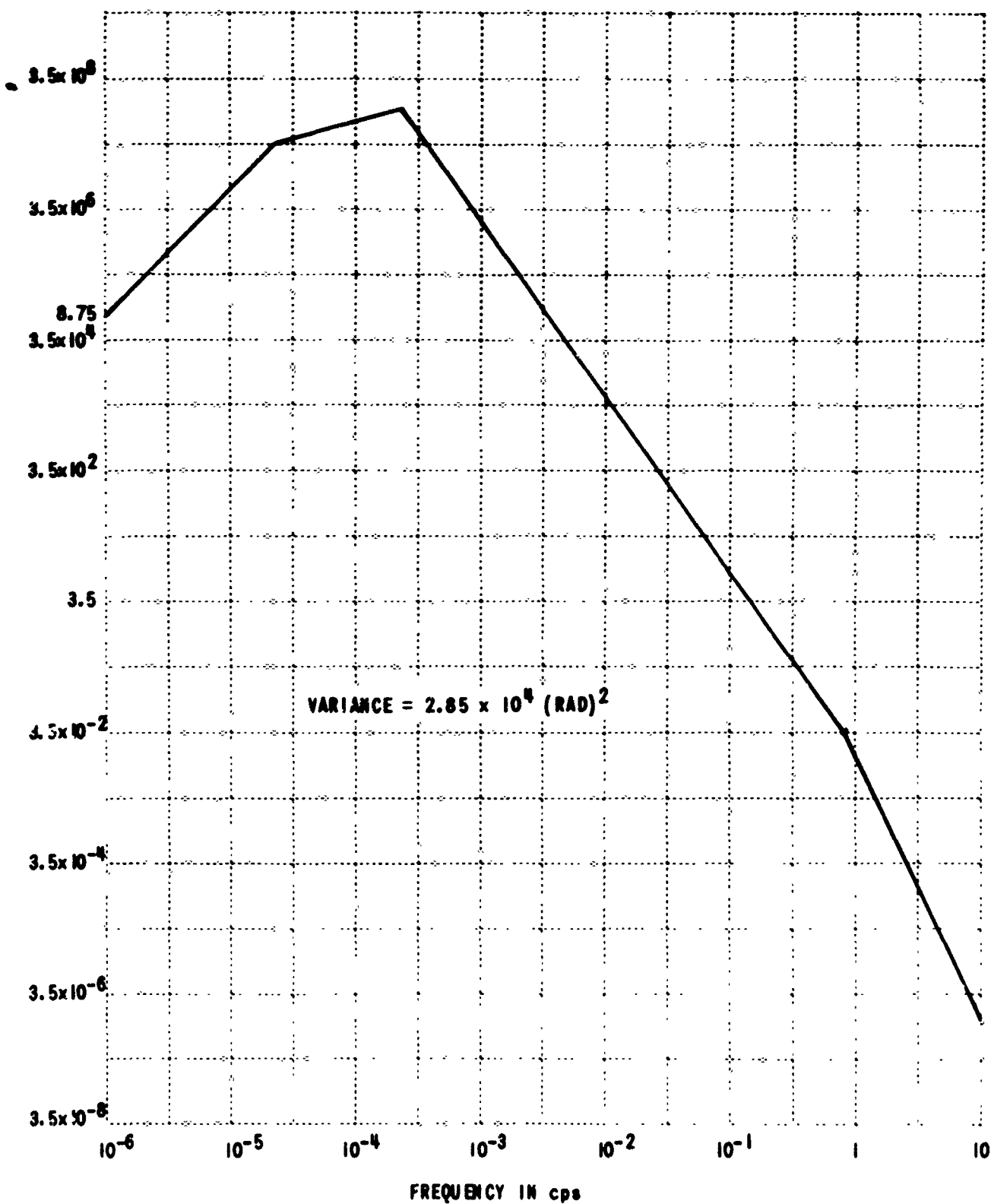
Figure D-7 SPECTRUM OF PHASE DIFFERENCE FLUCTUATIONS EXPECTED IN U. S.
FOR 10 MILE, X-BAND BASELINE USING 30 FT DIAMETER ANTENNAS,
300,000 FT PATH AND MEAN WIND OF 20 FPS

represents the situation when the target is fixed. If the target moves, the line of sight is rotated through a turbulent field and one might expect the spectrum to have higher frequency components than does the spectrum for a fixed target. However in the case of the satellite, the linear velocity of the line of sight evaluated at 2000-5000 feet altitude is much less than the assumed mean wind speed of 20 fps so that the spectrum of Figure D-7 should represent to a high degree of accuracy the spectrum due to the moving line of sight.

Effects of Random Phase Fluctuations on Power Density

Consider that the fields radiated from four separated antennas are so phased that the fields from each antenna are in phase except for a random fluctuation of phase in each field = ϕ_i.

We shall assume that the ϕ_i are independent chance variables having a normal distribution with mean value zero and standard deviation σ.

The net field at the focal spot can be reppesented by

$$|E| = \left| \sum_{i=1}^{4} \exp\{-\phi_i\} \right| \tag{D-2}$$

The probability of observing a value ϕ_j is $p(\phi_j) \, d\phi_j$ $\qquad$ (D-3)

$$p(\phi_j) = \frac{1}{\sqrt{2\pi\sigma^2}} \, exp\left\{-\frac{\phi_j^2}{2\sigma^2}\right\}$$

and since the ϕ_j

are independent

$$p(\phi_j, \phi_k, \phi_\ell, \phi_m) = p(\phi_j) \, p(\phi_k) \, p(\phi_\ell) \, p(\phi_m) \qquad (D-4)$$

Then the mean squared value of the field, $\overline{|E|^2}$, is the power in the

focal spot and in Appendix D-1, it is shown that $\overline{|E|^2}$ is

$$\overline{|E|^2} = 4 + 12 \, exp\left\{-\sigma^2\right\} \qquad (D-5)$$

This formula has the expected variation with σ^2. As the

phase fluctuations go to zero, the power goes to 16, i.e., to 4^2, as

expected. When the phase fluctuations become so large that the four

antennas act as four incoherent sources, the net power is the sum of the

powers radiated (four in this case).

Consider a system in which the appropriate phase corrections

to obtain a focus in the absence of atmospheric refractive fluctuations

were developed from geometry. Although it is highly unrealistic to do

so, we shall further assume that the phase correction so obtained is

perfect and we shall then calculate the effects of the random nature
of the troposphere upon the power density in the focal spot.

$$\text{From Figure D-7,} \quad \sigma^2 = \frac{2.85 \times 10^4}{2} = 1.42 \times 10^4 \text{ per path}$$

Consequently,

$$\overline{|E|^2} = 4 + 12 \, exp\left\{-1.42 \times 10^4\right\} \approx 4$$

or the system is completely incoherent so that some sort of active phase
compensation is required.

Prediction Problem

The previous section considered the degradation caused by
tropospheric phase fluctuations for a stationary satellite of known
position, and indicated that phase fluctuations would cause the system
to fail unless active phase compensation were utilized. In the actual
satellite problem however, the target is moving and we are required
to predict, from our measurements, what the required phase will be
to focus at the satellites' new position.

One way of accomplishing the prediction problem is to measure
the phase difference between antennas as a function of time. If τ
is the travel time between the satellite and the ground station and $\phi(t_i)$

is the phase difference between the two antennas at a time t_1 , the

phase difference at a time $t_2 = t_1 + \tau$

$$\phi(t_2) \approx \phi(t_1) + \phi'(t_1)\, \tau \qquad \text{(D-6)}$$

where $\phi'(t_1)$ is the time derivative of $\phi(t)$ evaluated at $t = t_1$.

The phase correction required to lead the target will be the conjugate

of Equation (D-6). If the atmosphere were ideal and there were no fluctuations

of refractive index all the variables in (D-6) would be proportional to

the time variation of geometrical quantities. Let us denote the phase

factors appropriate to pure geometrical factors with the subscript

zero. Thus

$$\phi(t) = \phi_0(t) + \phi_\wedge(t) \qquad \text{(D-7)}$$

where $\phi_r(t)$ is the random component of the phase difference between

the two antennas.

    Combining (D-6) and (D-7) we see the predicted correction $\Delta\phi(\tau)$

is

$$\Delta\phi(\tau) = -\left\{ \left[\phi_0'(t_1) \right] \tau + \left[\phi_\wedge'(t_1) \right] \tau \right\} \qquad \text{(D-8)}$$

As will be shown, the second term on the right hand side of (D-8) contains a source of error which must be evaluated. Referring to the basic concepts inherent in (D-8), while the rate of change of the phase due to geometrical considerations may lead to a reasonable prediction, the instantaneous frequency (or rate of change of phase) due to the random phase fluctuations may only lead to reasonable predictions if the lead time is short enough. The error in Equation (D-8) lies in the second term which is a stochastic variable. Define

$$\left[\phi_\lambda'(t)\right] \tau = f(t, \tau) \qquad \text{(D-9)}$$

$\phi_\lambda(t)$ and $\phi_\lambda'(t)$ are normally distributed variables. The variance of $f(t,\tau)$ is

$$\text{var}\left[f(t,\tau)\right] = \tau^2 \, \text{var}\left[\phi_\lambda'(t)\right] \qquad \text{(D-10)}$$

In order to evaluate (D-10) we require the variance of $\phi_\lambda'(t)$. It can be shown that if $\phi_\lambda(t)$ has a power spectrum $S(\omega)$, the power spectrum of $\phi_\lambda'(t)$ is $4\pi^2 f^2 S(f)$. The variance of $\phi_\lambda'(t)$ is the area under the curve of the power spectrum and is

$$\text{var}\left[\phi_\lambda'(t)\right] = 4\pi^2 \int_0^\infty f^2 S(f) \, df \qquad \text{(D-11)}$$

The ordinate values of Figure D-7 have been multiplied by $4\pi^2$ and by the square of the value of the abscissa and the result plotted as the power spectrum of $\phi'_\Lambda(t)$ in Figure D-8. The area under the curve, the variance of $\phi'_\Lambda(t)$, is found to be 3.45 (radians/sec)^2. The standard deviation of the instantaneous frequency fluctuation is 1.86 radians/sec.

Now the lead time required for a satellite at 2200 miles and six degrees above the horizon is 0.118 seconds. (This assumes that all data processing on the ground takes place in a few tens of microseconds.)

$$\mathrm{var}\left[f(t,\tau) \right] = \tau^2 \, \mathrm{var}\left[\phi'_\Lambda(t) \right] = .048 \left(radians \right)^2 \qquad (D\text{-}12)$$

On the average, then, we would predict a change in phase, due to the random nature of the atmosphere, which has a variance of .048 (radians)^2. Now the prediction time must be the travel time from the earth to the satellite - but the troposphere extends to only 30,000 feet and the radio wave spends something less than one-half millisecond in the random troposphere. We would like to know how much the phase (difference) can change in a half millisecond.
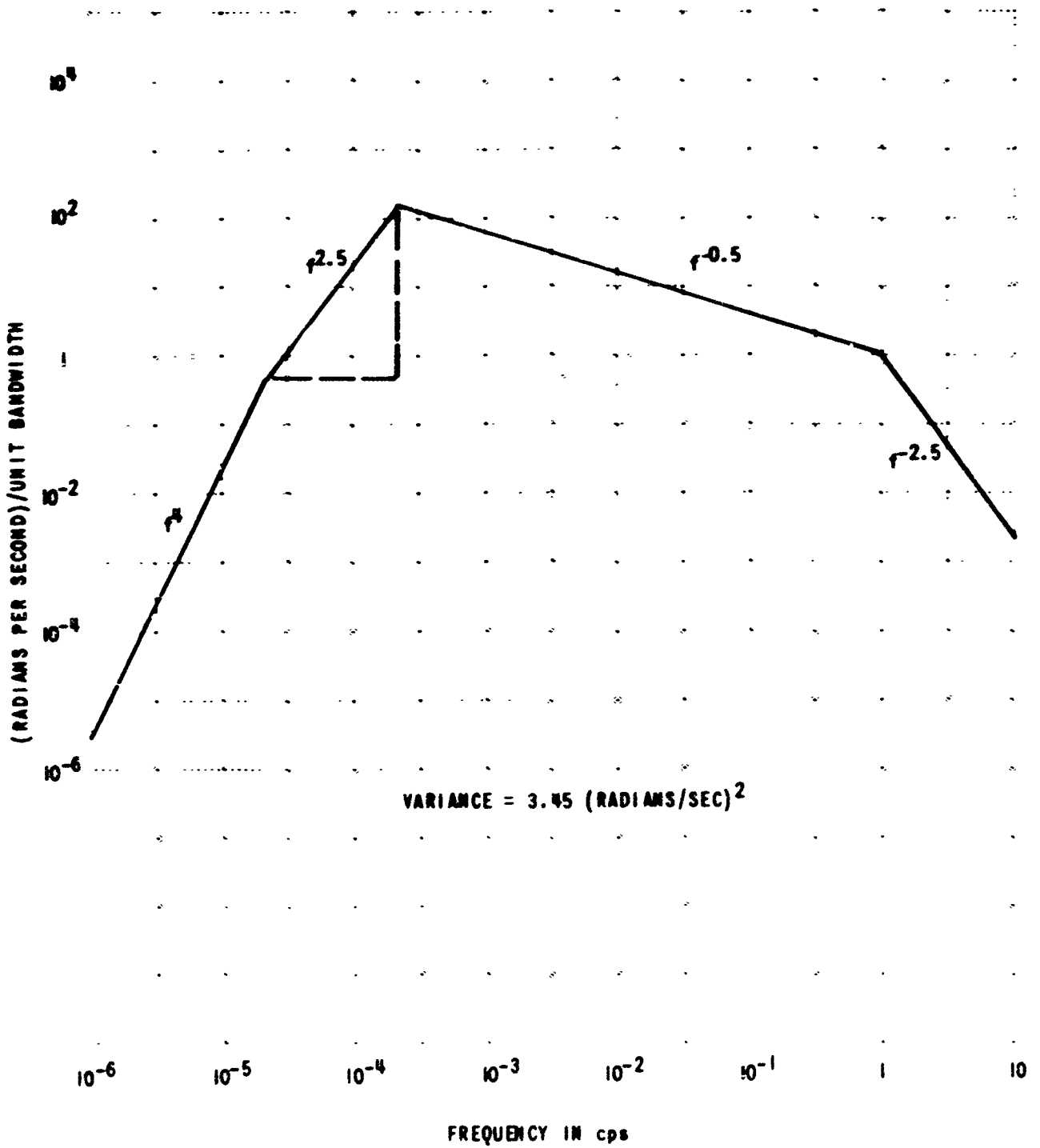
Figure D-8 SPECTRUM OF FLUCTUATIONS OF PHASE RATE

In Appendix D-2 we show that the mean squared phase fluctuation which can occur in a time t' is

$$\text{var}\left[\Delta\phi(t')\right] = 2\,\text{var}\left[\phi(t)\right]\left\{1 - \rho(t')\right\} = (t')^2\,\text{var}\left[\dot{\phi}(t)\right] \quad \text{D-2(7)}$$

The mean square value of the phase change in one millisecond is therefore

$$\text{var}\left[\Delta\phi\right] \approx \frac{1}{4} \times 10^{-6}(3.45) \sim 10^{-6}\,(\text{radians})^2 \quad \text{(D-13)}$$

However, our prediction technique programs a mean squared phase correction of .048 (radians)^2.

The difference between equations (D-13) and (D-14) is an estimate of the mean squared error incurred in this prediction process. Mean squared phase error

$$\sigma^2 = \text{var}\left[\phi(t,\tau)\right] - \text{var}\left[\Delta\phi\right] \approx .048\,(\text{radians})^2 \quad \text{(D-14)}$$
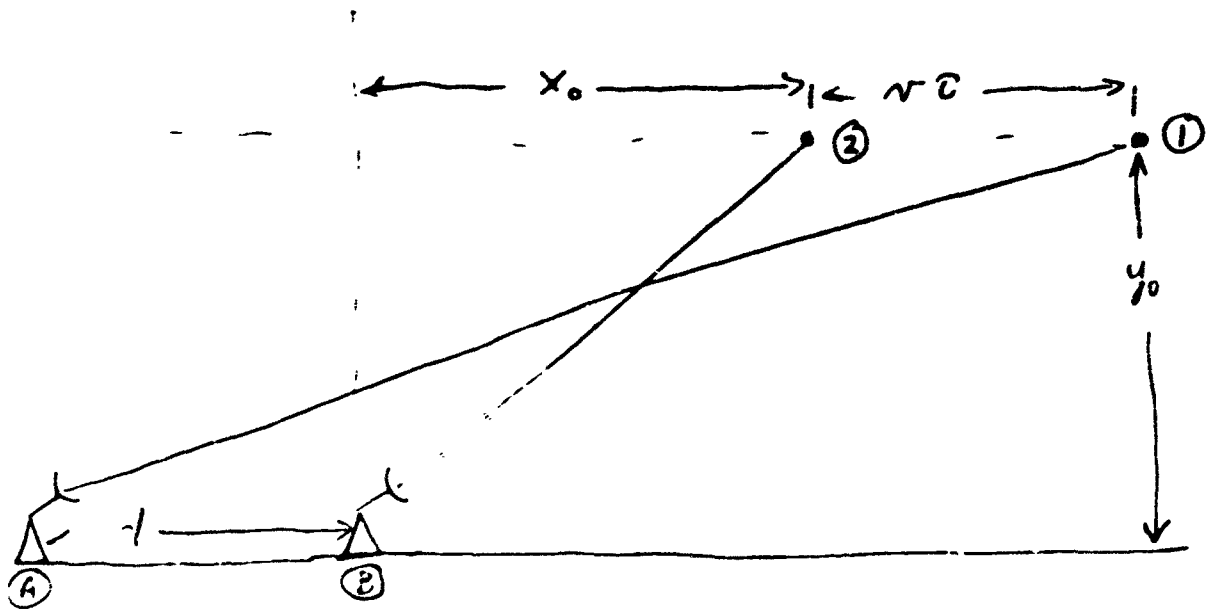
The average power in the focal spot will then be

$$\overline{|E|^2} = 4 + 12\,\exp\left\{-.048\right\} \sim 16 \quad \text{(D-15)}$$

D-21

and this four antenna system will act like a coherent system.

Satellite Velocity Correction

The previous analyses are approximate since they assume that the velocity of the satellite can be neglected in determining the phase difference between antennas at any instant of time.

The above sketch exaggerates the real situation but does clearly illustrate the physical situation. The satellite at position 1 is further from antenna A than it is from antenna B. By the time the signal emitted at position 1 reaches antenna A, a signal emitted from position 2, travelling over the shorter path r_2 will reach antenna B. Satellite position 2 is displaced a distance $N\tau$ (where N is the satellite velocity) from position 1. The time of propagation between position 1 and antenna A is t_{A1}

$$t_{A1} = \frac{r_1}{c} = \frac{r_2}{c} + \tau$$

The phase difference between antennas will therefore be

$$\theta = \omega \tau$$

We solve for θ as follows:

$$c^2 \tau^2 + 2c\tau r_2 + r_2^2 = r_1^2$$

$$c^2 \tau^2 + 2c\tau r_2 + x_o^2 + y_o^2 = [x_o + d + r\tau]^2 + y_o^2$$

Let $z = c\tau$, $\beta = \dfrac{v}{c}$ and rearranging terms we get

$$z^2(1-\beta^2) + 2z[r_2 - \beta(x_o+d)] - (2x_o+d)d = 0$$

$$z = \frac{-[r_2 - \beta(x_o+d)] \mp \left\{ [r_2 - \beta(x_o+d)]^2 + (1-\beta^2)(2x_o+d)d \right\}^{1/2}}{(1-\beta^2)}$$

Let R denote $\left\{ [r_2 - \beta(x_o+d)]^2 + (1-\beta^2)(2x_o+d)d \right\}^{1/2}$

$$R = r_2 \left[1 - \left\{ \frac{2\beta(x_o+d)}{r_2} - \frac{\beta^2 x_o^2}{r_2^2} - \frac{(2x_o+d)d}{r_2^2} \right\} \right]^{1/2}$$

We use the binomial expansion of $(1-x)^{1/2}$, keeping all terms with coefficients less than β^2 or $\frac{1}{r^2}$ to obtain:

$$R = r_2 - \beta(x_0+d) + \frac{\beta^2 x_0^2}{2r_2} + \frac{(x_0+d/2)d}{r_2} - \frac{\beta^2(x_0+d)^2}{2r_2} + \frac{\beta(x_0+d/2)(x_0+d)d}{r_2^2}$$

$$\zeta = 1+\beta^2 \left\{ \frac{(x_0+d/2)}{r_2} \left[1 - \frac{\beta(x_0+d)}{r_2} - \beta^2 \right] \right\} \approx \frac{d(x_0+d/2)}{r_2} \left[1 + \frac{\beta(x_0+d)}{r_2} \right]$$

The phase difference between antennas is θ

$$\theta = \omega \tau = \frac{\omega \zeta}{c} = \frac{2\pi d}{\lambda} \left(\frac{x_0+d/2}{r_2} \right) \left[1 + \frac{\beta(x_0+d)}{r_2} \right] \qquad \text{(D-16)}$$

It should be noted that when the velocity of the satellite is neglected $(\beta \sim 0)$

$$\theta_{STATIC} = \frac{2\pi d}{\lambda} \left[\frac{(x_0+d/2)}{r_2} \right] \approx \frac{2\pi d}{\lambda} \cos E$$

and the usual interferometer formula obtains (far field approximation).

In order to estimate the magnitude of the correction factor $\frac{\beta(x_0+d)}{r_2}$ note that the velocity term is maximized for large x_0 implying low elevation angles. At low elevation angles for a 2200 mile satellite

$$\frac{x_0+d}{r_2} \approx \frac{x_0+d/2}{r_2} = \cos E$$

where E is the elevation angle referred to the center of the array.

Accordingly we write (D-16) as

$$\theta = \frac{2\pi d}{\lambda} \cos E \left[1 + \beta \cos E \right] = \frac{2\pi d}{\lambda} \cos E \left[1 + \frac{N_r}{c} \right] \qquad \text{(D-17)}$$

where N_r is the radial component of the satellite velocity.

An estimate of the magnitude of the velocity dependent term can be made by assuming that after the satellite emits its pulse at position 2, we freeze the satellite in space (a highly theoretical proposition). We then ask, if we transmitted the conjugate of the phase, whether we would focus on the satellite.

At low elevation angles

$$\cos E \sim 1$$

$$\frac{2\pi d}{\lambda} \cos E \sim \frac{2\pi (5 \times 10^4)}{10^{-1}} = 3.16 \times 10^{-6} \text{ radians}$$

$$\beta \cos E \sim \beta = \frac{8 \times 10^3}{3 \times 10^8} = 2.67 \times 10^{-5}$$

The correction term is of the order of 84 radians and since, in general, the correction term will not be an integral multiple of 2π radians, it must be accounted for if deep fading signals are to be avoided.

D-25

Since the required correction is proportional to d, the distance between antennas, decreasing the separation between antennas as well as increasing the minimum elevation angle will lessen the problem. For example, an antenna separation of 500 feet and elevation angle of 45° will result in a required correction of approximately 1/2 radian which _may_ be acceptable. We conclude, however, that an active phase compensation system, with an added satellite velocity correction, will be required to obtain a fully coherent, efficient communication system using widely spaced anternas.

Summary and Recommendations

In Appendix D-3 we examine the accuracy of a linear prediction technique and find that errors due to linear prediction are negligibly small. In general then we have shown that using "typical" propagation data, the X-band communication system under consideration can be used down to elevation angles as low as 6° if an appropriate correction for the satellite velocity is added to the active phase compensation mode of operation.

It should be recognized that this fully coherent system at low elevation angles has only a 12 db advantage over a far simpler system employing single thirty foot dishes at each terminal. The cost of the fully coherent system is not known but ultimately the question must be answered in terms of just how much 12 db is worth.

Up to this point, we have not considered the question of system bandwidth. It is clear, because of the separation between antennas, that in addition to the radio frequency phasing required to focus the antenna system, envelope delay must be inserted in the system. Without envelope delay, the maximum allowable bit rate would be something like 3.57×10^3. The maximum multipath delay for a 14 mile baseline is 140 microseconds. If the data pulse from each transmitter is twice that length, the transmissions from each antenna will overlap and coherent operation can be obtained. While the bit rate is greater than that normally available via conventional HF circuits it is still a far cry from the minimum desirable information bandwidth of two megacycles. Envelope delay is a real requirement then. If bandwidths of greater than two megacycles are to be achieved, the range from each transmitter to the satellite must be known to better than one-half microsecond. The ability to measure the range of each antenna to the satellite and the adjust envelope delay will set the limits on the maximum bandwidth of the system.

REFERENCES

1. K. A. Norton, J. W. Herbstreit, et al. National Bureau of Standards Monograph 33, November 1, 1961.

2. M. C. Thompson, H. B. Janes and A. W. Kirkpatrick, JGR $\underline{65}$, 193, 1960.

3. Handbook of Geophysics, Revised Edition, USAF, ARDC, Macmillan Co., New York, 1960.

Calculation of Power in Focal Spot

Let the fields radiated by each of four antennas have unit amplitude. Let each field have a phase factor which is the sum of two terms:

1) a term to insure perfect focus in the absence of propagation phase fluctuations;

2) a term $\phi_j(t)$ which represents the atmospheric propagation fluctuations.

The second term is a random variable. The available experimental data show that the $\phi_j(t)$ are normally distributed and, if the antennas are separated by more than 100 meters, that phase fluctuations are uncorrelated. Accordingly,

$$p(\phi_j) = \frac{1}{\sqrt{2\pi\sigma^2}} \exp\left\{-\frac{\phi_j^2}{2\sigma^2}\right\} \qquad \text{where } \sigma^2 \text{ is the variance of } \phi_j$$

$$p(\phi_j, \phi_k, \phi_\ell, \phi_m) = \prod_{m=1}^{4} \frac{1}{\sqrt{2\pi\sigma_m^2}} \exp\left\{-\frac{\phi_m^2}{2\sigma_m^2}\right\}$$

Defining the resulting field magnitude as R, we write

$$R = \left| \sum_{j=1}^{4} exp\{i\,\phi_j\} \right| = \left| \sum_{j}^{4} \cos\phi_j + i \sin\phi_j \right|$$

$$R^2 = \left(\sum_{j}^{4} \cos\phi_j \right)^2 + \left(\sum_{j}^{4} \sin\phi_j \right)^2$$

$$R^2 = 4 + 2\left[\cos\phi_1 \cos\phi_2 + \cos\phi_1 \cos\phi_3 + \cos\phi_2 \cos\phi_3 \right] + 2\left[\sin\phi_1 \sin\phi_2 + \sin\phi_1 \sin\phi_3 \right.$$
$$\left. + \sin\phi_2 \sin\phi_3 \right]$$

$$\overline{R^2} = 4 + 2\iint [\text{cosine terms}]\, p(\phi_i; \phi_j)\, d\phi_i\, d\phi_j + 2\iint (\text{Sine terms})\, p(\phi_i, \phi_j)\, d\phi_i\, d\phi_j$$

Let us look at cosine terms

$$\iint \cos\phi_1 \cos\phi_2\, p(\phi_1, \phi_2)\, d\phi_1\, d\phi_2 = \left[\int \cos\phi_1\, p(\phi_1)\, d\phi_1 \right]^2$$

because of the independence of the phases

$$\int_{-\infty}^{\infty} \cos\phi_1 \, \frac{1}{\sqrt{2\pi\sigma^2}} exp\left\{ -\frac{\phi_1^2}{2\sigma^2} \right\} d\phi_1 = e^{-\sigma^2/2}$$

so that

$$\iint (\cos \text{ terms})\, p(\phi_i, \phi_j)\, d\phi_i\, d\phi_j = 12\, e^{-\sigma^2}$$

The sine term integrals are of form

$$\int \int \sin\phi_j \, \sin\phi_k \, P(\phi_j, \phi_k) \, d\phi_j \, d\phi_k = \left[\int_{-\infty}^{\infty} \sin\phi_i \, P(\phi_i) \, d\phi_i \right]^2$$

because of the independence of the probability distributions and

$$\int_{-\infty}^{\infty} \sin\phi_i \, \frac{1}{\sqrt{2\pi\sigma^2}} \, \exp\left\{ -\frac{\phi_i^2}{2\sigma^2} \right\} = 0$$

Therefore

$$\overline{R^2} = 4 + 12 \, e^{-\sigma^2}$$

We can readily generalize our result to the power in the focal spot resulting from the phasing of n identical antennas and transmitters

$$\overline{R^2} = n + n(n-1) \, e^{-\sigma^2}$$

For n sufficiently large and σ^2 small

$$\overline{R^2} \approx n^2 \, e^{-\sigma^2}$$

APPENDIX D-2

Rate of Phase Fluctuation

If $\phi(t)$ is a chance variable from a Gaussian process such that the probability of obtaining a value between ϕ and $\phi + \Delta\phi$ is $P(\phi)d\phi$ then

$$P(\phi) = \frac{1}{\sqrt{2\pi\sigma^2}} \, exp\left\{-\frac{\phi^2}{2\sigma^2}\right\}$$

D-2(1)

The probability that ϕ can change by an amount $\Delta\phi$ in a time τ is

$$P(\Delta\dot\phi) = \frac{1}{\sqrt{4\pi\sigma^2[1-\rho(\tau)]}} \, exp\left\{-\frac{(\Delta\phi)^2}{4\sigma^2[1-\rho(\tau)]}\right\}$$

D-2(2)

where σ^2 is the variance of ϕ

$\rho(\tau)$ is the normalized autocorrelation function of $\phi(t)$

It is clear that $\Delta\phi$ is normally distributed with variance

$$var(\Delta\phi) = 2\sigma^2[1-\rho(\tau)] = [2\,var\,\phi(t)][1-\rho(\tau)]$$

D-2(3)

Linear Prediction Theory

In this section we shall estimate the error accruing from simple linear prediction. The basic problem arises from the fact that linear prediction is a first order approximation to a power series expansion. A function analytic in a region may be expanded in a converging power series

$$f(x+\alpha) = f(x) + f'(x)(\alpha) + f''(x)\frac{\alpha^2}{2!} + f'''(x)\frac{\alpha^3}{3!}$$

Linear prediction uses only the first derivative of the function and assumes that the higher order terms are negligble.

Consider the geometry sketched in the accompanying figure. r_1 is the radius of the earth. r_2 represents the radius of the satellite orbit. ϕ, the phase difference between two antennas separated a distance d (using far-field approximation)

$$\phi = \frac{2\pi d}{\lambda}\sin\chi = \frac{2\pi d}{\lambda}\frac{\sin\theta}{[1+k^2-2k\cos\theta]^{1/2}} = k\, f(\theta)$$

where $\quad K = \dfrac{2\pi d}{\lambda}$

$$f(\theta) = \dfrac{\sin\theta}{\sqrt{1 + k^2 - 2k\cos\theta}}$$

$$k = \dfrac{r_1}{r_2}$$

Defining $\quad \psi = \phi /_K = \sin\chi$

$$\psi(t+\tau) = \psi(t) + \psi'(t)\,\tau + \psi''(t)\dfrac{\tau^2}{2!} + \psi'''(t)\dfrac{\tau^3}{3!} + \cdots$$

$$\mathcal{E}_Y = \psi(t+\tau) - \left[\psi(t) + \psi'(t)\,\tau\right] = \psi''(t)\dfrac{\tau^2}{2!} + \psi'''(t)\dfrac{\tau^3}{3!} + \cdots$$

$\mathcal{E}_Y$ is the error in ψ we make using linear prediction theory

$$\psi'(t) = \dfrac{d\psi}{d\chi}\,\dfrac{d\chi}{d\theta}\,\dfrac{d\theta}{dt} = \omega\,\dfrac{d\psi}{d\chi}\,\dfrac{d\chi}{d\theta}$$

$$\psi''(t) = \omega^2\left[\dfrac{d\psi}{d\chi}\,\dfrac{d^2\chi}{d\theta^2} + \dfrac{d^2\psi}{d\chi^2}\left(\dfrac{d\chi}{d\theta}\right)^2\right]$$

$$\psi'''(t) = \omega^3\left[\dfrac{d\psi}{d\chi}\,\dfrac{d^3\chi}{d\theta^3} + 3\dfrac{d^2\psi}{d\chi^2}\,\dfrac{d\chi}{d\theta}\,\dfrac{d^2\chi}{d\theta^2} + \dfrac{d^3\psi}{d\chi^3}\left(\dfrac{d\chi}{d\theta}\right)^3\right]$$

$$\dot{y}'(t) = \omega \cos \chi \, \frac{d\chi}{d\theta}$$

$$\dot{y}''(t) = \omega^2 \left[\cos \chi \, \frac{d^2\chi}{d\theta^2} - \sin \chi \left(\frac{d\chi}{d\theta} \right)^2 \right]$$

$$\dot{y}'''(t) = \omega^3 \left[\cos \chi \, \frac{d^3\chi}{d\theta^3} - 3 \sin \chi \, \frac{d\chi}{d\theta} \, \frac{d^2\chi}{d\theta^2} - \cos \chi \left(\frac{d\chi}{d\theta} \right)^3 \right]$$

$$\frac{d\chi}{d\theta} = \frac{1 - k \cos \theta}{1 + k^2 - 2k \cos \theta}$$

$$\frac{d^2\chi}{d\theta^2} = \frac{(k^2 - 1) k \sin \theta}{\left(1 + k^2 - 2k \cos \theta \right)^2}$$

$$\frac{d^3\chi}{d\theta^3} = \frac{k (k^2 - 1) \left[(1 + k^2) \cos \theta - 2k (1 + \sin^2 \theta) \right]}{\left[1 + k^2 - 2k \cos \theta \right]^3}$$

We shall evaluate the error incurred in linear prediction theory by neglecting the higher order terms of the power series at Zenith angles $\chi = 0$, 78, and 84 degrees.

$\underline{\chi = 0°}$

After some algebra

$$\mathcal{E}_\psi \qquad = -1.56 \times 10^{-14}$$

$$\mathcal{L}\, \psi'(t) \qquad = 4.38 \times 10^{-5}$$

$$\underline{\underline{\chi = 78°}}$$

$$\mathcal{E}_\psi = -7.86 \times 10^{-10} + 2.16 \times 10^{-14} + \ldots$$

$$\mathcal{L}\, \psi'(t) = 7.72 \times 10^{-6}$$

$$\chi = 84°$$

$$\mathcal{E}_\psi = -5.79 \times 10^{-10} + 1.72 \times 10^{-14}$$

$$\mathcal{L}\, \psi'(t) = 3.4 \times 10^{-6}$$

It would appear therefore that linear prediction theory is more than adequate.

APPENDIX D-4

Far Field Approximation

With reference to Figure D-4-1 on page D-39:

$$r_a^2 = r_1^2 + r_2^2 - 2r_1 r_2 \cos(\theta - \alpha)$$

$$r_b^2 = r_1^2 + r_2^2 - 2r_1 r_2 \cos(\theta + \alpha)$$

$$S \equiv r_b - r_a = \left[r_1^2 + r_2^2 - 2r_1 r_2 \cos(\theta + \alpha) \right]^{1/2} - \left[r_1^2 + r_2^2 - 2r_1 r_2 \cos(\theta - \alpha) \right]^{1/2}$$

$$S = r_2 \left\{ \left[1 + k^2 - 2k \cos(\theta + \alpha) \right]^{1/2} - \left[1 + k^2 - 2k \cos(\theta - \alpha) \right]^{1/2} \right\}^{1/2}$$

$\phi_t =$ exact phase difference between the two antennas $= \dfrac{2\pi S}{\lambda}$

$$\phi_A = \frac{2\pi r_2}{\lambda} \left[\gamma(\theta + \alpha) - \gamma(\theta - \alpha) \right]$$

where $\gamma(\theta) \equiv \left(1 + k^2 - 2k \cos\theta \right)^{1/2}$

$$\phi_A(\theta + \omega\tau) = \phi_A(\theta) + \phi'(\theta)\, \omega\tau + \phi_A''(\theta) \frac{(\omega\tau)^2}{2!} + \cdots$$

Error in ϕ_A caused by neglect of higher order terms is ε_{ϕ_A}

$$\varepsilon_{\phi_A} = \frac{1}{2} \phi''(\theta) (\omega\tau)^2 + \frac{(\omega\tau)^3}{3!} \phi_A'''(\theta) + \cdots$$

$$\phi_A''(\theta) = \frac{2\pi r_2}{\lambda}\left[g''(\theta \cdot \alpha) - g'(\theta - \alpha)\right]$$

$$\phi_A'''(\theta) = \frac{2\pi r_2}{\lambda}\left[g'''(\theta + \alpha) - g''(\theta - \alpha)\right]$$

$$\phi_A''(\theta) = \frac{2\pi r_2}{\lambda}\left[\left(g''(\theta) + g'''(\theta)\alpha + g^{(4)}\frac{(\theta)\alpha^2}{2!} + \cdots \right) - \left(g''(\theta) - \alpha g'''(\theta) + \frac{\alpha^2 g^{(4)}(\theta)}{2!} + \cdots \right)\right]$$

$$\phi_A''(\theta) = \frac{2\pi r_2}{\lambda}\left[2\alpha\, g'''(\theta) + \cdots \right]$$

$$\phi_A'''(\theta) = \frac{2\pi r_2}{\lambda}\left[2\alpha\, g^4(\theta) + \cdots \right]$$

$$g(\theta) = \left(1 + k^2 - 2k\cos\theta\right)^{1/2}$$

$$g'(\theta) = \frac{1}{2}\frac{2k\sin\theta}{(1 + k^2 - 2k\cos\theta)^{1/2}} \equiv k\, f'(\theta)$$

$$\phi_A''(\theta) = 2\alpha k \left(\frac{2\pi r_2}{\lambda}\right) f''(\theta)$$

$$\phi_A'''(\theta) = 2\alpha k \left(\frac{2\pi r_2}{\lambda}\right) f'''(\theta)$$

We must compare

$$\varepsilon_\phi = \frac{1}{2}\left(\frac{2\pi d}{\lambda}\right) f''(\theta)\, (\omega\tau)^2 \qquad \text{where } d = \text{antenna baseline}$$

with

$$\varepsilon_{\phi_A} = \frac{1}{2}\, 2\alpha k \left(\frac{2\pi r_2}{\lambda}\right) f''(\theta)\,(\omega\tau)^2$$

$$\frac{\varepsilon_\phi}{\varepsilon_{\phi_A}} = \frac{\frac{2\pi d}{\lambda}}{2\alpha \frac{r_1}{r_2}\left(\frac{2\pi r_2}{\lambda}\right)} = \frac{d}{2\alpha r_1}\,.$$
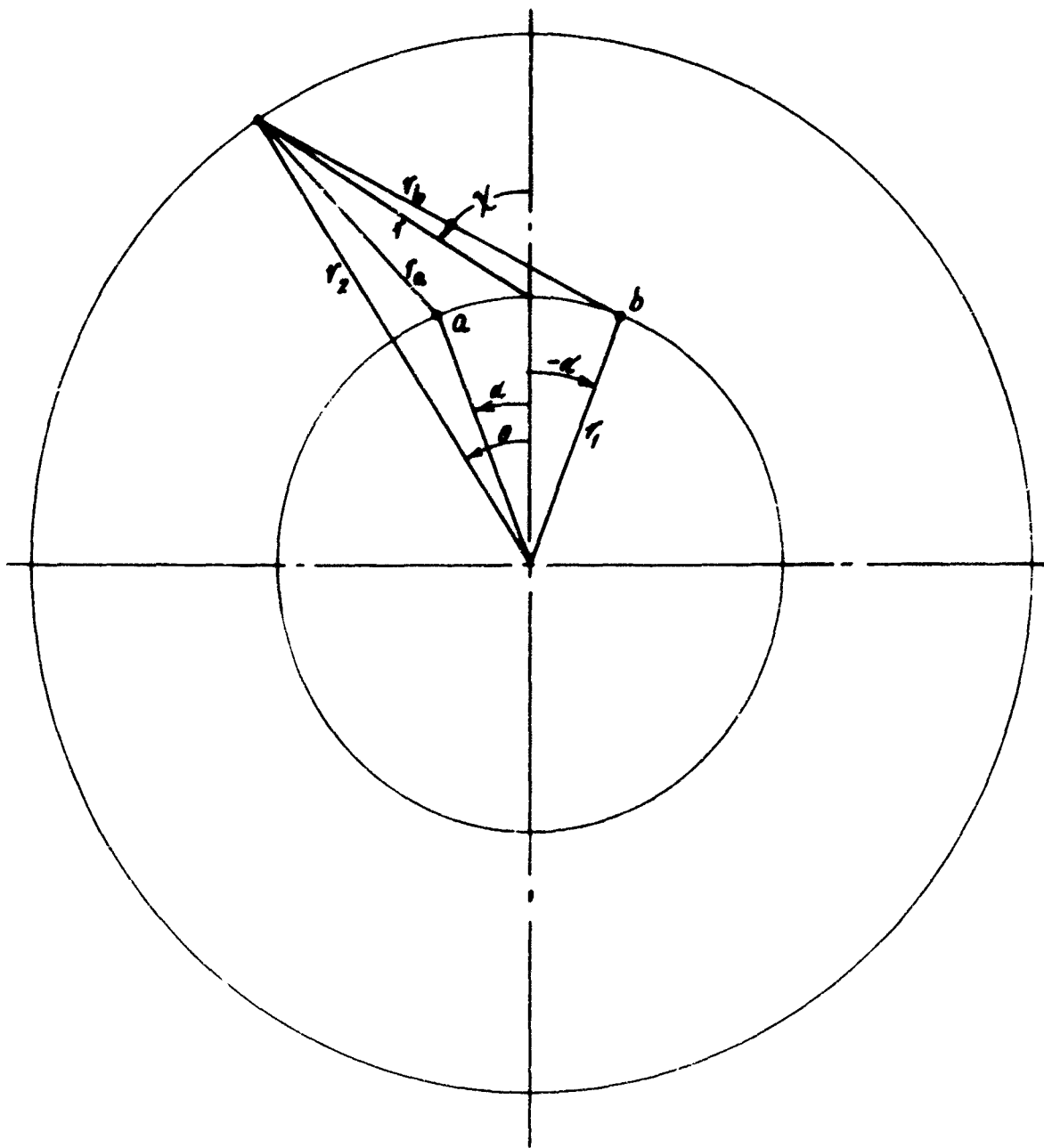
Figure D-4-1